Design, Analysis, and Optimization of Vibrational Control Strategies

Sevak Tahmasian

Dissertation submitted to the Faculty of the

Virginia Polytechnic Institute and State University

in partial fulfillment of the requirements for the degree of

Doctor of Philosophy

in

Engineering Mechanics

Craig A. Woolsey, Chair

Muhammad R. Hajj

Mark R. Paul

Shane D. Ross

April 27, 2015

Blacksburg, Virginia

Keywords: Vibrational Control, Geometric Control, Averaging, Mechanical Control-Affine Systems, Underactuated Mechanical Systems, Input Optimization, Biomimetic Systems

Design, Analysis, and Optimization of Vibrational Control Strategies

Sevak Tahmasian

ABSTRACT

This dissertation presents novel vibrational control strategies for mechanical control-affine systems with high-frequency, high-amplitude inputs. Since these control systems use high-frequency, zero-mean, periodic inputs, averaging techniques are widely used in the analysis of their dynamics. By studying their time-averaged approximations, new properties of the averaged dynamics of this class of systems are revealed. Using these properties, the problem of input optimization of vibrational control systems was formulated and solved by transforming the problem to a constrained optimization one.

Geometric control theory provides powerful tools for studying the control properties of control-affine systems. Using the concepts of vibrational and geometric controls and averaging tools, a closed-loop control strategy for trajectory tracking of a class of underactuated mechanical control-affine systems is developed. In the developed control law, the fact that for underactuated systems, the actuated coordinates together with the corresponding generalized velocities can be considered as generalized inputs for the unactuated dynamics plays the main role. Using the developed control method, both actuated and unactuated coordinates of the system are able to follow slowly time-varying prescribed trajectories on average. The developed control method is applied for altitude control of flapping wing micro-air vehicles by considering the sweeping (flapping) angle of the wings as the inputs. Using the feathering

(pitch) angles of the wings as additional inputs, and using non-symmetric flapping, the control method is then extended for three-dimensional flight control of flapping wing micro-air vehicles.

This work was partially supported by the National Science Foundation under Grant No. CMMI-1435484.

Dedication

Dedicated to my family for their never-ceasing love.

Acknowledgments

I would like to thank my advisor, Dr. Craig Woolsey, who helped and supported me patiently and sincerely during my studies. Without his guidance and support it would not be possible to accomplish this. Besides benefiting from his broad scientific and technical knowledge, I learned professional supervising and academic behavior from him, not to mention all the English grammar.

I also would like to thank my committee members, Dr. Muhammad Hajj, Dr. Mark Paul, and Dr. Shane Ross who were kind enough to serve in my committee. During the courses which I passed with all three of them I learned lots of scientific and technical knowledge and teaching strategies. For five semesters I was grader of Dr. Mark Paul's classes which increased my experience and provided financial support.

During my studies at Virginia Tech, I passed very useful courses with Dr. Mayuresh Patil, Dr. Rolf Mueller, Dr. Mark Cramer, and Dr. Raffaella De Vita , which hereby I want to thank them. Moreover, I benefited from great weekly seminars and meetings with Dr. Robert Canfield and Dr. Andrew Kurdila which I need to thank them also.

I want to express my gratitudes to Dr. Scott Case, Dr. Eric Paterson, and Dr. Mark Stremler for providing me the opportunity to serve as instructor of record for five semesters in the Engineering Science and Mechanics, and Aerospace and Ocean Engineering departments at Virginia Tech. I also want to thank Dr. Scott Hendricks, Dr. Glenn Kraige, and Dr. Jonathan Black for being a great help in my teachings.

I also want to thank the staff of the Engineering Science and Mechanics, Aerospace and Ocean Engineering, and Mechanical Engineering departments for providing help and support during my studies. I would like to especially mention Lisa Smith, Rachel Hall Smith, Amanda Stanley, Anne-Marie Bracken, Shannon Bennett, and Amy Burchett for always being ready to help.

My friends and colleagues created a friendly atmosphere for me during my studies. I would like to thank all my friends at Virginia Tech for their help, comments, and suggestions during my research and courses, especially Dr. Haithem Taha, Dr. Alireza Samimi, Dr. Amir Bozorg Magham, Artur Wolek, and Farid Jafari. I especially want to thank Parisa, who though far from me, never ceased to encourage me during my studies.

I would like to thank the College of Engineering Dean's Office at Virginia Tech for providing financial support during my last academic year of studies. And I want to thank all who made this possible.

Contents

1 Introduction **1**

1.1 Vibrational Control 2

1.2 Contributions 12

1.3 Outline 13

2 Mathematical Preliminaries: Control Systems and Averaging **15**

2.1 Control-Affine Systems 15

2.2 Controllability of Control-Affine Systems 18

2.3 The Symmetric Product 22

2.4 Averaging Theorem 23

2.5 Higher-Order Averaging 26

2.6 Summary 27

3 Some Properties of the Averaged Dynamics **29**

3.1 Introduction 30

3.2 On the Commutativity of Linearization and Averaging 32

3.3 Averaging of High-Frequency Mechanical Control Systems 35

3.4 Effects of the Inputs Relative Phase Shifting on the Averaged Dynamics . . . 39

3.5 Conclusions 43

4 Control of Underactuated Mechanical Systems Using High-Frequency Inputs **44**

4.1 Introduction 45

4.2 The Control Method 47

4.3 Selection of Control Parameters 51

4.4 Control of Higher Dimensional, Multi-Input Systems 54

4.5 Example 1: A 4-DOF Control System 60

4.6 Example 2: Flapping Plate in Uniform Flow 65

4.6.1 Equations of motion and aerodynamic model 67

4.6.2 Closed-loop control 70

4.7 Conclusions 76

4.8 Acknowledgment 77

5 Flight Control of Flapping Wing Micro Air Vehicles 78

5.1 Introduction 79

5.2 Equations of Longitudinal Motion 83

5.3 Aerodynamic Model 90

5.4 Averaging and Control of Longitudinal Flight 93

5.5 Simulation and Numerical Results 98

5.6 Control of Three Dimensional Flight 105

5.6.1 Equations of three dimensional motion 105

5.6.2 Control of three dimensional motion 108

5.6.3 Numerical results for three dimensional motion 110

5.7 Conclusions 115

6 Input Optimization of Vibrational Control Systems 116

6.1 Introduction 117

6.2 Input Optimization of 1-DOF Control-Affine Systems 119

6.3 Input Optimization of Higher-Dimensional Systems 124

6.3.1 Example 1: Input optimization of a 3-DOF system 131

6.3.2 Example 2: Planar two-link mechanism on a cart 133

6.4 Selection of Design Parameters for Input Optimization 140

6.5 Conclusions 143

7 Summary and Future Work **145**

7.1 Vibrational Control of a Two-Link Mechanism on a Cart 148

7.1.1 Two-link mechanism on a cart without gravity 151

7.1.2 Two-link mechanism on a cart with gravity 154

7.2 Conclusions 158

A Proof of Theorem 3.4.1 **159**

B Proof of Proposition 4.4.1 **162**

C Proof of Theorem 6.2.1 **165**

D Proof of Theorem 6.3.1 **168**

Bibliography **171**

List of Figures

2.1 a) Lack of accessibility, b) accessibility but not local controllability, c) local controllability, at a point x_0 (shaded regions are accessible). Adapted from [Bullo and Lewis, 2005, Ch. 7] 22

3.1 Averaging and Linearization 34

3.2 Portrait of root locus of the linearized system (3.24) for $0 \leq \phi_0 \leq \pi$ 42

3.3 Time histories of the actual and averaged systems for $\phi_0 = 0$ 42

3.4 Time histories of the actual and averaged systems for $\phi_0 = 0.733$ 43

4.1 Time history of actuated coordinates θ_1 and θ_2 65

4.2 Time history of unactuated coordinates θ_3 and θ_4 66

4.3 Notation for the oscillating wing 67

4.4 Aerodynamic and control forces on the flapping device 68

4.5 Variations of y, z, and θ with respect to time in hovering motion 74

4.6 Variations of y with respect to time in hovering motion using modified controller 74

4.7 Variations of y, z, and θ following a harmonic trajectory with $\omega = 50\,\text{rad/s}$. 75

4.8 Variations of y, z, and θ following a harmonic trajectory with $\omega = 17\,\text{rad/s}$. 76

5.1 The inertial and body coordinate frames (side view) 84

5.2 The wing angles and wing coordinate frame 84

5.3 Time histories of X, Z and θ for hovering flight without wing inertia effects . 102

5.4 Time histories of X, Z and θ for a circular desired trajectory without wing inertia effects 103

5.5 X-Z path for a circular desired trajectory without wing inertia effects 103

5.6 Time histories of X, Z and θ following a circular trajectory when considering the wing effects 104

5.7 The vehicle X-Z path, following a circular trajectory when considering the wing effects 104

5.8 Time histories of X, Y and Z following trajectory 1 112

5.9 Time histories of ϕ, θ and ψ following trajectory 1 112

5.10 The 3-D trajectory 1 of the FWMAV 113

5.11 Time histories of X, Y and Z following trajectory 2 113

5.12 Time histories of ϕ, θ and ψ following trajectory 2 114

5.13 The 3-D trajectory 2 of the FWMAV 114

6.1 Three T-periodic, zero-mean functions with different amplitudes and the input parameter $\mu_{11} = 1$ 122

6.2 Time histories of the original and averaged systems when using the optimum inputs 133

6.3 Two-link mechanism on a cart 134

6.4 Time histories of $x(t)$ of the two-link mechanism on a cart 138

6.5 Time histories of $\theta_1(t)$ of the two-link mechanism on a cart 139

6.6 Time histories of $\theta_2(t)$ in the two-link mechanism on a cart 139

7.1 Two-link mechanism 148

7.2 Time histories of the actual and averaged dynamics of the two-link mechanism 150

7.3 Time histories of $x(t)$ of the two-link mechanism on a cart 154

7.4 Time histories of $\theta_1(t)$ of the two-link mechanism on a cart 154

7.5 Time histories of $\theta_2(t)$ in the two-link mechanism on a cart 155

7.6 Two-link mechanism on a cart with gravity 155

7.7 Time histories of $x(t)$ in the two-link mechanism on a cart with gravity . . . 157

7.8 Time histories of $\theta_1(t)$ in the two-link mechansim on a cart with gravity . . . 157

7.9 Time histories of $\theta_2(t)$ in the two-link mechanism on a cart with gravity . . . 158

Chapter 1

Introduction

This dissertation presents vibrational control and input optimization of classes of mechanical control systems. Based on the concepts of vibrational and geometric control, a novel method to control a class of underactuated mechanical systems is developed. Using cleverly designed high-frequency inputs, the system tracks slowly-varying prescribed trajectories on average. Many engineered systems, including those that mimic living creatures, are underactuated by design and require advanced control methods. Using the method developed here, flight control of flapping wing micro-air vehicles (FWMAV), as an example of underactuated biomimetic systems, is considered in this dissertation.

Optimization of design parameters and input optimization of high-frequency biomimetic systems were two main motivations of this research. Using smaller actuators and less power are two important factors in design of small biomimetic devices. The input optimization

problem considered here is determining the waveform (shape), amplitude, and the relative phase of inputs to minimize their amplitudes while accomplishing some control objective. Using available averaging techniques and the results obtained in this dissertation, the input optimization problem for high-frequency mechanical systems is formulated as a constrained optimization problem, which may be solved using well-developed analytical or numerical methods.

1.1 Vibrational Control

Vibrational control is influencing the behavior of dynamic systems using high-frequency, zero-mean inputs. The principle of vibrational control stems from the well known effect of stabilizing the unstable (upper) equilibrium position of a pendulum by vibrating its pivot along the vertical line with an amplitude as small as desired, provided that a "sufficiently" high frequency is used. The pendulum, known as Stephenson-Kapitza pendulum (usually Kapitza's pendulum), was first described by A. Stephenson in 1908. Later, P. Kapitza developed the theory underlying the stabilization of its unstable equilibrium point in 1951. The interesting observation in stabilizing Kapitza's pendulum is that unlike conventional stabilizing methods, it does not need any feedback from the states of the system (position or velocity), and its unstable equilibrium will be asymptotically stable if the frequency of vibrations is greater than a certain value, depending on the length of the pendulum and the amplitude of the vibrations.

The principle of vibrational control for linear dynamical systems was first introduced by Meerkov [1977, 1980]. The principle consists of the introduction of zero mean vibrations of the dynamic system parameters which modify the properties of the system in a desired manner. As mentioned for the special case of Kapitza's pendulum, the benefit of vibrational control is that unlike conventional methods containing feedback or feedforward, it does not require measurements of deviations and disturbances. Depending on the class of the dynamical system, vibrational control may be effective for ensuring the stability, the desired properties of the transient response, and the desired properties of the dynamical system response to the external disturbances. Vibrational control also can be useful for systems described by partial differential equations, where it is necessary to stabilize all modes of oscillations simultaneously. In many cases it is impossible to measure all the modes and apply feedback, but introduction of vibrations can stabilize all the modes simultaneously. One example is the problem of glow discharge stabilization in continuous powerful gas lasers [Meerkov, 1980].

The theory of vibrational control for nonlinear systems and vibrational stabilizability was developed by Meerkov [1982] for a class of nonlinear systems, and later by Bellman et al. [1986a] for more general classes of nonlinear systems. In a subsequent paper, Bellman et al. [1986b] addressed the vibrational controllability and transient behavior of nonlinear systems. Bentsman [1987] extended the nonlinear vibrational control theory to the case of nonlinear multiplicative vibrations, by applying the technique to the example of a catalytic reactor. In his work, Bentsman showed that for the method to be effective, one needs to have a fairly

accurate description of the system dynamics. He mentioned this fact along with physical limitations on the magnitudes and frequencies of the vibrations in actual systems as the disadvantages of the vibrational control method.

Since in vibrational control methods high-frequency, periodic inputs are used, averaging techniques are useful tools for analysis. Averaging is a perturbation method which transforms a time-periodic system into a time-invariant approximation [Guckenheimer and Holmes, 1983; Sanders and Verhulst, 1985]. In [Guckenheimer and Holmes, 1983] it is stated that the average of a Hamiltonian system forced by a bounded high-frequency perturbation can be computed by averaging its Hamiltonian. For the case of mechanical systems with high-frequency, high-amplitude inputs, Baillieul [1993] introduced the notion of *averaged potential* for underactuated mechanical control systems subject to periodic forcing. Underactuated systems have fewer actuators than their degrees of freedom (DOF).

In his work, Baillieul [1993] considered underactuated mechanical systems with their cyclic coordinates being actuated directly by high-frequency periodic forcing. An example of this class of systems is the well known cart and pendulum system [Fantoni and Lozano, 2002], with the cart being forced by a periodic forcing. Assuming the velocity of the actuated cyclic coordinate (the velocity of the cart in the cart-pendulum system) to be the input of the dynamics of the unactuated coordinate (the dynamics of pendulum in the cart-pendulum system), he derived the reduced dynamics of the unactuated subsystem (the dynamics of the pendulum with the cart velocity as its input). He showed that the dynamics of unactuated subsystem itself prescribes the dynamics of a Lagrangian control system, with its Lagrangian

called the *reduced Lagrangian*. The reduced Lagrangian determined in this way contains both kinetic and potential energies, with the potential energy called the *augmented potential*. By applying the Legendre transformation, the Hamiltonian control system corresponding to the actuated subsystem (reduced Lagrangian) can be determined. The time average of the determined Hamiltonian control system is Hamiltonian itself (called the *averaged Hamiltonian system*). The Hamiltonian function corresponding to the averaged Hamiltonian system may be interpreted as an averaged total energy (kinetic plus potential energies). The potential part of this averaged energy is called the averaged potential.

Baillieul then showed that the unactuated coordinates evolve ("hover") in a small neighborhood of the strict minimum points of the averaged potential. The radius of the neighborhood depends on the frequency of the inputs, and decreases by increasing the frequency. Note that the strict minimum points of the averaged potential may not be even an equilibrium point of the original time varying system. The equilibrium points of the averaged system are not the equilibrium points of the original, time-varying system necessarily. For a thorough description of averaged potential and its application in stabilization of underactuated mechanical systems, together with the example of stabilization of a cart-pendulum system on an inclined (including vertical) surface, see [Baillieul, 1993; Weibel et al., 1995, 1997].

Later Weibel and Baillieul [1998] developed more theorems on the concept of averaged potential, and applied the concept for open-loop stabilization and bifurcation analysis of a rotating planar pendulum, and presented a thorough comparison of the averaged phase portraits and Poincaré maps of the system with different control parameters. They applied the averaged

potential for control of systems with more degrees of freedom, such as heavy rotating chains with periodic excitation at one end. Baillieul [1999] also studied the connection between geometry of second-order underactuated mechanical control systems (geometric control) with the theory of averaged Lagrangian and Hamiltonian systems and averaged potential.

In a later article, Baillieul [2000] introduced a new averaged potential term resulting from averaging of the whole underactuated system dynamics, instead of averaging the dynamics of the unactuated subsystem only. He showed that the comparison of the two averaged potentials resulting from the two methods is in fact a comparison of force controlled and acceleration controlled systems, while mentioning their advantages and disadvantages.

Bullo [2002] extended the concept of averaged potential for *simple* mechanical control systems, i.e., systems without any nonholonomic constraint, and systems with integrable inputs. He stated the conditions under which the averaged system remains simple again. He showed that the concept of averaged potential is related to the definition of the *symmetric product* (see Section 3.3), and applied the results for open-loop control of an underactuated two-link mechanism.

Using time-periodic input and averaging techniques, and by modulating of the feedback error amplitude, Suzuki and Nakamura [1997]; Nakamura et al. [1997] also tried the nonlinear control of free joint manipulators. Choosing a time-periodic input for the first joint of an underactuated two-link manipulator, they showed that when the amplitude of periodic input remains small, the Poincaré map of the system forms an elliptic closed manifold. As the amplitude grows, the Poincaré map shows chaotic behavior. They proposed a series of

positioning control strategies where the amplitude modulation of the error signal was used for feedback control to a desired elliptic manifold. They verified their results by series of experiments which showed the effectiveness of the method.

Hong et al. [1999]; Hong [2002] also investigated the open-loop vibrational control of underactuated mechanical systems with amplitude and frequency modulation. By first positioning the actuated joint in their desired locations, they applied periodic oscillatory inputs to the actuated joints to bring the unactuated joints to their desired locations.

Another approach to vibrational control of underactuated mechanical systems is the use of geometric control and concepts in differential geometry to determine the necessary oscillatory inputs for stabilization and trajectory tracking. This approach is one of the main interests of this dissertation. The main idea underlying the differential geometry and averaging approach is expressed clearly by Brockett [1989], which we mention in brief.

Consider the driftless control system

$$\dot{\boldsymbol{x}} = \boldsymbol{g}_1(\boldsymbol{x})u + \boldsymbol{g}_2(\boldsymbol{x})v$$

where $\boldsymbol{g}_1(\boldsymbol{x})$ and $\boldsymbol{g}_2(\boldsymbol{x})$ are the input vector fields, and u and v are the inputs. (Driftless or drift-free control systems have zero dynamics in the absence of controls [Sastry, 1999].) As a control system, u can drive $\boldsymbol{x}$ in the direction defined (spanned) by $\boldsymbol{g}_1(\boldsymbol{x})$, and v can drive $\boldsymbol{x}$ in the direction defined (spanned) by $\boldsymbol{g}_2(\boldsymbol{x})$. But by working together, the inputs can also drive $\boldsymbol{x}$ in the direction defined (spanned) by the Lie bracket of the two vector fields

$\boldsymbol{g}_1(\boldsymbol{x})$ and $\boldsymbol{g}_2(\boldsymbol{x})$, shown as $[\boldsymbol{g}_1(\boldsymbol{x}), \boldsymbol{g}_2(\boldsymbol{x})]$. If one chooses coordinates such that $\boldsymbol{x} = \mathbf{0}$ is the nominal operating point, and $\boldsymbol{g}_1 = [1, 0, 0, \ldots]^T$ and $\boldsymbol{g}_2 = [0, 1, 0, \ldots]^T$, then one can see that for u and v periodic of period T and $\boldsymbol{x}(0) = \mathbf{0}$,

$$\boldsymbol{x}(T) \approx A\,[\boldsymbol{g}_1(\boldsymbol{x}), \boldsymbol{g}_2(\boldsymbol{x})]$$

with the vector $[\boldsymbol{g}_1(\boldsymbol{x}), \boldsymbol{g}_2(\boldsymbol{x})]$ evaluated at $\boldsymbol{x} = \mathbf{0}$, and A being the area defined by the closed curve described by the first and second components of $\boldsymbol{x}$. Thus in an average sense

$$\dot{\boldsymbol{x}} = \frac{A}{T}\,[\boldsymbol{g}_1(\boldsymbol{x}), \boldsymbol{g}_2(\boldsymbol{x})]$$

Using the mentioned approach above, Sussmann and Liu [1991] considered approximate trajectory tracking of controllable driftless systems using high-frequency, high-amplitude inputs. Their approach was to construct a driftless *extended system* using the input vector fields of the original driftless system and the Lie brackets between them. Since the extended system gives rise to more trajectories than the original system, by introducing new inputs, called *extended inputs*, they constructed trajectories for the extended system and showed that the original system will follow them approximately.

Using oscillatory inputs and averaging techniques, Gurvits [1992] developed open-loop and closed-loop solutions for motion planning of driftless systems, and used the method for stabilization of a rolling disk. Leonard and Krishnaprasad [1995] addressed the open-loop control of driftless left-invariant underactuated systems using low-frequency, small-amplitude

periodic inputs (unlike most of the vibrational control methods). They used n^{th} ($n \geq 1$) order averaging to construct open-loop controls for point to point maneuvering of the systems which require up to $n-1$ iteration of Lie brackets to satisfy the Lie algebra controllability rank condition [Sastry, 1999, Ch. 11]. They applied their method for the control of a 6-DOF autonomous underwater vehicle (AUV), once considering four inputs and once three inputs. For the definition of left-invariant vector fields and left-invariant control systems see [Sastry, 1999; Bullo and Lewis, 2005]. Examples include airplanes, satellites and underwater vehicles.

Bullo et al. [2000] provided controllability tests and motion control algorithms for a class of underactuated mechanical control systems. They considered an important class of mechanical systems with the features that the configuration space is a Lie group, the Lagrangian is equal to the kinetic energy, and the external forces applied to the system are fixed with respect to the body. These systems, if underactuated, offer a control challenge as they have nonzero drift, their linearization at zero velocity is not controllable, they are not stabilizable by continuous state feedback, and exponential stabilization cannot be achieved by smooth time-varying feedback. Examples of such systems are planar bodies, satellites and underwater vehicles. They designed motion planning algorithms to solve the problem of point-to-point reconfiguration, static interpolation, and exponential stabilization, and used their result for the control of a planar rigid body with two input forces. Vibrational control of examples of this class of systems are considered in Chapters 6 and 7 of this dissertation.

Vela and Burdick [2003b] used their developed technique of presenting higher order averaging approximations via Lie brackets (generalized averaging theorem) for control of underactuated

mechanical systems. They developed stabilizing control laws for a class of underactuated mechanical control systems with drift. They used sinusoidal inputs for indirect actuation of unactuated coordinates, and determined control laws to exponentially stabilize the averaged system. They also used their method for the control of biomimetic locomotion and applied it for point stabilization and trajectory tracking of a kinematic biped and snakeboard [Vela and Burdick, 2003c]. Snakeboards, roller-racers, and unicycle wheeled robots are underactuated mechanical systems which have been used extensively in geometric control and oscillatory control literature as examples of nonholonomic mechanical systems [Krishnaprasad and Tsakiris, 1995; Kolmanovsky and McClamroch, 1995; Bloch et al., 1996; Bullo and Lewis, 2003].

In a major work on oscillatory control systems, Martinez et al. [2002, 2003a] investigated the behavior of finite dimensional analytic systems subject to high-frequency, high-amplitude oscillatory inputs. They recovered and extended a variety of point stabilization and trajectory tracking results using oscillatory controls. The results are also presented in [Bullo, 2004; Bullo and Lewis, 2005]. An overview of motion planning and oscillatory control of underactuated robots is presented by Martinez et al. [2003b].

Control of underactuated mechanical systems with unactuated cyclic coordinates is also considered by Sanyal et al. [2005]. Using high-frequency, high-amplitude periodic inputs, geometric control, and averaging theory, their goal was to achieve full controllability of a reduced dynamics obtained by eliminating the cyclic coordinates. Lalish et al. [2007] used oscillatory control methods for control of constant speed planar unicycle-type vehicles, such

as unmanned aerial vehicles. In their work, they related the dynamics of the original system to another dynamical model that is less constrained, and designed an oscillatory regulator for control of a limit cycle behavior. The idea was based on defining a center of oscillation and using a parameterized oscillatory input to produce desirable center of oscillation dynamics.

Many attempts to control biomimetic locomotion systems using sinusoidal inputs have also been done. Morgansen et al. [2001] used the concept of controllability and accessibility for control-affine systems to produce forward propulsion and turning gaits for planar carangiform robot fish and verified their results by experiment. In a later work, Morgansen et al. [2002] used higher order averaging techniques and state feedback for trajectory stabilization of the mentioned robot fish. Vela et al. [2002] studied oscillatory shape deformation as a propulsion means for robotic underwater vehicles, and extended their control method based on higher order averaging techniques and oscillatory inputs for this class of systems. Morgansen et al. [2007] used geometric mechanics and geometric nonlinear control theory for construction of a trajectory tracking algorithm for a free-swimming underwater vehicle. The vehicle performed three dimensional motion using a two-link actuated tail and two independently actuated pectoral fins. By particular choice of oscillatory actuation of the four joints, they constructed maneuvers such as forward swimming, in and out of plane turning, surfacing, and diving, and verified their results using a prototype fin-actuated underwater vehicle. Vibrational control, geometric control, and the averaging theory also have been widely used in analysis and control of other biomimetic systems such as FWMAVs [Schenato, 2003] and snake robots [Liljeback et al., 2010].

1.2 Contributions

The main contributions of this dissertation are the following.

- Determining the effects of waveform (shape) and relative phasing of the inputs on the averaged dynamics of high-frequency mechanical control-affine systems.

- Developing a closed-loop control method for trajectory tracking of a class of underactuated mechanical systems using high-frequency inputs. In this method both actuated and unactuated coordinates follow slowly-varying desired trajectories on average.

- Three-dimensional flight control of FWMAVs. Using the developed control method in this dissertation and state feedback, a control method for tracking of three-dimensional slowly-varying trajectories by a FWMAV device was developed.

- Input optimization of high-frequency mechanical control-affine systems. Using the results obtained in this dissertation and averaging tools, the problem of input amplitude minimization for high-frequency mechanical control systems was transformed to a regular constrained optimization problem, which can be solved using well developed analytical or numerical methods.

- Investigation of the commutativity of linearization and averaging of nonlinear time-periodic systems. In this dissertation it was shown that switching the order of linearization and averaging of a nonlinear, time-periodic system results in two distinct

linear, time-invariant systems which become equivalent in the limit that the perturbations are infinitesimal and the frequency of oscillations is arbitrarily high.

1.3 Outline

The structure of this dissertation is as follows. In Chapter 2 the mathematical concepts used in this dissertation are presented. After presenting the general form of control-affine systems, the controllability and accessibility of this class of systems are discussed in brief and the concept of symmetric product as used in this dissertation is presented. The averaging theorem is discussed in detail and a higher-order averaging method is presented. In Chapter 3 two different methods of determining the stability of periodic orbits of time-periodic systems are compared. Averaging of mechanical control-affine systems with high-frequency, high-amplitude inputs is presented and the effect of relative phase of the inputs on the stability properties of the averaged and original systems is studied. In Chapter 4 a control method for control of a class of underactuated mechanical systems based on vibrational control and averaging is developed. After discussing the idea for 2-DOF mechanical systems with one input, the method is extended to higher-dimensional mechanical systems. The method is then used for control of a 4-DOF system with two inputs, and a 3-DOF system with one input. In Chapter 5, after deriving the equations of motion and introducing the model used to represent aerodynamic forces and moments, the method developed in Chapter 4 is used for control of three-dimensional flight of FWMAVs. Optimization of input amplitudes in

vibrational control systems is presented in Chapter 6. By selecting the best waveform for the inputs, a cost function is developed to determine the amplitude and relative phase of the inputs. Summary and possible future work, along with vibrational control of a planar two-link mechanism on a cart system as a potential future work, are presented in Chapter 7.

Chapter 2

Mathematical Preliminaries: Control Systems and Averaging

This chapter presents the mathematical concepts and tools used in this dissertation. The necessary concepts in control systems and geometric control are presented and controllability of control-affine systems is discussed. The *symmetric product*, averaging theorem, and higher order averaging of time-periodic dynamical systems are discussed in detail.

2.1 Control-Affine Systems

A general class of nonlinear control systems is described by the following system of ordinary differential equations:

$$\dot{\boldsymbol{x}} = \boldsymbol{f}(\boldsymbol{x}, \boldsymbol{u}) \tag{2.1}$$

where $\boldsymbol{x} = (x_1, \ldots, x_n)^T$ is the state vector, $\boldsymbol{u} = (u_1, \ldots, u_m)^T$ is the vector of inputs, and $\boldsymbol{f}$ is a (smooth) vector field in $\boldsymbol{x}$ and $\boldsymbol{u}$. A broad subclass of nonlinear control systems is the subset of systems (2.1) which are linear in their inputs. In general this class of control systems, called *control-affine systems* or *input-linear systems*, can be written in the following form

$$\dot{\boldsymbol{x}} = \boldsymbol{f}(\boldsymbol{x}) + \sum_{j=1}^{m} \boldsymbol{g}_j(\boldsymbol{x}) u_j \tag{2.2}$$

where $\boldsymbol{f}$ and $\boldsymbol{g}_j$, $j \in \{1, \ldots, m\}$, are smooth vector fields called the *drift vector field* and the *input vector fields* respectively, and u_j, $j \in \{1, \ldots, m\}$, are the inputs. The drift vector field $\boldsymbol{f}$ specifies the dynamics of the system in the absence of controls. A control-affine system for which the drift vector field is identically zero is called a driftless or drift-free control system (and in some literature, a *nonholonomic control system*). While the state history $\boldsymbol{x}(t)$ may evolve in Euclidean space, a more general model allows the state history to evolve on an n-dimensional *smooth* manifold M. For an introduction to differential geometry and definition of smooth manifold see [Nijmeijer and van der Schaft, 1990, Ch. 2], [Jurdjevic, 1997], and [Bullo and Lewis, 2005, Ch. 3].

Mechanical control-affine systems are a broad class of control-affine systems. The dynamic equations of an n-DOF mechanical control-affine system with m ($m \leq n$) independent inputs are in the form

$$\boldsymbol{M}(\boldsymbol{q})\ddot{\boldsymbol{q}} = \boldsymbol{f}(\boldsymbol{q}, \dot{\boldsymbol{q}}) + \boldsymbol{u} \tag{2.3}$$

where $\boldsymbol{q} = (q_1, \ldots, q_n)^T$ is the vector of generalized coordinates on an n-dimensional smooth

manifold Q called *configuration manifold*, $\boldsymbol{M}(\boldsymbol{q})$ is the (invertible) generalized inertia matrix, $\boldsymbol{u} = (u_1, \ldots, u_m, 0, \ldots, 0)^T$ is the input vector, and $\boldsymbol{f}(\boldsymbol{q}, \dot{\boldsymbol{q}})$ is a vector containing linear and/or nonlinear terms in $\boldsymbol{q}$ and $\dot{\boldsymbol{q}}$. If system (2.3) has fewer actuators than its degrees of freedom, i.e., $m < n$, it is called underactuated mechanical control-affine system. In this case the coordinates q_i, $i \in \{1, \ldots, m\}$, directly driven by the inputs are called actuated coordinates, and the rest of the coordinates q_i, $i \in \{m+1, \ldots, n\}$, are called unactuated coordinates. Otherwise if $m = n$, the system is called fully actuated.

Since $\boldsymbol{M}(\boldsymbol{q})$ is non-singular, system (2.3) can be rewritten as

$$\ddot{\boldsymbol{q}} = \boldsymbol{g}(\boldsymbol{q}, \dot{\boldsymbol{q}}) + \sum_{j=1}^{m} \boldsymbol{h}_j(\boldsymbol{q}) u_j \tag{2.4}$$

where $\boldsymbol{g} = \boldsymbol{M}^{-1}\boldsymbol{f}$ and $\boldsymbol{h}_j$ is the j^{th} column of $\boldsymbol{M}^{-1}$. (The arguments $\boldsymbol{q}$ and $\dot{\boldsymbol{q}}$ are suppressed here and elsewhere for brevity.) Defining the state vector $\boldsymbol{x} = (\boldsymbol{q}^T, \dot{\boldsymbol{q}}^T)^T$, system (2.4) can be written in the first order form of

$$\dot{\boldsymbol{x}} = \boldsymbol{Z}(\boldsymbol{x}) + \sum_{j=1}^{m} \boldsymbol{Y}_j(\boldsymbol{x}) u_j \tag{2.5}$$

where $\boldsymbol{Z} = (\dot{\boldsymbol{q}}^T, \boldsymbol{g}^T)^T$ and $\boldsymbol{Y}_j = (\boldsymbol{0}_{1\times n}, \boldsymbol{h}_j^T)^T$. The state vector $\boldsymbol{x}$ is evolving on a $2n$-dimensional smooth manifold M, called the *state manifold*, which is the *tangent bundle* of the configuration manifold Q. (The collection of all tangent vectors at $\boldsymbol{q}$ is the *tangent space* at $\boldsymbol{q}$, denoted by $T_{\boldsymbol{q}}Q$. The disjoint union of all tangent spaces of Q is called the tangent bundle of Q, denoted by TQ.)

2.2 Controllability of Control-Affine Systems

It is not always possible to steer the control system (2.1) from an initial point (state) $\boldsymbol{x}_0$ at time t_0 to a desired point $\boldsymbol{x}_1$ at time $t_1 > t_0$. The system (2.1) is called *controllable at a point* $\boldsymbol{x}_0$ if there exist a time $t_1 > t_0$ and admissible inputs u_j, $j \in \{1, \ldots, m\}$, to steer the system from point $\boldsymbol{x}_0$ at time t_0 to any point $\boldsymbol{x}_1$ in its neighborhood at time t_1 (i.e. $\boldsymbol{x}(t_1) = \boldsymbol{x}_1$). The system is called *controllable* if it is controllable at any point $\boldsymbol{x}$. To see the precise definition and variants see [Nijmeijer and van der Schaft, 1990; Sastry, 1999; Bullo and Lewis, 2005].

Controllability of linear time-invariant control systems is easy to determine. Linear time-invariant control system are in the form of

$$\dot{\boldsymbol{x}} = \boldsymbol{A}\boldsymbol{x} + \sum_{j=1}^{m} \boldsymbol{b}_j u_j \tag{2.6}$$

where $\boldsymbol{A}$ is the constant $n \times n$ state matrix and $\boldsymbol{b}_j$, $j \in \{1, \ldots, m\}$, are $n \times 1$ vectors. System (2.6) is controllable if and only if the controllability Gramian $\boldsymbol{M}_c = \begin{bmatrix} \boldsymbol{B} & \boldsymbol{A}\boldsymbol{B} & \ldots & \boldsymbol{A}^{n-1}\boldsymbol{B} \end{bmatrix}$ has full rank (i.e., $\operatorname{rank}(\boldsymbol{M}_c) = n$), where $\boldsymbol{B} = [\boldsymbol{b}_1 \ \ldots \ \boldsymbol{b}_m]$ [Sastry, 1999; Khalil, 1996; Ogata, 2010]. Since for a linear time-invariant system the controllability Gramian matrix $\boldsymbol{M}_c$ is constant, a linear system controllable in one point is controllable everywhere.

The controllability Gramian test can often be used to check the local controllability of nonlinear control systems in the general form of (2.1) at an equilibrium point $(\boldsymbol{x}_\mathrm{e}, \boldsymbol{u}_\mathrm{e})$, (i.e.

where $\boldsymbol{f}(\boldsymbol{x}_\mathrm{e}, \boldsymbol{u}_\mathrm{e}) = \boldsymbol{0}$) [Brockett, 1983]. If the linear system resulting from linearization of nonlinear system (2.1) about an equilibrium point $(\boldsymbol{x}_\mathrm{e}, \boldsymbol{u}_\mathrm{e})$ is controllable, then the nonlinear system is locally controllable at that point, though still may not globally controllable [Sastry, 1999]. The linearization of (2.1) about its equilibrium point is determined by

$$\boldsymbol{\delta\dot{x}} = \left.\frac{\partial \boldsymbol{f}}{\partial \boldsymbol{x}}\right|_{(\boldsymbol{x}_\mathrm{e}, \boldsymbol{u}_\mathrm{e})} \boldsymbol{\delta x} + \left.\frac{\partial \boldsymbol{f}}{\partial \boldsymbol{u}}\right|_{(\boldsymbol{x}_\mathrm{e}, \boldsymbol{u}_\mathrm{e})} \boldsymbol{\delta u}$$

where $\boldsymbol{\delta x} = \boldsymbol{x} - \boldsymbol{x}_\mathrm{e}$ and $\boldsymbol{\delta u} = \boldsymbol{u} - \boldsymbol{u}_\mathrm{e}$ are the state and input vectors of the linearized system, respectively.

For the control-affine system (2.2), an equilibrium point $\boldsymbol{x}_\mathrm{e}$ is determined for the system with zero input (i.e., $\boldsymbol{f}(\boldsymbol{x}_\mathrm{e}) = \boldsymbol{0}$). The linearization of system (2.2) about an equilibrium point $\boldsymbol{x}_\mathrm{e}$ is given by

$$\boldsymbol{\delta\dot{x}} = \left.\frac{\partial \boldsymbol{f}}{\partial \boldsymbol{x}}\right|_{\boldsymbol{x}=\boldsymbol{x}_\mathrm{e}} \boldsymbol{\delta x} + \sum_{j=1}^{m} \boldsymbol{g}_j(\boldsymbol{x}_\mathrm{e}) u_j \tag{2.7}$$

where $\boldsymbol{\delta x} = \boldsymbol{x} - \boldsymbol{x}_\mathrm{e}$ is the state vector of the linearized system.

The controllability of the linearized approximation of a nonlinear system about an equilibrium point is only a sufficient condition for local controllability of the nonlinear system at that equilibrium point, but not necessary. Since a nonlinear system may lose much of its structure by linearization, the nonlinear system can be controllable while its linearization is not. Controllability of the control-affine system (2.2) depends on the Lie brackets of its drift and input vector fields. The Lie bracket between two smooth vector fields $\boldsymbol{X}(\boldsymbol{x})$ and $\boldsymbol{Y}(\boldsymbol{x})$

is defined as

$$[\boldsymbol{X}(\boldsymbol{x}), \boldsymbol{Y}(\boldsymbol{x})] = \frac{\partial \boldsymbol{Y}(\boldsymbol{x})}{\partial \boldsymbol{x}} \boldsymbol{X}(\boldsymbol{x}) - \frac{\partial \boldsymbol{X}(\boldsymbol{x})}{\partial \boldsymbol{x}} \boldsymbol{Y}(\boldsymbol{x}) \tag{2.8}$$

Controllability of nonlinear control systems has been studied by Brockett [1972], Sussmann and Jurdjevic [1972], Hermann and Krener [1977], Sussmann [1983, 1987], and others. To discuss the controllability of control-affine system (2.2), first consider the drift-free case, where $\boldsymbol{f}(\boldsymbol{x}) = \boldsymbol{0}$:

$$\dot{\boldsymbol{x}} = \sum_{j=1}^{m} \boldsymbol{g}_j(\boldsymbol{x}) u_j \tag{2.9}$$

Consider the vector space (formally, the *distribution*) $\Delta(\boldsymbol{x})$ generated by the input vector fields $\boldsymbol{g}_j$, $j \in \{1, \ldots, m\}$, and the Lie brackets between them as

$$\Delta = \text{span}\{[\boldsymbol{X}_k, [\boldsymbol{X}_{k-1}, [\ldots, [\boldsymbol{X}_2, \boldsymbol{X}_1] \ldots]]]\} \tag{2.10}$$

where $\boldsymbol{X}_i \in \{\boldsymbol{g}_1, \ldots, \boldsymbol{g}_m\}$, $i \in \{1, \ldots, k\}$, $k = 1, 2, \ldots$. The control system (2.9) is controllable at $\boldsymbol{x} \in M$, if and only if $\Delta = T_{\boldsymbol{x}} M$, i.e., the input vector fields and the Lie brackets between them span the tangent space of M at $\boldsymbol{x}$, or $\dim\Delta = n$.

As for the control-affine systems with drift, one can always write them as a driftless control-affine system by treating $\boldsymbol{f}(\boldsymbol{x})$ as an input vector field for which the input is always one. Using $\boldsymbol{g}_0(\boldsymbol{x}) = \boldsymbol{f}(\boldsymbol{x})$ and $u_0 = 1$, system (2.2) can be written as [Sastry, 1999]

$$\dot{\boldsymbol{x}} = \sum_{j=0}^{m} \boldsymbol{g}_j(\boldsymbol{x}) u_j \tag{2.11}$$

So one can form the vector space $\bar{\Delta}$ using (2.10) where $\boldsymbol{X}_i \in \{\boldsymbol{f}, \boldsymbol{g}_1, \ldots, \boldsymbol{g}_m\}$, $i \in \{1, \ldots, k\}$, $k = 1, 2, \ldots$, and check the dimension of $\bar{\Delta}$. However, though in the driftless system (2.9) the system can be steered in both positive and negative directions of the input vector $\boldsymbol{g}_j$, $j \in \{1, \ldots, m\}$, by switching the sign of its corresponding input u_j, this is not the case in system (2.11). Since u_0 is constant, system (2.11) can only be steered in one direction along the input vector field $\boldsymbol{g}_0$. However by making switchings only in $\boldsymbol{u}$ the evolution of $\boldsymbol{x}$ still can be steered in directions involving the brackets of $\boldsymbol{g}_0 = \boldsymbol{f}$ and $\boldsymbol{g}_j$, $j \in \{1, \ldots, m\}$. Although generally we can now only steer along the positive or negative directions of these brackets. This causes the rank condition only to predict *accessibility* of the control-affine systems with drift. System (2.2) is accessible from a point $\boldsymbol{x}$ if there exist admissible inputs u_j, $j \in \{1, \ldots, m\}$, for the system to be steered to a non-empty neighborhood of $\boldsymbol{x}$. For driftless control-affine systems, accessibility and controllability are equivalent. But for control-affine system (2.2) with drift, if $\dim\bar{\Delta} = n$ at a point $\boldsymbol{x}$, then the system is accessible at that point, i.e., the system may only be steered to parts of the neighborhood of $\boldsymbol{x}$ (accessible region). If point $\boldsymbol{x}$ is an interior point of the accessible region then the system is controllable at $\boldsymbol{x}$ (see Figure 2.1). However, checking this criterion to determine the controllability of control-affine systems with drift, and nonlinear systems in general, is still a challenging problem. For a few theorems on determining the accessibility or controllability of special classes of fully actuated or underactuated control-affine systems see [Nijmeijer and van der Schaft, 1990; Lewis and Murray, 1997; Manikonda and Krishnaprasad, 2002; Cortes and Martinez, 2003; Bullo and Lewis, 2005].

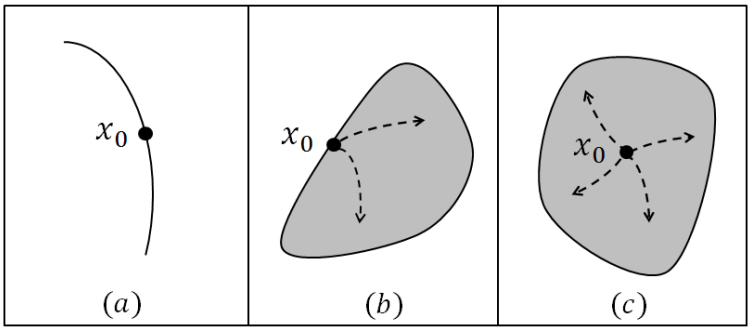

Figure 2.1: a) Lack of accessibility, b) accessibility but not local controllability, c) local controllability, at a point x_0 (shaded regions are accessible). Adapted from [Bullo and Lewis, 2005, Ch. 7]

2.3 The Symmetric Product

The *Symmetric product* is an important element for determining the controllability or accessibility and averaged dynamics of mechanical control-affine systems with high-frequency, high-amplitude inputs. The definition of the symmetric product is presented in [Crouch, 1981; Bullo and Lewis, 2005, Ch. 3]. For notational simplicity, the notion of symmetric product used here is slightly different from that used by Bullo [2002] and Bullo and Lewis [2005, Ch. 3].

Consider mechanical control-affine system (2.5) and the $2n$-dimensional drift vector field $\boldsymbol{Z}(\boldsymbol{x})$ and input vector fields $\boldsymbol{Y}_i(\boldsymbol{x})$ and $\boldsymbol{Y}_j(\boldsymbol{x})$. In [Bullo, 2002] the symmetric product of two input vector fields, denoted as $\langle \boldsymbol{Y}_i : \boldsymbol{Y}_j \rangle$, is defined as the last n components of the vector field

$$\langle \boldsymbol{Y}_i : \boldsymbol{Y}_j \rangle^{\text{lift}}(\boldsymbol{x}) = [\boldsymbol{Y}_j(\boldsymbol{x}), [\boldsymbol{Z}(\boldsymbol{x}), \boldsymbol{Y}_i(\boldsymbol{x})]] \tag{2.12}$$

where $[\cdot, \cdot]$ represents the Lie bracket of vector fields. The superscript "lift" indicates the

correspondence between the $2n$-dimensional vector field on the right and the n-dimensional vector field $\langle \boldsymbol{Y}_i : \boldsymbol{Y}_j \rangle$ defined by the last n rows of $\langle \cdot : \cdot \rangle^{\text{lift}}$. As the name of the symmetric product indicates, $\langle \boldsymbol{Y}_i : \boldsymbol{Y}_j \rangle^{\text{lift}}(\boldsymbol{x}) = \langle \boldsymbol{Y}_j : \boldsymbol{Y}_i \rangle^{\text{lift}}(\boldsymbol{x})$.

In this dissertation we consider a broad class of mechanical control-affine systems (2.3) where the vector field $\boldsymbol{f}(\boldsymbol{q}, \dot{\boldsymbol{q}})$ contains homogeneous polynomials in $\dot{\boldsymbol{q}}$ of degree two and/or less. For this class of mechanical control systems, the first n components of the $2n$-dimensional vector field $\langle \boldsymbol{Y}_i : \boldsymbol{Y}_j \rangle^{\text{lift}}(\boldsymbol{x})$ defined in (2.12) are zero [Bullo, 2002].

Using this observation, we introduce a slight abuse of established vocabulary and define the $2n$-dimensional vector field in (2.12) as the symmetric product between input vector fields, i.e.,

$$\langle \boldsymbol{Y}_i : \boldsymbol{Y}_j \rangle(\boldsymbol{x}) = \langle \boldsymbol{Y}_j : \boldsymbol{Y}_i \rangle(\boldsymbol{x}) = [\boldsymbol{Y}_j(\boldsymbol{x}), [\boldsymbol{Z}(\boldsymbol{x}), \boldsymbol{Y}_i(\boldsymbol{x})]] \tag{2.13}$$

2.4 Averaging Theorem

The idea of averaging is to approximate a time-periodic dynamical system by a time-invariant one. The averaging method was first used in problems of celestial mechanics in the 19^{th} century. But its first use in oscillatory dynamical systems appeared in the 1920's by van der Pol's well known works. Its wide use in perturbation studies of nonlinear systems started after major works of Bogoliubov and Mitropolsky [Bogoliubov and Mitropolsky, 1961]. For the history of development and discussion of the averaging techniques see [Mitropolsky, 1967] and references therein.

Consider a time-varying dynamical system

$$\dot{\boldsymbol{x}} = \epsilon \boldsymbol{f}(\boldsymbol{x}, t), \quad \boldsymbol{x}(0) = \boldsymbol{x}_0 \tag{2.14}$$

where $0 < \epsilon \ll 1$ and the vector field $\boldsymbol{f}(\boldsymbol{x}, t)$ is continuously differentiable in its first argument and T-periodic in its second argument. The averaged dynamics of system (2.14) is defined as [Guckenheimer and Holmes, 1983; Sanders and Verhulst, 1985]

$$\dot{\bar{\boldsymbol{x}}} = \epsilon \bar{\boldsymbol{f}}(\bar{\boldsymbol{x}}), \quad \bar{\boldsymbol{x}}(0) = \boldsymbol{x}_0 \tag{2.15}$$

where

$$\bar{\boldsymbol{f}}(\boldsymbol{x}) = \frac{1}{T} \int_0^T \boldsymbol{f}(\boldsymbol{x}, t) dt \tag{2.16}$$

Theorem 2.4.1 *(First order averaging theorem [Bullo, 2002]): Consider the time-periodic system* (2.14) *and its averaged approximation* (2.15)*. There exists a positive* ϵ_0 *such that for all* $0 < \epsilon \leq \epsilon_0$*,*

1. $\|\boldsymbol{x}(t) - \bar{\boldsymbol{x}}(t)\| = O(\epsilon)$ *as* $\epsilon \to 0$ *on the time scale* $\frac{1}{\epsilon}$*, and*

2. *if the origin is a hyperbolically stable critical point for* $\bar{\boldsymbol{f}}$*, then* $\|\boldsymbol{x}(t) - \bar{\boldsymbol{x}}(t)\| = O(\epsilon)$ *as* $\epsilon \to 0$ *for all* $t \in \mathbb{R}^+$*, and the differential equation* (2.14) *possesses a unique periodic orbit which is hyperbolically stable and belongs to an* $O(\epsilon)$ *neighborhood of the origin.*

Theorem 2.4.1 can also be used for system

$$\dot{\boldsymbol{x}} = \boldsymbol{f}(\boldsymbol{x}, t/\epsilon)$$

which using a change of variable $\tau = \frac{t}{\epsilon}$ can be transformed into (2.14) [Bullo, 2002].

Finding the maximum value of ϵ_0 for a system for which Theorem 2.4.1 is still valid is not easy, and often experimental and numerical results may be used [Bellman et al., 1985]. Meerkov [1973] has proposed an analytic method to determine the maximum acceptable range of ϵ_0 which results in a conservative value.

The last result of Theorem 2.4.1 is useful when studying the dynamics and stability of periodic orbits of nonlinear time-periodic (NLTP) systems. Though determining the stability of periodic orbits is usually a hard task, checking the stability of an equilibrium point of a nonlinear time-invariant (NLTI) system is mush easier. For the latter, one may use Lyapunov's indirect method, and the center manifold theorem in special cases [Khalil, 1996]. In Lyapunov's indirect method, the NLTI system is linearized about its equilibrium point to obtain a linear time-invariant (LTI) system. According to Lyapunov's indirect method, stability of the LTI system implies stability of the equilibrium point of the NLTI system, which according to the averaging theorem implies stability of the periodic orbit of the NLTP system corresponding to that equilibrium point.

In another approach for stability analysis of periodic orbits of a NLTP system, the system is linearized about its periodic orbit to obtain a linear time-periodic (LTP) system. Using

the averaging theorem, the resulted LTP system is averaged to get its corresponding LTI system. The stability of the resulting LTI system implies stability of the periodic orbit of the NLTP system. Comparison of the two mentioned methods is presented in Section 3.2. Floquet theory [Hartman, 1964] is also an available tool for stability analysis of time-periodic systems.

2.5 Higher-Order Averaging

Since the averaged system (2.15) is an $O(\epsilon)$ approximation of the time-periodic system (2.14), the averaging method mentioned in Section 2.4 is called first-order averaging. To determine more precise time-invariant approximations, higher order averaging methods have been developed which are discussed in [Bogoliubov and Mitropolsky, 1961; Sanders and Verhulst, 1985]. Later, using Floquet theory [Hartman, 1964] and the notion of Lie brackets, Sarychev [2001b,a] and Vela [2003]; Vela and Burdick [2003a] developed a general averaging algorithm for determining higher order averaging approximations. The averaged approximation of (2.14) can be shown as a power series expansion in the form of

$$\dot{\bar{\boldsymbol{x}}} = \sum_{n=1}^{\infty} \epsilon^n \boldsymbol{\Lambda}^{(n)} \tag{2.17}$$

where the vector fields $\mathbf{\Lambda}^{(i)}$ can be determined using Lie brackets. For example the cases $i \in \{1, 2, 3\}$ are

$$\mathbf{\Lambda}^{(1)} = \bar{\boldsymbol{f}}$$
$$\mathbf{\Lambda}^{(2)} = \tfrac{1}{2}\overline{\left[\int_0^t \boldsymbol{f}_\tau d\tau, \boldsymbol{f}_t\right]}$$
$$\mathbf{\Lambda}^{(3)} = -\tfrac{1}{2}T\left[\mathbf{\Lambda}^{(1)}, \mathbf{\Lambda}^{(2)}\right] + \tfrac{1}{3}\overline{\left[\int_0^t \boldsymbol{f}_\tau d\tau, \left[\int_0^t \boldsymbol{f}_\tau d\tau, \boldsymbol{f}_t\right]\right]}$$

where $\boldsymbol{f}_t = \boldsymbol{f}(\boldsymbol{x}, t)$, $[\cdot, \cdot]$ is the Lie bracket of vector fields, and the overbar denotes averaging using (2.16). Using this series expansion, the third order averaging approximation ($O(\epsilon^3)$) of the system (2.14), for example, is

$$\dot{\bar{\boldsymbol{x}}} = \epsilon\bar{\boldsymbol{f}} + \frac{1}{2}\epsilon^2\overline{\left[\int_0^t \boldsymbol{f}_\tau d\tau, \boldsymbol{f}_t\right]} - \frac{1}{4}T\epsilon^3\left[\bar{\boldsymbol{f}}, \overline{\left[\int_0^t \boldsymbol{f}_\tau d\tau, \boldsymbol{f}_t\right]}\right] + \frac{1}{3}\epsilon^3\overline{\left[\int_0^t \boldsymbol{f}_\tau d\tau, \left[\int_0^t \boldsymbol{f}_\tau d\tau, \boldsymbol{f}_t\right]\right]}$$

As is evident, using higher-order averaging is not very promising, since the terms to be determined become very complicated.

2.6 Summary

In this chapter the mathematical preliminaries used in this dissertation were presented. The control systems in general, and mechanical control-affine systems in particular, were introduced. The ideas of controllability and accessibility of mechanical control-affine systems were discussed in brief, and the concept of symmetric product were presented. The averaging

theorem and higher order averaging techniques for time-periodic dynamical systems were presented in detail. For additional background and more details concerning the concepts presented here, the reader is referred to the literature cited in the preceding discussion.

Chapter 3

Some Properties of the Averaged Dynamics

The comparison of two of the existing methods for stability analysis of periodic orbits of nonlinear time-periodic (NLTP) systems is presented. It is shown that the methods result in two different linear time-invariant (LTI) systems. Averaging of a class of mechanical control-affine systems with high-frequency, high-amplitude inputs is discussed. Using the concept of symmetric product, the averaged dynamics of this class of systems can be shown in a closed form. The effects of relative phase shifting of the high-frequency inputs on the averaged dynamics of a mechanical control-affine system are also analyzed.

3.1 Introduction

Averaging provides useful tool for stability analysis of the periodic orbits of time-periodic systems. According to the averaging theorem, the averaged dynamics of a time-periodic system has an equilibrium point corresponding to each periodic orbit of the time-periodic system (if there are any). Moreover, if the averaged dynamics possesses a hyperbolic equilibrium point, the time-periodic system possesses a hyperbolic periodic orbit corresponding to that equilibrium point. Therefore by averaging a time-periodic system and linearizing its averaged dynamics about one of its equilibrium points, one obtains a LTI system with the same stability characteristics as the periodic orbit of the time-periodic system corresponding to that equilibrium point. On the other hand, one may first linearize the time-periodic system about its periodic orbit and then determine the averaged dynamics of the resulting linear time-periodic (LTP) system. The result once again is a LTI system. In this dissertation it is shown that the LTI systems determined by two methods are not identical.

Averaging techniques can be used for the analysis of the dynamics of mechanical control systems which use high-frequency periodic inputs for control. High-frequency inputs are able to influence the stability properties of a dynamical system. The simplest example is Kapitza's pendulum, an inverted pendulum which uses high-frequency vertical oscillations for stabilization of its unstable equilibrium point (i.e., upward position). In this dissertation we are mostly interested in mechanical control-affine systems with high-frequency, high-amplitude inputs. In the usual perturbed systems, noises, disturbances, and other inputs are

considered as perturbations to the dominant dynamics of the system. But in control systems with high-frequency, high-amplitude inputs, the main dynamics of the system without control are instead a perturbation to the dominant high-amplitude inputs [Bullo, 2002]. Examples include biolocomotion or biomimetic systems such as flying insects, fish, flapping wing micro-air vehicles, and robotic fish.

For a mechanical control-affine system with high-frequency, high-amplitude, zero-mean, periodic inputs, averaging techniques can be used to determine its approximate time-invariant (averaged) dynamics. For a broad class of such systems, using the averaging theorem and the variation of constants formula, a closed form averaged dynamics is determined by Bullo [2002]; Bullo and Lewis [2005], which we present in this chapter in detail. Also we investigate the effects of relative phase shifting of the inputs. One interesting observation is if all the inputs are being shifted by the same amount, the effect on the averaged dynamics appears as a change of initial conditions only. But if the inputs are being shifted by different amounts (i.e., if the input phases are shifted relative to one another), the averaged dynamic equations and the stability properties of the averaged dynamics may also change.

In this chapter the commutativity of averaging and linearization is discussed in Section 3.2. After discussing the averaging of mechanical control-affine system with high-frequency, high-amplitude inputs in Section 3.3, the effects of the relative phase shifting of the inputs on the averaged dynamics of such systems are presented in Section 3.4.

3.2 On the Commutativity of Linearization and Averaging

Consider time-varying system

$$\dot{\boldsymbol{x}} = \epsilon \boldsymbol{f}(\boldsymbol{x}, t), \quad \boldsymbol{x}(0) = \boldsymbol{x}_0 \tag{3.1}$$

where $\boldsymbol{f}$ is T-periodic in its second argument, and its averaged dynamics

$$\dot{\bar{\boldsymbol{x}}} = \epsilon \bar{\boldsymbol{f}}(\bar{\boldsymbol{x}}), \quad \bar{\boldsymbol{x}}(0) = \boldsymbol{x}_0 \tag{3.2}$$

where

$$\bar{\boldsymbol{f}}(\boldsymbol{x}) = \frac{1}{T} \int_0^T \boldsymbol{f}(\boldsymbol{x}, t) dt \tag{3.3}$$

Suppose that system (3.2) possesses an equilibrium point $\boldsymbol{x}_{\mathrm{e}}$. Linearizing system (3.2) about this equilibrium point results in the LTI system

$$\dot{\boldsymbol{\delta}\bar{\boldsymbol{x}}} = \epsilon \bar{\boldsymbol{A}} \boldsymbol{\delta}\bar{\boldsymbol{x}} \tag{3.4}$$

where

$$\bar{\boldsymbol{A}} = \frac{\partial \bar{\boldsymbol{f}}(\boldsymbol{x})}{\partial \boldsymbol{x}}\Big|_{\boldsymbol{x}=\boldsymbol{x}_{\mathrm{e}}} \tag{3.5}$$

is the constant state matrix. According to Theorem 2.4.1, if $\boldsymbol{x}_{\mathrm{e}}$ is a hyperbolic equilibrium point of (3.2), then there exists $\epsilon_0 > 0$ such that for all $0 < \epsilon \leq \epsilon_0$, the system (3.1) possesses a unique hyperbolic periodic orbit $\boldsymbol{x}_{\mathrm{p}}(t) = \boldsymbol{x}_{\mathrm{p}}(t+T) = \boldsymbol{x}_{\mathrm{e}} + O(\epsilon)$ of the same stability properties as $\boldsymbol{x}_{\mathrm{e}}$.

On the other hand, linearizing system (3.1) about its periodic orbit $\boldsymbol{x}_{\mathrm{p}}(t)$ results in LTP system

$$\dot{\boldsymbol{\delta y}} = \epsilon \boldsymbol{B}(t) \boldsymbol{\delta y} \tag{3.6}$$

where

$$\boldsymbol{B}(t) = \frac{\partial \boldsymbol{f}(\boldsymbol{y}, t)}{\partial \boldsymbol{y}}\Big|_{\boldsymbol{y}=\boldsymbol{x}_{\mathrm{p}}(t)}.$$

Since $\boldsymbol{f}(\boldsymbol{x}, t)$ is T-periodic in its second argument, $\boldsymbol{B}(t)$ is also T-periodic. The first order averaged form of equation (3.6) is

$$\dot{\bar{\boldsymbol{\delta y}}} = \epsilon \bar{\boldsymbol{B}} \bar{\boldsymbol{\delta y}} \tag{3.7}$$

where

$$\bar{\boldsymbol{B}} = \frac{1}{T} \int_0^T \boldsymbol{B}(t) dt. \tag{3.8}$$

In summary one may average the NLTP system (3.1) and then linearize about the equilibrium point $\boldsymbol{x}_{\mathrm{e}}$ to obtain the LTI system (3.4). Or one may linearize the NLTP system (3.1) around the periodic orbit $\boldsymbol{x}_{\mathrm{p}}(t)$ and then average to obtain the LTI system (3.7). However, the LTI systems (3.4) and (3.7) that result from these two approximation sequences are not identical, as depicted in Figure 3.1. To appreciate the disparity between the systems (3.4) and (3.7), we

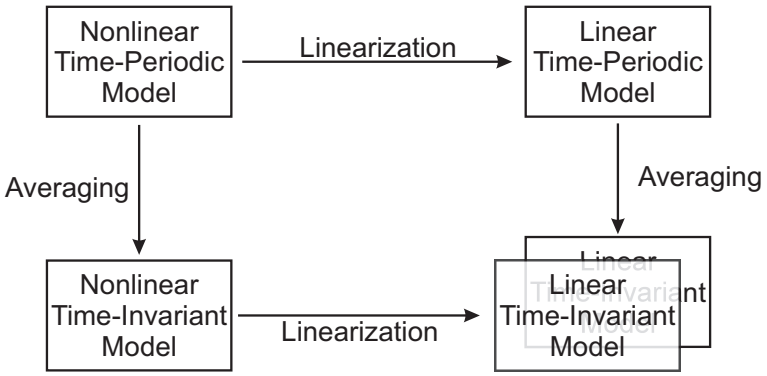

Figure 3.1: Averaging and Linearization

consider the error that accrues during the first-order averaging and linearization. Using the Taylor series expansion of $\boldsymbol{f}(\boldsymbol{x},t)$ around $\boldsymbol{x}_{\mathrm{e}}$, and assuming that $\|\boldsymbol{x}(t)-\boldsymbol{x}_{\mathrm{e}}\|$ is sufficiently small, one finds that [Taha et al., 2015]

$$\begin{aligned}
\bar{\boldsymbol{B}} &= \frac{1}{T}\int_0^T \boldsymbol{B}(t)dt = \frac{1}{T}\int_0^T \frac{\partial \boldsymbol{f}(\boldsymbol{x},t)}{\partial \boldsymbol{x}}\Big|_{\boldsymbol{x}=\boldsymbol{x}_{\mathrm{p}(t)}} dt \\
&= \frac{1}{T}\int_0^T \frac{\partial \boldsymbol{f}(\boldsymbol{x},t)}{\partial \boldsymbol{x}}\Big|_{\boldsymbol{x}=\boldsymbol{x}_{\mathrm{e}}+O(\epsilon)} dt \\
&= \frac{1}{T}\int_0^T \left(\frac{\partial \boldsymbol{f}(\boldsymbol{x},t)}{\partial \boldsymbol{x}}\Big|_{\boldsymbol{x}=\boldsymbol{x}_{\mathrm{e}}} + O(\epsilon)\right) dt \\
&= \frac{1}{T}\int_0^T \frac{\partial \boldsymbol{f}(\boldsymbol{x},t)}{\partial \boldsymbol{x}}\Big|_{\boldsymbol{x}=\boldsymbol{x}_{\mathrm{e}}} dt + O(\epsilon) \\
&= \left[\frac{\partial}{\partial \boldsymbol{x}}\left(\frac{1}{T}\int_0^T \boldsymbol{f}(\boldsymbol{x},t)dt\right)\right]_{\boldsymbol{x}=\boldsymbol{x}_{\mathrm{e}}} + O(\epsilon) \\
&= \frac{\partial \bar{\boldsymbol{f}}(\boldsymbol{x})}{\partial \boldsymbol{x}}\Big|_{\boldsymbol{x}=\boldsymbol{x}_{\mathrm{e}}} + O(\epsilon) \\
&= \bar{\boldsymbol{A}} + O(\epsilon)
\end{aligned} \tag{3.9}$$

Thus, if $\boldsymbol{\delta}\bar{\boldsymbol{x}}(t)$ and $\boldsymbol{\delta}\bar{\boldsymbol{y}}(t)$ are solutions of (3.4) and (3.7) starting from initial conditions $\boldsymbol{\delta}\bar{\boldsymbol{x}}_0$ and $\boldsymbol{\delta}\bar{\boldsymbol{y}}_0$ respectively with $\|\boldsymbol{\delta}\bar{\boldsymbol{x}}_0-\boldsymbol{\delta}\bar{\boldsymbol{y}}_0\| = O(\epsilon)$, then $\|\boldsymbol{\delta}\bar{\boldsymbol{x}}(t)-\boldsymbol{\delta}\bar{\boldsymbol{y}}(t)\| = O(\epsilon)$ on a time scale

$\frac{1}{\epsilon}$. Moreover if the hyperbolic equilibrium point $\boldsymbol{x}_{\mathrm{e}}$ of (3.2), and therefore the hyperbolic periodic orbit $\boldsymbol{x}_{\mathrm{p}}(t)$ of (3.1), is stable, then the LTI systems (3.4) and (3.7) are stable and $\|\boldsymbol{\delta\bar{x}}(t) - \boldsymbol{\delta\bar{y}}(t)\| = O(\epsilon)$ for $t \in [0, \infty)$. Note that if instead of a periodic orbit the NLPT system (3.1) possesses an equilibrium point, the processes of linearizing and averaging do indeed commute so that the resulting approximations (3.4) and (3.7) are equivalent.

3.3 Averaging of High-Frequency Mechanical Control Systems

As discussed in Section 2.1, the general form of an n-DOF mechanical control-affine system with m ($m \leq n$) independent inputs is in the from of

$$\ddot{\boldsymbol{q}} = \boldsymbol{f}(\boldsymbol{q}, \dot{\boldsymbol{q}}) + \sum_{i=1}^{m} \boldsymbol{g}_i(\boldsymbol{q}) u_i(t), \quad \boldsymbol{q}(0) = \boldsymbol{q}_0,\ \dot{\boldsymbol{q}}(0) = \boldsymbol{v}_0 \tag{3.10}$$

where $\boldsymbol{q} = (q_1\ \ldots\ q_n)^T$ is the vector of generalized coordinates, $\boldsymbol{f}$ and $\boldsymbol{g}_i$, $i \in \{1, \ldots, m\}$, are drift and input vector fields respectively, and $u_i(t)$, $i \in \{1, \ldots, m\}$, are the inputs. Suppose that $\boldsymbol{f}$ and $\boldsymbol{g}_i$ contain twice differentiable polynomials in $\boldsymbol{q}$, and the polynomials in $\boldsymbol{f}$ are homogeneous in $\dot{\boldsymbol{q}}$ of degree two and/or less. Also suppose that $u_i(t)$, $i \in \{1, \ldots, m\}$, are high-frequency, high-amplitude inputs in the form of

$$u_i(t) = \omega v_i(\omega t) \tag{3.11}$$

where ω is the (high) frequency and $v_i(t)$, $i \in \{1, \ldots, m\}$, are zero-mean, T-periodic functions.

Defining the state vector $\boldsymbol{x} = (\boldsymbol{q}^T,\ \dot{\boldsymbol{q}}^T)^T$ and using inputs defined in (3.11), system (3.10) can be written in the first order form of

$$\dot{\boldsymbol{x}} = \boldsymbol{Z}(\boldsymbol{x}) + \sum_{i=1}^{m} \boldsymbol{Y}_i(\boldsymbol{x}) \left(\frac{1}{\epsilon}\right) v_i \left(\frac{t}{\epsilon}\right), \quad \boldsymbol{x}(0) = \boldsymbol{x}_0 = (\boldsymbol{q}_0^T,\ \boldsymbol{v}_0^T)^T \tag{3.12}$$

where $\boldsymbol{Z}(\boldsymbol{x}) = (\dot{\boldsymbol{q}}^T,\ \boldsymbol{f}^T(\boldsymbol{q}, \dot{\boldsymbol{q}}))^T$, $\boldsymbol{Y}_i(\boldsymbol{x}) = (\boldsymbol{0}_{1\times n},\ \boldsymbol{g}_i^T(\boldsymbol{q}))^T$, and $\epsilon = \frac{1}{\omega}$ is a small positive number (since ω is big).

For the inputs considered as (3.11) and following [Bullo and Lewis, 2005], define scalars κ_i, λ_{ij}, and μ_{ij}, $i, j \in \{1, \ldots, m\}$, as

$$\kappa_i = \frac{1}{T} \int_0^T \int_0^t v_i(\tau) d\tau dt \tag{3.13}$$

$$\lambda_{ij} = \frac{1}{T} \int_0^T \left(\int_0^t v_i(\tau) d\tau \right) \left(\int_0^t v_j(\tau) d\tau \right) dt \tag{3.14}$$

and

$$\mu_{ij} = \frac{1}{2}(\lambda_{ij} - \kappa_i \kappa_j). \tag{3.15}$$

Also, as mentioned in Section 2.3, for any two input vector fields $\boldsymbol{Y}_i(\boldsymbol{x})$ and $\boldsymbol{Y}_j(\boldsymbol{x})$, $i, j \in \{1, \ldots, m\}$, in (3.12), we define the symmetric product between them as

$$\langle \boldsymbol{Y}_i : \boldsymbol{Y}_j \rangle(\boldsymbol{x}) = [\boldsymbol{Y}_j(\boldsymbol{x}), [\boldsymbol{Z}(\boldsymbol{x}), \boldsymbol{Y}_i(\boldsymbol{x})]] \tag{3.16}$$

where $[\cdot,\cdot]$ denotes the Lie bracket of vector fields as defined in (2.8).

Using the general averaging theorem, variation of constants formula [Bullo, 2002], and specific properties of time-dependent vector fields, Bullo and Lewis [2005, Ch. 9] determined the averaged dynamics of (3.12) as follows.

Theorem 3.3.1 *(Adapted from [Bullo and Lewis, 2005, Ch. 9]): Consider system* (3.12) *with the initial conditions of* $\boldsymbol{x}(0) = \boldsymbol{x}_0$ *where the inputs* $v_i(t)$, $i \in \{1, \ldots, m\}$, *are zero-mean,* T*-periodic functions. Also consider*

$$\dot{\bar{\boldsymbol{x}}} = \boldsymbol{Z}(\bar{\boldsymbol{x}}) - \sum_{i,j=1}^{m} \mu_{ij} \langle \boldsymbol{Y}_i : \boldsymbol{Y}_j \rangle (\bar{\boldsymbol{x}}) \tag{3.17}$$

with the initial conditions of $\bar{\boldsymbol{x}}(0) = \bar{\boldsymbol{x}}_0 = \boldsymbol{x}_0 + \sum_{i=1}^{m} \kappa_i \boldsymbol{Y}_i(\boldsymbol{x}_0)$, *where* $\bar{\boldsymbol{x}} = (\bar{\boldsymbol{q}}^T,\ \dot{\bar{\boldsymbol{q}}}^T)^T$ *is the state vector.*

Then there exists a positive ϵ_0 *such that for all* $0 < \epsilon \leq \epsilon_0$, $\boldsymbol{q}(t) = \bar{\boldsymbol{q}}(t) + O(\epsilon)$ *as* $\epsilon \to 0$ *on the time scale 1. Furthermore if the system* (3.17) *possesses a hyperbolically stable equilibrium point* $\bar{\boldsymbol{x}}_{\mathrm{e}}$, *then the system* (3.12) *possesses a unique, hyperbolically stable periodic orbit within an* $O(\epsilon)$ *neighborhood of the equilibrium point* $\bar{\boldsymbol{x}}_{\mathrm{e}}$, *and the approximation* $\boldsymbol{q}(t) = \bar{\boldsymbol{q}}(t) + O(\epsilon)$ *is valid for all time* $t \geq 0$.

We call system (3.17) the averaged form or the averaged dynamics of time-periodic system (3.12).

Remark 3.3.2 *: Note that since the first* n *components of the input vector fields* $\boldsymbol{Y}_i(\boldsymbol{x})$,

$i \in \{1, \ldots, m\}$, are zero, the initial conditions of the averaged dynamics (3.17) *may also be written as* $\bar{\boldsymbol{q}}(0) = \boldsymbol{q}_0$ *and* $\dot{\bar{\boldsymbol{q}}}(0) = \boldsymbol{v}_0 + \sum_{i=1}^{m} \kappa_i \boldsymbol{g}_i(\boldsymbol{q}_0)$*. Note that, while the initial configuration is identical for the time-varying and averaged systems, the initial velocity is not.*

Theorem 3.3.1 can be expressed in more general form for the first order, multiple-time-scale system

$$\frac{d\boldsymbol{x}}{dt} = \boldsymbol{Z}(\boldsymbol{x}, t) + \sum_{i=1}^{m} \boldsymbol{Y}_i(\boldsymbol{x}, t) \left(\frac{1}{\epsilon}\right) v_i(t, \tau) \tag{3.18}$$

where $\tau = \frac{t}{\epsilon}$ and t are the *fast* and *slow time-scales*, respectively. Assuming these time scales are sufficiently well separated, averaging can be done over the fast time-scale τ, and the averaged dynamics can be written as [Bullo and Lewis, 2005, Ch. 9]

$$\frac{d\bar{\boldsymbol{x}}}{dt} = \boldsymbol{Z}(\bar{\boldsymbol{x}}, t) - \sum_{i,j=1}^{m} \mu_{ij}(t) \langle \boldsymbol{Y}_i : \boldsymbol{Y}_j \rangle(\bar{\boldsymbol{x}}, t) \tag{3.19}$$

It is evident that the averaged system (3.19) is not time-invariant, but slowly varying. In averaging of the system (3.19) one assumes that the drift and input vector fields, which contain slowly varying functions of t, remain constant during the short time ϵT, which is the period of the fast-varying periodic functions $v_i(t, \tau)$. For more on multiple-time-scale methods and its applications see [Kokotovic et al., 1980; Saksena et al., 1984; Kokotovic, 1984] and the references therein.

3.4 Effects of the Inputs Relative Phase Shifting on the Averaged Dynamics

In this section the effects of the relative phase shifting of the inputs on mechanical control-affine systems with high-frequency, high-amplitude inputs are investigated.

Theorem 3.4.1 *: Consider the control-affine system* (3.12)*, and the system*

$$\dot{\boldsymbol{y}} = \boldsymbol{Z}(\boldsymbol{y}) + \sum_{i=1}^{m} \boldsymbol{Y}_i(\boldsymbol{y}) \left(\frac{1}{\epsilon}\right) w_i \left(\frac{t}{\epsilon}\right) \tag{3.20}$$

with the initial conditions of $\boldsymbol{y}(0) = \boldsymbol{x}_0$*, and where* $w_i(t) = v_i(t + \phi_0)$*,* $i \in \{1, \ldots, m\}$*, and* $0 \leq \phi_0 \leq T$*. For any* $0 \leq \phi_0 \leq T$*, systems* (3.12) *and* (3.20) *have identical averaged dynamics with different initial conditions (different initial velocities).*

Proof: See Appendix A.

Therefore by phase shifting of all the inputs by the same amount ϕ_0, the averaged dynamics of the system (3.12) does not change. But since in general $\kappa_i \neq \kappa_{s_i}$, the initial conditions of the two averaged dynamics may be different. The theorem does not hold if at least one of the inputs is shifted by a different phase amount. The latter case may even change the stability properties of the averaged and original dynamics. To make this clear we present the following example.

Example 1: Consider the following 2-DOF system with two high-frequency, high-amplitude inputs $u_i(t) = \omega v_i(\omega t)$, $i \in \{1, 2\}$,

$$\begin{cases} \ddot{q}_1 = \dot{q}_1^2 - \dot{q}_2^2 - \dot{q}_1 + q_1 - q_2 + 2q_2 u_1(t) \\ \ddot{q}_2 = \dot{q}_1^2 + \dot{q}_2^2 - 0.8\dot{q}_2 - 3q_1 + 3q_1 u_2(t) \end{cases} \tag{3.21}$$

Using the state vector $\boldsymbol{x} = (q_1,\ q_2,\ \dot{q}_1,\ \dot{q}_2)^T$, system (3.21) can be written as

$$\dot{\boldsymbol{x}} = \underbrace{\begin{pmatrix} x_3 \\ x_4 \\ x_3^2 - x_4^2 - x_3 + x_1 - x_2 \\ x_3^2 + x_4^2 - 0.8x_4 - 3x_1 \end{pmatrix}}_{\boldsymbol{Z}(\boldsymbol{x})} + \underbrace{\begin{pmatrix} 0 \\ 0 \\ 2x_2 \\ 0 \end{pmatrix}}_{\boldsymbol{Y_1}(\boldsymbol{x})} \omega v_1(\omega t) + \underbrace{\begin{pmatrix} 0 \\ 0 \\ 0 \\ 3x_1 \end{pmatrix}}_{\boldsymbol{Y_2}(\boldsymbol{x})} \omega v_2(\omega t) \tag{3.22}$$

Considering $v_1(t) = \cos t$ and $v_2(t) = \cos(t + \phi_0)$, one determines $\kappa_1 = 0$, $\kappa_2 = -\sin\phi_0$, $\lambda_{11} = \frac{1}{2}$, $\lambda_{22} = 1 - \frac{1}{2}\cos 2\phi_0$, and $\lambda_{12} = \lambda_{21} = \frac{1}{2}\cos\phi_0$, and so $\mu_{11} = \mu_{22} = \frac{1}{4}$, $\mu_{12} = \mu_{21} = \frac{1}{4}\cos\phi_0$. Using (3.16) and (3.17) the averaged dynamics of (3.22) can be determined as

$$\begin{cases} \dot{\bar{x}}_1 = \bar{x}_3 \\ \dot{\bar{x}}_2 = \bar{x}_4 \\ \dot{\bar{x}}_3 = \bar{x}_3^2 - \bar{x}_4^2 - \bar{x}_3 - 4.5\bar{x}_1^2 + 2\bar{x}_2^2 + (1 - 3\cos\phi_0)\bar{x}_1 - \bar{x}_2 \\ \dot{\bar{x}}_4 = \bar{x}_3^2 + \bar{x}_4^2 - 0.8\bar{x}_4 + 4.5\bar{x}_1^2 + 2\bar{x}_2^2 - 3\bar{x}_1 - 3\bar{x}_2\cos\phi_0 \end{cases} \tag{3.23}$$

where $\bar{\boldsymbol{x}} = (\bar{x}_1,\ \bar{x}_2,\ \bar{x}_3,\ \bar{x}_4)^T$ is the state vector of the averaged dynamics. The origin is an equilibrium point of both the original time-varying system (3.22) and its averaged dynamics (3.23). Linearizing the averaged dynamics about the origin, one gets the linear system

$$\boldsymbol{\delta}\dot{\bar{\boldsymbol{x}}} = \begin{pmatrix} 0 & 0 & 1 & 0 \\ 0 & 0 & 0 & 1 \\ 1 - 3\cos\phi_0 & -1 & -1 & 0 \\ -3 & -3\cos\phi_0 & 0 & -0.8 \end{pmatrix} \boldsymbol{\delta}\bar{\boldsymbol{x}} \tag{3.24}$$

where $\boldsymbol{\delta}\bar{\boldsymbol{x}}$ is the state vector of the linearized system. Using the eigenvalues of the state matrix of the linearized system (3.24) one finds that the linear system is unstable for $0.6957 < \phi_0 < 5.5875$, and stable otherwise (note that $0 \leq \phi_0 \leq 2\pi$). Therefore the origin is an unstable equilibrium point of the time-varying system (3.22) for $0.6957 < \phi_0 < 5.5875$, and a stable one otherwise.

A portrait of the root locus of the linearized system (3.24) for different values of ϕ_0, and the responses of the time-varying system and its averaged dynamics for $\phi_0 = 0$ and $\phi_0 = 0.733$ are presented in Figures 3.2 through 3.4. The initial conditions for the simulations are $\boldsymbol{x}(0) = (0.1, -0.1, 0, 0)^T$, and $\omega = 50$. Note that since the state matrix of the linear system varies in terms of $\cos\phi_0$, which is bounded, the branches of the root locus of the linear system shown in Figure 3.2 have finite lengths as shown, and none of them approaches infinity. Also note that since the origin is a stable equilibrium point for the system for $\phi_0 = 0$, according to Theorem 3.4.1 it still will be stable if both the inputs are shifted by the same amount of

$0 \leq \phi_0 \leq 2\pi$, i.e., $v_1(t) = v_2(t) = \cos(t + \phi_0)$. In such a case the averaged dynamics will be the same as (3.23) determined for $\phi_0 = 0$. In Figure 3.4, though the origin is an unstable equilibrium point, the new equilibrium points which emerge from the bifurcation are stable for $\phi_0 \leq 1.434$ and $\phi_0 \geq 4.849$. Therefore for $\phi_0 = 0.733$ the averaging is still valid for all time $t > 0$.

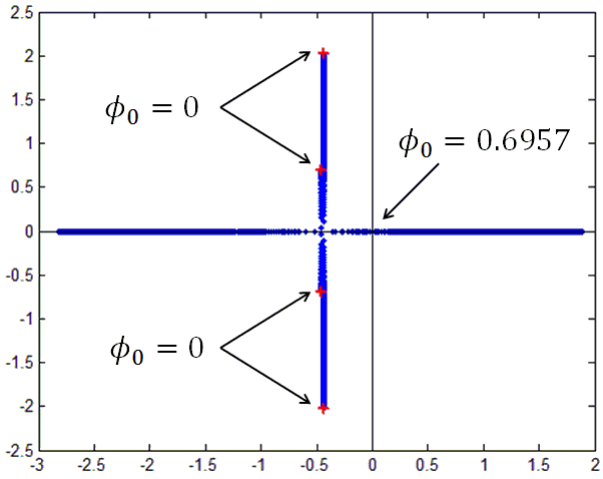

Figure 3.2: Portrait of root locus of the linearized system (3.24) for $0 \leq \phi_0 \leq \pi$

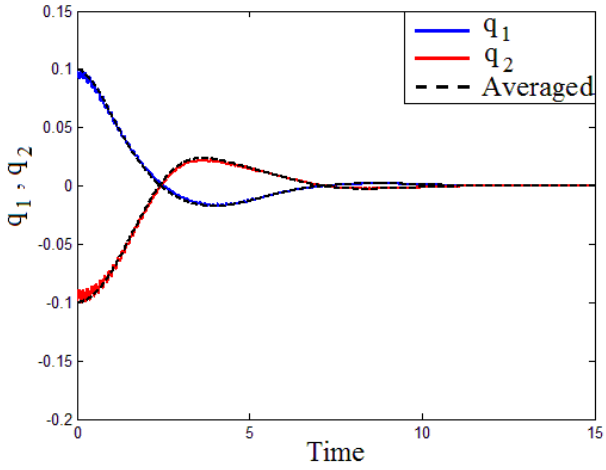

Figure 3.3: Time histories of the actual and averaged systems for $\phi_0 = 0$

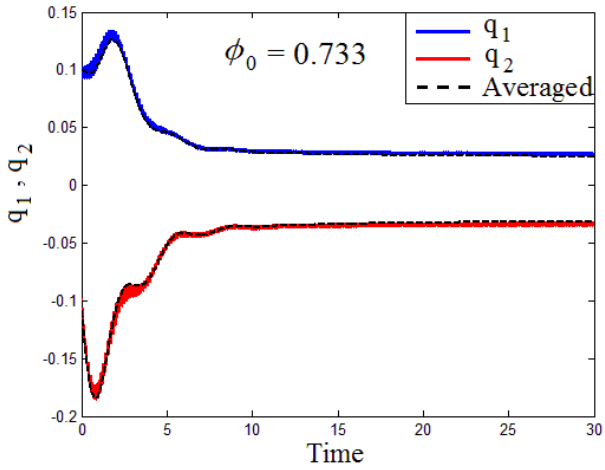

Figure 3.4: Time histories of the actual and averaged systems for $\phi_0 = 0.733$

3.5 Conclusions

In this chapter it was shown that when studying the stability of a time-periodic system using averaging, linearization, and the Floquet theorem, the order of averaging and linearization matters and they do not commute. After presenting the averaging of mechanical control-affine systems with high-frequency, high-amplitude inputs, the effects of the relative phase shifting of the inputs on mechanical control systems were investigated. It was shown that when shifting all the inputs by the same amount, the stability properties of the system do not change, and the effect is a change of initial condition and transient response of the system. But if the inputs are phase shifted by different amounts, the stability properties of the system may also change.

Chapter 4

Control of Underactuated Mechanical Systems Using High-Frequency Inputs

This chapter presents a control design technique which enables approximate reference trajectory tracking for a class of underactuated mechanical systems [Tahmasian and Woolsey, 2015a]. The control law comprises two terms. The first involves feedback of the trajectory tracking error in the actuated coordinates. Building on the concept of vibrational control, the second term imposes high-frequency periodic inputs that are modulated by the tracking error in the unactuated coordinates. Under appropriate conditions on the system structure and the commanded trajectory, and with sufficient separation between the time scales of the vibrational forcing and the commanded trajectory, the approach provides convergence in both the actuated and unactuated coordinates. The procedure is first described for a two degree-of-freedom system with one input. Generalizing to higher-dimensional, underactuated

systems, the approach is then applied to a four degree-of-freedom system with two inputs. A final example involves control of a rigid plate that is flapping in a uniform flow, a three degree-of-freedom system with one input. More general applications include biomimetic locomotion systems, such as underwater vehicles with articulating fins and flapping wing micro-air vehicles.

4.1 Introduction

Underactuated mechanical systems have fewer actuators than degrees of freedom. Examples arise in mobile robotics, for example, where size, weight, and power constraints may dictate the use of fewer components. Examples also arise in nature. Creatures such as flying insects, birds, and fish are able to move effectively and efficiently even though they are underactuated. Many of these systems are characterized by the use of oscillatory control to generate motion. This chapter describes a particular oscillatory control approach for a class of underactuated mechanical systems.

One reason that oscillatory control is prevalent is that underactuated mechanical systems often cannot be stabilized using smooth, static state feedback [Brockett, 1983]. This observation motivated the development of time-varying control synthesis methods, first for drift-free systems (i.e., systems that only move while control inputs are being applied) and later for systems with drift. Following early work on stabilization using high-frequency, high-amplitude inputs [Meerkov, 1980; Bellman et al., 1986a,b], a number of researchers have explored the

use of vibrational control for underactuated systems (see [Sastry, 1999, Ch. 11], [Bullo, 2002], and [Bullo and Lewis, 2005, Ch. 12]).

Averaging theory provides useful tools for analyzing vibrational control systems [Guckenheimer and Holmes, 1983; Sanders and Verhulst, 1985]. First order averaging, as considered in this dissertation, is effective when there is sufficient time-scale separation between oscillatory forcing and slower modes of motion, though some applications to biological or biomimetic locomotion have required higher order averaging [Morgansen et al., 2002; Vela and Burdick, 2003b; Vela, 2003; Sanyal et al., 2005].

This chapter presents an oscillatory control design approach which enables approximate reference trajectory tracking for a class of underactuated mechanical systems. The purpose of the controller is to follow slowly varying desired trajectories in both the actuated and unactuated degrees of freedom on average. The approach relies on the observation that, in underactuated systems with appropriate structure, the actuated coordinates together with the corresponding generalized velocities can be considered as generalized inputs for the unactuated coordinates [Weibel and Baillieul, 1998]. The control law comprises two terms. The first involves feedback of the trajectory tracking error in the actuated coordinates. Building on the concept of vibrational control, the second term imposes high-frequency periodic inputs that are modulated by the tracking error in the unactuated coordinates.

Having defined a controller structure, one must then determine suitable values for the control parameters. In doing so, one must ensure that the desired, slowly varying trajectories are *feasible* for the dynamics of the time-averaged, unactuated degrees of freedom. The result

is a set of conditions on both the system structure and the desired trajectory. Building on earlier results for oscillatory control ([Bullo, 2002; Martinez et al., 2003a], [Bullo and Lewis, 2005, Ch. 12]), a technique is proposed for designing nonlinear feedback, with high frequency periodic forcing, to control a class of underactuated mechanical systems with drift.

The chapter is organized as follows. The proposed control method is initially developed for 2-DOF, single-input mechanical systems in Section 4.2. The selection of control parameters is discussed in Section 4.3. In Section 4.4 the proposed control method is extended for control of higher dimensional, multi-input systems. Two examples are presented in Sections 4.5 and 4.6, respectively. The first example is a 4-DOF, 2-input system. The second is a 3-DOF, 1-input system that describes the motion of a rigid flapping plate in a uniform flow. Section 4.7 provides a brief summary and conclusions and suggests directions for continuing work.

4.2 The Control Method

Consider a 2-DOF mechanical system with one input. The actuated coordinate is denoted q_{a} and the unactuated coordinate is denoted q_{u}. Defining the configuration vector $\boldsymbol{q} = (q_{\mathrm{a}}, q_{\mathrm{u}})^T$, the equations of motion are

$$\boldsymbol{M}(\boldsymbol{q}) \begin{pmatrix} \ddot{q}_{\mathrm{a}} \\ \\ \ddot{q}_{\mathrm{u}} \end{pmatrix} = \begin{pmatrix} f_{\mathrm{a}}(\boldsymbol{q}, \dot{\boldsymbol{q}}) \\ \\ f_{\mathrm{u}}(\boldsymbol{q}, \dot{\boldsymbol{q}}) \end{pmatrix} + \begin{pmatrix} u \\ \\ 0 \end{pmatrix} \tag{4.1}$$

where $\boldsymbol{M}(\boldsymbol{q})$ is the positive definite generalized inertia matrix, u denotes the input and $f_{\mathrm{a}}(\boldsymbol{q}, \dot{\boldsymbol{q}})$ and $f_{\mathrm{u}}(\boldsymbol{q}, \dot{\boldsymbol{q}})$ are twice continuously differentiable functions comprising homogeneous polynomials in $\dot{\boldsymbol{q}}$ of degree two or less. These functions contain centripetal and Coriolis effects, damping and gravity forces as well as any non-conservative external forces that satisfy the assumed functional form. Since the matrix $\boldsymbol{M}$ is invertible, equation (4.1) can be written as

$$\ddot{\boldsymbol{q}} = \boldsymbol{M}^{-1}(\boldsymbol{q})\boldsymbol{f}(\boldsymbol{q}, \dot{\boldsymbol{q}}) + \boldsymbol{M}^{-1}(\boldsymbol{q})\boldsymbol{u}$$

where $\boldsymbol{u} = (u\ ,\ 0)^T$ and $\boldsymbol{f} = (f_{\mathrm{a}}\ ,\ f_{\mathrm{u}})^T$. More succinctly, one may write

$$\ddot{\boldsymbol{q}} = \boldsymbol{g}(\boldsymbol{q}, \dot{\boldsymbol{q}}) + \boldsymbol{h}(\boldsymbol{q})u \tag{4.2}$$

where $\boldsymbol{g} = \boldsymbol{M}^{-1}\boldsymbol{f}$ and $\boldsymbol{h}$ is the first column of $\boldsymbol{M}^{-1}$ as discussed in Section 2.1. Using the state vector $\boldsymbol{x} = (\boldsymbol{q}^T,\ \dot{\boldsymbol{q}}^T)^T$, the system (4.2) can be written in the first order form

$$\dot{\boldsymbol{x}} = \begin{pmatrix} \dot{\boldsymbol{q}} \\ \\ \boldsymbol{g}(\boldsymbol{q}, \dot{\boldsymbol{q}}) \end{pmatrix} + \begin{pmatrix} \boldsymbol{0}_{2\times 1} \\ \\ \boldsymbol{h}(\boldsymbol{q}) \end{pmatrix} u \tag{4.3}$$

The goal is to find an input u such that on average both coordinates q_{a} and q_{u} follow slowly varying desired trajectories $q_{\mathrm{ad}}(t)$ and $q_{\mathrm{ud}}(t)$ respectively. The phrase "on average" is made more precise when referring to the averaging theorem.

In vibrational control, the actuated coordinates and their corresponding generalized velocities can be considered as inputs to the unactuated dynamics. The proposed control law contains

high-frequency forcing of the actuated coordinates which can be adjusted to assure stability of the system. To ensure that both actuated and unactuated coordinates follow low-frequency desired trajectories on average, the input also contains state feedback terms. The main idea is a feedback control law comprising two components: one that provides proportional-derivative tracking in the actuated coordinate and a second that imposes high frequency oscillations, scaled by the tracking error in the unactuated coordinate. The resulting closed-loop system is in a form amenable to direct averaging.

Proposition 4.2.1 *Let* $e_{\mathrm{a}} = q_{\mathrm{ad}} - q_{\mathrm{a}}$ *and* $e_{\mathrm{u}} = q_{\mathrm{ud}} - q_{\mathrm{u}}$ *represent the trajectory following errors. Also let*

$$u(t) = [k_{\mathrm{p}} e_{\mathrm{a}}(t) + k_{\mathrm{d}} \dot{e}_{\mathrm{a}}(t)] + [(1 + k_{\mathrm{u}} e_{\mathrm{u}}(t))\, v(t)] \tag{4.4}$$

where k_{p}, k_{d} *and* k_{u} *are control parameters and where* $v(t) = v_0(t)\omega \cos \omega t$ *is a prescribed periodic input, with a high forcing frequency* ω *and a slowly varying large amplitude* $v_0(t)\omega$. *The input* (4.4) *transforms the system* (4.3) *into the form*

$$\dot{\boldsymbol{x}} = \boldsymbol{Z}(\boldsymbol{x}, t) + \boldsymbol{Y}(\boldsymbol{x}, t) \frac{1}{\epsilon} \cos\left(\frac{t}{\epsilon}\right) \tag{4.5}$$

where $\epsilon = \frac{1}{\omega}$,

$$\boldsymbol{Z}(\boldsymbol{x}, t) = \begin{pmatrix} \dot{\boldsymbol{q}} \\ \\ \boldsymbol{g}(\boldsymbol{q}, \dot{\boldsymbol{q}}) + \big(k_{\mathrm{p}} e_{\mathrm{a}} + k_{\mathrm{d}} \dot{e}_{\mathrm{a}}\big) \boldsymbol{h}(\boldsymbol{q}) \end{pmatrix} \tag{4.6}$$

and

$$\boldsymbol{Y}(\boldsymbol{x},t) = \begin{pmatrix} \mathbf{0}_{2\times 1} \\ v_0(t)\left(1 + k_{\mathrm{u}} e_{\mathrm{u}}\right)\boldsymbol{h}(\boldsymbol{q}) \end{pmatrix} \tag{4.7}$$

Proof: Substituting input (4.4) into equation (4.3) along with the explicit function $v(t)$ and regrouping, one obtains

$$\ddot{\boldsymbol{q}} = \boldsymbol{g}(\boldsymbol{q},\dot{\boldsymbol{q}}) + k_{\mathrm{p}} e_{\mathrm{a}} \boldsymbol{h}(\boldsymbol{q}) + k_{\mathrm{d}} \dot{e}_{\mathrm{a}} \boldsymbol{h}(\boldsymbol{q}) + v_0(t)\big(1 + k_{\mathrm{u}} e_{\mathrm{u}}\big)\boldsymbol{h}(\boldsymbol{q})\omega \cos \omega t \tag{4.8}$$

Defining $\epsilon = \frac{1}{\omega}$ and using the state vector $\boldsymbol{x}$, equation (4.8) can be rewritten in the concise first order form

$$\dot{\boldsymbol{x}} = \boldsymbol{Z}(\boldsymbol{x},t) + \boldsymbol{Y}(\boldsymbol{x},t)\frac{1}{\epsilon}\cos\left(\frac{t}{\epsilon}\right) \tag{4.9}$$

with $\boldsymbol{Z}$ and $\boldsymbol{Y}$ being defined as (4.6) and (4.7) respectively. □

Assuming that ω is large (ϵ is small) relative to the characteristic frequencies of the unforced system, equation (4.5) exhibits a fast and a slow time scale ($\frac{t}{\epsilon}$ and t, respectively). To find the averaged form of equation (4.5), we refer to Theorem 3.3.1 for averaging of affine connection systems subject to oscillatory controls, and its more general form of (3.19) for multiple time-scale systems [Bullo and Lewis, 2005, Ch. 9]. A key observation is that the controller structure proposed in (4.4) satisfies the conditions of Theorem 3.3.1.

Theorem 3.3.1 makes the phrase "on average" more precise. For example, assume that the averaged system (3.19) is time-invariant (i.e., there is no explicit time variation at the slow time scale) and suppose that $\epsilon \leq \epsilon_0$. If the initial state of (3.18) is within the region

of attraction of an exponentially stable equilibrium for the averaged system (3.19), then $\boldsymbol{q}(t) = \bar{\boldsymbol{q}}(t) + O(\epsilon)$ as $\epsilon \to 0$ for all $t \geq 0$.

Comparing equation (4.5) with the general form of (3.18), it can be seen that in this case $m = 1$ and $v_1(\tau) = \cos\tau$, and so $T = 2\pi$. Using equations (3.13) through (3.15) one can find $\kappa_1 = 0$ and $\mu_{11} = \lambda_{11} = \frac{1}{4}$. So the fast-time-averaged form of the system (4.5) is in the form

$$\dot{\bar{\boldsymbol{x}}} = \boldsymbol{Z}(\bar{\boldsymbol{x}}, t) - \frac{1}{4}\langle \boldsymbol{Y}(\bar{\boldsymbol{x}}, t) : \boldsymbol{Y}(\bar{\boldsymbol{x}}, t)\rangle \tag{4.10}$$

with the symmetric product defined as (3.16). In equation (4.10), the high-frequency input in (4.9) has been averaged out; the only remaining time-dependent terms are slowly varying terms due to $q_{\mathrm{ad}}(t)$ and $q_{\mathrm{ud}}(t)$. If these desired trajectories are constant, the averaged system (4.10) will be time-invariant.

Remark 4.2.2 *: Though we have used $v(t) = v_0(t)\omega\cos\omega t$ as the oscillatory part of the input* (4.4)*, in general one may use $v(t) = v_0(t)\omega w(\omega t)$ where $w(t)$ is a periodic, zero-mean function with unit amplitude, such as sine, square, or triangular functions.*

4.3 Selection of Control Parameters

Having found the averaged approximation of equation (4.5), one seeks control parameters k_{p}, k_{d} and k_{u}, and the time-varying amplitude of the high frequency input, $v_0(t)$, to ensure trajectory tracking by the system. The method suggested here is first to find the amplitude

$v_0(t)$ using the averaged equation of motion of the unactuated coordinate, and then to find the other three (constant) parameters k_p, k_d, and k_u to guarantee stability and desired performance of the system.

Since the system is supposed to follow the slowly varying desired trajectories $q_\mathrm{ad}(t)$ and $q_\mathrm{ud}(t)$ on average, basic feasibility requires that

$$\dot{\boldsymbol{x}}_\mathrm{d}(t) = \boldsymbol{Z}_g(\boldsymbol{x}_\mathrm{d}, t) - \frac{1}{4}\left\langle \boldsymbol{Y}(\boldsymbol{x}_\mathrm{d}, t) : \boldsymbol{Y}(\boldsymbol{x}_\mathrm{d}, t) \right\rangle \tag{4.11}$$

where $\boldsymbol{x}_\mathrm{d} = (q_{\mathrm{a_d}},\ q_{\mathrm{u_d}},\ \dot{q}_{\mathrm{a_d}},\ \dot{q}_{\mathrm{u_d}})^T$. Since the input does not affect the unactuated coordinate directly (see equation (4.1)) the control parameters may or may not appear in the averaged dynamics for the unactuated coordinate. Written explicitly, the fourth equation of (4.11) takes the following form

$$\begin{aligned}\ddot{q}_\mathrm{ud}(t) - g_2(\boldsymbol{q}_\mathrm{d}, \dot{\boldsymbol{q}}_\mathrm{d}) =& \frac{1}{4}v_0^2(t)\Big[2k_\mathrm{u}h_2^2(\boldsymbol{q}) + h_1^2(\boldsymbol{q})\frac{\partial^2 g_2}{\partial \dot{q}_\mathrm{a}^2} + h_2^2(\boldsymbol{q})\frac{\partial^2 g_2}{\partial \dot{q}_\mathrm{u}^2} + 2h_1(\boldsymbol{q})h_2(\boldsymbol{q})\frac{\partial^2 g_2}{\partial \dot{q}_\mathrm{a}\partial \dot{q}_\mathrm{u}} \\ & - 2h_1(\boldsymbol{q})\frac{\partial h_2}{\partial q_\mathrm{a}} - 2h_2(\boldsymbol{q})\frac{\partial h_2}{\partial q_\mathrm{u}}\Big]_{\boldsymbol{q}=\boldsymbol{q}_\mathrm{d}}\end{aligned} \tag{4.12}$$

where the right hand side is simply the last (fourth) element of $\frac{1}{4}\left\langle \boldsymbol{Y} : \boldsymbol{Y} \right\rangle$. Equation (4.12) may be interpreted as a condition on both the system structure and the desired trajectory.

Remark 4.3.1 *We may choose the non-zero amplitude $v_0(t)$ such that* (4.12) *holds identi-*

cally for a given desired trajectory $\boldsymbol{q}_{\mathrm{d}}(t)$ *provided*

$$\operatorname{sign}\Big(\Big[2k_{\mathrm{u}}h_2^2(\boldsymbol{q}) + h_1^2(\boldsymbol{q})\frac{\partial^2 g_2}{\partial \dot{q}_{\mathrm{a}}^2} + 2h_1(\boldsymbol{q})h_2(\boldsymbol{q})\frac{\partial^2 g_2}{\partial \dot{q}_{\mathrm{a}}\partial \dot{q}_{\mathrm{u}}} + h_2^2(\boldsymbol{q})\frac{\partial^2 g_2}{\partial \dot{q}_{\mathrm{u}}^2} - 2h_1(\boldsymbol{q})\frac{\partial h_2}{\partial q_{\mathrm{a}}} - 2h_2(\boldsymbol{q})\frac{\partial h_2}{\partial q_{\mathrm{u}}}\Big]_{\boldsymbol{q}=\boldsymbol{q}_{\mathrm{d}}}\Big) = \operatorname{sign}\Big(\ddot{\bar{q}}_{\mathrm{ud}}(t) - g_2(\boldsymbol{q}_{\mathrm{d}}, \dot{\boldsymbol{q}}_{\mathrm{d}})\Big) \neq 0 \tag{4.13}$$

It is evident that in this case if the desired trajectories are time-invariant, then the amplitude v_0 *is constant. If the left hand side of equation* (4.12) *is zero, then* $\boldsymbol{q}_{\mathrm{d}}(t)$ *is a natural trajectory of the unactuated dynamics. In this case the system follows unactuated desired trajectory* $q_{\mathrm{ud}}(t)$ *without need of the vibrational part of the input. So as determined from equation* (4.12), $v_0(t) = 0$.

The term in square brackets on the right hand side of equation (4.12) *corresponds to the last element of the symmetric product* $\langle \boldsymbol{Y} : \boldsymbol{Y} \rangle$, *which shows the influence of this symmetric product over the unactuated coordinate. If the expression inside the square brackets in* (4.12) *vanishes for some desired trajectory* $\boldsymbol{q}_{\mathrm{d}}(t)$, *this influence over the unactuated coordinate is lost. In this case the amplitude* $v_0(t)$ *cannot be determined, and the proposed controller cannot be used. An obvious case where this might occur is if there is no coupling between the actuated and unactuated coordinates.*

After solving (4.12) for the amplitude $v_0(t)$ and substituting into equation (4.10), one may seek values for the control parameters k_{u}, k_{p}, and k_{d} which provide the desired stability and performance. For example, one may linearize the averaged equations about the slowly varying desired motion to obtain a (slow) time-varying linear system, parameterized by the control

gains. Suitable control parameter values may be determined through a stability analysis of this slowly varying linear system (see [Tsakalis and Ioannou, 1993, Ch. 4]). (In the case where the desired motion for the averaged system is constant, this process yields a linear time-invariant system and stability analysis simply involves examining how the eigenvalues of its state matrix vary with the control parameters.)

4.4 Control of Higher Dimensional, Multi-Input Systems

The procedure described for control of 2-DOF underactuated systems can be extended to underactuated systems with more degrees of freedom. Consider an n-DOF underactuated system with $m < n$ independent inputs but with at least as many inputs as unactuated degrees of freedom: $\frac{n}{2} \leq m < n$. Let the vector $\boldsymbol{q}_{\mathrm{a}} = (q_1, \ldots, q_m)^T$ denote the m actuated generalized coordinates and let $\boldsymbol{q}_{\mathrm{u}} = (q_{m+1}, \ldots, q_n)^T$ denote the $l = n - m$ unactuated ones. Assuming there is no loss of control effectiveness (i.e., assuming the inputs remain independent and ignoring control limits), there is no loss of generality in writing:

$$\boldsymbol{M}(\boldsymbol{q}) \begin{pmatrix} \ddot{\boldsymbol{q}}_{\mathrm{a}} \\ \\ \ddot{\boldsymbol{q}}_{\mathrm{u}} \end{pmatrix} = \begin{pmatrix} \boldsymbol{f}_{\mathrm{a}}(\boldsymbol{q}, \dot{\boldsymbol{q}}) \\ \\ \boldsymbol{f}_{\mathrm{u}}(\boldsymbol{q}, \dot{\boldsymbol{q}}) \end{pmatrix} + \begin{pmatrix} \boldsymbol{I}_m \\ \\ \boldsymbol{0}_{l \times m} \end{pmatrix} \boldsymbol{u} \tag{4.14}$$

Here $\boldsymbol{M}$ is the positive definite generalized inertia matrix, $\boldsymbol{I}_m$ is the $m \times m$ identity matrix and $\boldsymbol{u} = (u_1, \ldots, u_m)^T$ is the input vector. The vector fields $\boldsymbol{f}_{\mathrm{a}}$ and $\boldsymbol{f}_{\mathrm{u}}$ are assumed to be

twice continuously differentiable and homogeneous polynomials in $\dot{\boldsymbol{q}}$ of degree two or less. The goal is for the actuated and unactuated coordinates $q_{\mathrm{a}_i} = q_i$ and $q_{\mathrm{u}_j} = q_{j+m}$ to follow slowly varying desired trajectories $q_{\mathrm{ad}_i}(t)$ and $q_{\mathrm{ud}_j}(t)$ for $i \in \{1, \ldots, m\}$ and $j \in \{1, \ldots, l\}$. Equation (4.14) can be rewritten more concisely as

$$\ddot{\boldsymbol{q}} = \boldsymbol{g}(\boldsymbol{q}, \dot{\boldsymbol{q}}) + \sum_{i=1}^{m} \boldsymbol{h}_i(\boldsymbol{q}) u_i \tag{4.15}$$

where $\boldsymbol{q} = (\boldsymbol{q}_{\mathrm{a}}^T\ ,\ \boldsymbol{q}_{\mathrm{u}}^T)^T$ is the vector of generalized coordinates, $\boldsymbol{g} = \boldsymbol{M}^{-1}(\boldsymbol{f}_{\mathrm{a}}^T\ ,\ \boldsymbol{f}_{\mathrm{u}}^T)^T$, and $\boldsymbol{h}_i$ is the i^{th} column of $\boldsymbol{M}^{-1}$.

Let $e_{\mathrm{a}_i} = q_{\mathrm{ad}_i} - q_{\mathrm{a}_i}$ represent the tracking error for the slowly varying desired motion in the i^{th} actuated degree of freedom. Consider the inputs

$$u_i(t) = k_{\mathrm{p}_i} e_{\mathrm{a}_i}(t) + k_{\mathrm{d}_i} \dot{e}_{\mathrm{a}_i}(t) + (1 + k_{\mathrm{u}_i} e_{\mathrm{u}_j}(t)) v_i(t) \qquad \text{for } i \in \{1, \ldots, m\} \tag{4.16}$$

where $v_i(t) = v_{0_i}(t)\omega \cos \omega t$ is a high frequency periodic input with a slowly varying amplitude $v_{0_i}(t)$. The term e_{u_j} represents the tracking error in *one* unactuated degree of freedom: $e_{\mathrm{u}_j} = q_{\mathrm{ud}_j} - q_{\mathrm{u}_j}$ for $j \in \{1, \ldots, l\}$, where q_{ud_j} is the slowly varying desired motion for the j^{th} unactuated degree of freedom. We require that a unique tracking error e_{u_j} be associated with each input component u_i; hence the requirement that there be at least as many inputs as unactuated degrees of freedom: $\frac{n}{2} \leq m < n$.

The challenge, as before, is to determine the amplitudes $v_{0_i}(t)$ and values of the control

parameters k_{p_i}, k_{d_i} and k_{u_i} (and possibly conditions on the structure and the desired motion) such that the time-averaged system behaves as desired.

Substituting $u_i(t)$ into equation (4.15) and rearranging, one obtains

$$\ddot{\boldsymbol{q}} = \boldsymbol{g}(\boldsymbol{q}, \dot{\boldsymbol{q}}) + \sum_{i=1}^{m} \big(k_{\mathrm{p}_i} e_{\mathrm{a}_i}(t) + k_{\mathrm{d}_i} \dot{e}_{\mathrm{a}_i}(t)\big) \boldsymbol{h}_i(\boldsymbol{q}) + \sum_{i=1}^{m} v_{0_i}(t)(1 + k_{\mathrm{u}_i} e_{\mathrm{u}_j}(t)) \boldsymbol{h}_i(\boldsymbol{q}) \omega \cos \omega t \quad (4.17)$$

Considering the state vector $\boldsymbol{x} = (\boldsymbol{q}^T\ ,\ \dot{\boldsymbol{q}}^T)^T$ and defining $\epsilon = \frac{1}{\omega}$ as before, equation (4.17) can be written as $2n$ first order differential equations

$$\dot{\boldsymbol{x}} = \boldsymbol{Z}(\boldsymbol{x}, t) + \boldsymbol{Y}(\boldsymbol{x}, t) \left(\frac{1}{\epsilon}\right) \cos\left(\frac{t}{\epsilon}\right) \quad (4.18)$$

where

$$\boldsymbol{Z}(\boldsymbol{x}, t) = \begin{pmatrix} \dot{\boldsymbol{q}} \\ \boldsymbol{g}(\boldsymbol{q}, \dot{\boldsymbol{q}}) + \sum_{i=1}^{m} \big(k_{\mathrm{p}_i} e_{\mathrm{a}_i}(t) + k_{\mathrm{d}_i} \dot{e}_{\mathrm{a}_i}(t)\big) \boldsymbol{h}_i(\boldsymbol{q}) \end{pmatrix} \quad (4.19)$$

and

$$\boldsymbol{Y}(\boldsymbol{x}, t) = \begin{pmatrix} \boldsymbol{0}_{n \times 1} \\ \sum_{i=1}^{m} v_{0_i}(t)\big(1 + k_{\mathrm{u}_i} e_{\mathrm{u}_j}(t)\big) \boldsymbol{h}_i(\boldsymbol{q}) \end{pmatrix} \quad (4.20)$$

Equation (4.18) is in standard averaging form and Theorem 3.3.1 can be used to find its averaged approximation. For this case $m = 1$ and $v_1(t) = \cos(t)$. Using equations (3.13) through (3.15) one finds $\kappa_1 = 0$ and $\lambda_{11} = \mu_{11} = \frac{1}{4}$. Therefore the averaged dynamics

of (4.18) is in the form

$$\dot{\bar{\boldsymbol{x}}} = \boldsymbol{Z}(\bar{\boldsymbol{x}}, t) - \frac{1}{4} \langle \boldsymbol{Y}(\bar{\boldsymbol{x}}, t) : \boldsymbol{Y}(\bar{\boldsymbol{x}}, t) \rangle \tag{4.21}$$

with the vector fields $\boldsymbol{Z}$ and $\boldsymbol{Y}$ defined as (4.19) and (4.20).

To find the control parameters, one must again choose the periodic forcing terms $v_{0_i}(t)$ (for $i \in \{1, \ldots, m\}$) such that the slowly varying desired motion is feasible; see Remark 4.3.1 concerning the 2-DOF, single-input case. For higher dimensional, multi-input systems, the first condition for the existence of feasible amplitudes $v_{0_i}(t)$ is that each amplitude must appear in at least one of the averaged equations of motion for the unactuated coordinates. To find the class of underactuated systems which meet this condition, consider system (4.15) with inputs

$$u_i(t) = k_{\mathrm{p}_i} e_i(t) + k_{\mathrm{d}_i} \dot{e}_i(t) + (1 + k_{\mathrm{u}_i} e_j(t))\, v_i(t), \quad \text{for } i \in \{1, \ldots, m\} \quad \text{and } j \in \{m+1, \ldots, n\} \tag{4.22}$$

where $e_k = q_{\mathrm{d}_k} - q_k$ (for $k \in \{1, \ldots, n\}$) are the components of the tracking error for the complete slowly varying desired trajectory. The terms $v_i(t) = v_{0_i}(t)\omega \cos \omega t$ are high frequency functions with slowly varying amplitudes; the real coefficients k_{p_i}, k_{d_i} and k_{u_i} are control parameters.

Under appropriate structural conditions on the equations of motion, one may choose the m inputs to influence the actuated coordinates in a way that effects desired behavior in the $l \leq m$ unactuated coordinates. Proposition 4.4.1 describes the class of underactuated

systems for which the amplitude $v_{0_i}(t)$ appears in the averaged dynamics of the j^{th} degree of freedom.

Proposition 4.4.1 *Consider system* (4.15) *with the inputs* u_i*, for* $i \in \{1, \ldots, m\}$*, defined as in* (4.22)*. For* $\bar{\boldsymbol{q}} = \boldsymbol{q}_{\text{d}}$ *the slowly varying amplitude* $v_{0_i}(t)$ *appears in the* $(n+k)^{\text{th}}$*, equation of the averaged approximation* (4.21) *provided there exists* $l \in \{1, \ldots, m\}$ *such that*

$$\sum_{r,s=1}^{n} \left(\frac{\partial^2 g_k(\boldsymbol{q}, \dot{\boldsymbol{q}})}{\partial \dot{q}_r \partial \dot{q}_s} h_{l_s}(\boldsymbol{q}) + 2k_{\text{u}_l} h_{l_k}(\boldsymbol{q}) \delta_{rp} - 2\frac{\partial h_{l_k}(\boldsymbol{q})}{\partial q_r} \right) \Big|_{\boldsymbol{q}=\boldsymbol{q}_{\text{d}}} h_{i_r}(\boldsymbol{q}_{\text{d}}) \neq 0 \tag{4.23}$$

or

$$\sum_{r,s=1}^{n} \left(\frac{\partial^2 g_k(\boldsymbol{q}, \dot{\boldsymbol{q}})}{\partial \dot{q}_r \partial \dot{q}_s} h_{i_s}(\boldsymbol{q}) + 2k_{\text{u}_i} h_{i_k}(\boldsymbol{q}) \delta_{rj} - 2\frac{\partial h_{i_k}(\boldsymbol{q})}{\partial q_r} \right) \Big|_{\boldsymbol{q}=\boldsymbol{q}_{\text{d}}} h_{l_r}(\boldsymbol{q}_{\text{d}}) \neq 0 \tag{4.24}$$

where h_{i_j} *is the* j^{th} *element of* $\boldsymbol{h}_i$ *and* δ_{ij} *represents the Kronecker delta function. The indices "p" and "j"* ($p, j \in \{m+1, \ldots, n\}$) *in the first and second inequalities, respectively, account for the particular unactuated coordinate whose tracking error is associated with the* i^{th} *input.*

Proof: See Appendix B.

Remark 4.4.2 *Note that conditions* (4.23) *and* (4.24) *are distinct because the index i is fixed. (One cannot exchange the indices i and l to obtain a single condition.)*

If all the parameters $v_{0_i}(t)$ appear in the last $l = n - m$ equations of (4.21), then after replacing the state vector $\boldsymbol{x}$ with the desired state vector $\boldsymbol{x}_{\text{d}}$, one obtains l algebraic equations to be satisfied. If this set of l equations with m unknowns is consistent (see the "sign" condition in

Remark 4.3.1, for example), one can find amplitudes $v_{0_i}(t)$ for which the dynamic equations of the unactuated averaged coordinates are satisfied for the desired trajectories. After substituting these determined parameters $v_{0_i}(t)$ into equation (4.21), one may seek parameters k_{p_i}, k_{d_i}, and k_{u_i} for which the system meets stability and performance requirements.

Following is a brief summary of the control design procedure.

Step 1. Verify that the model structure satisfies the conditions of Theorem 3.3.1.

Step 2. Define the inputs given in equation (4.16).

Step 3. Verify that the closed-loop system structure, together with the choice of desired trajectory, satisfies equation (4.23) or (4.24) in Proposition 4.4.1.

Step 4. Compute the averaged dynamics (4.21).

Step 5. Analyze the averaged dynamics to obtain conditions on the control parameters that guarantee asymptotically stable tracking.

4.5 Example 1: A 4-DOF Control System

Consider the following dimensionless system with actuated coordinates $\boldsymbol{q}_{\mathrm{a}} = (\theta_1,\, \theta_2)^T$, unactuated coordinates $\boldsymbol{q}_{\mathrm{u}} = (\theta_3,\, \theta_4)^T$ and equations of motion

$$\begin{cases} \ddot{\theta}_1 = -\dot{\theta}_2^2 - 2\dot{\theta}_1 \cos\theta_3 + 1 + u_1 \\ \ddot{\theta}_2 = -\dot{\theta}_1\dot{\theta}_4 \sin\theta_3 - 2\dot{\theta}_2 + u_2 \\ \ddot{\theta}_3 = \dot{\theta}_1^2 + \dot{\theta}_2^2 - \dot{\theta}_3^2 \sin\theta_4 - 2\dot{\theta}_3 - 4 \\ \ddot{\theta}_4 = -\dot{\theta}_1^2 + \dot{\theta}_2^2 - 2\dot{\theta}_4 - 1 \end{cases} \tag{4.25}$$

The dynamic equations are twice differentiable and polynomial in the velocities of degree two or less. (The equations do not represent the dynamics of any particular physical system.) The control objective is to follow prescribed slowly varying trajectories in each coordinate direction, on average.

To begin, by checking conditions (4.23) and (4.24) it can be seen that both inputs u_1 and u_2 affect the averaged dynamics of the unactuated coordinates θ_3 and θ_4. So either of the inputs may be defined using the tracking error of either of the unactuated coordinates. For example, assigning θ_3 to u_1 and θ_4 to u_2 the inputs are

$$u_1(t) = k_{\mathrm{p}_1} e_{\theta_1}(t) + k_{\mathrm{d}_1} \dot{e}_{\theta_1}(t) + \big(1 + k_{\mathrm{p}_3} e_{\theta_3}(t)\big) v_1(t)$$

$$u_2(t) = k_{\mathrm{p}_2} e_{\theta_2}(t) + k_{\mathrm{d}_2} \dot{e}_{\theta_2}(t) + \big(1 + k_{\mathrm{p}_4} e_{\theta_4}(t)\big) v_2(t)$$

where $v_1(t) = v_{1_0}(t)\omega\cos\omega t$ and $v_2(t) = v_{2_0}(t)\omega\cos\omega t$ are two high frequency inputs. Defining $\Omega_i = \dot{\theta}_i$, $i \in \{1,2,3,4\}$, equations of motion (4.25) can be written as eight first order differential equations. Using the procedure described in Section 4.4, and defining $\bar{e}_i = \theta_{\mathrm{d}_i}(t) - \bar{\theta}_i$, $i \in \{1,2,3,4\}$, the averaged closed-loop equations of motion can be determined as

$$
\begin{cases}
\dot{\bar{\theta}}_1 = \bar{\Omega}_1 \\
\dot{\bar{\theta}}_2 = \bar{\Omega}_2 \\
\dot{\bar{\theta}}_3 = \bar{\Omega}_3 \\
\dot{\bar{\theta}}_4 = \bar{\Omega}_4 \\
\dot{\bar{\Omega}}_1 = -\bar{\Omega}_2^2 - 2\bar{\Omega}_1\cos\bar{\theta}_3 + 1 + k_{\mathrm{p}_1}\bar{e}_1 + k_{\mathrm{d}_1}\dot{\bar{e}}_1 - \frac{1}{2}v_{2_0}^2(t)(1+k_{\mathrm{p}_3}\bar{e}_3)^2 \\
\dot{\bar{\Omega}}_2 = -\bar{\Omega}_1\bar{\Omega}_4\sin\bar{\theta}_3 - 2\bar{\Omega}_2 + k_{\mathrm{p}_2}\bar{e}_2 + k_{\mathrm{d}_2}\dot{\bar{e}}_2 \\
\dot{\bar{\Omega}}_3 = \bar{\Omega}_1^2 + \bar{\Omega}_2^2 - \bar{\Omega}_3^2\sin\bar{\theta}_4 - 2\bar{\Omega}_3 - 4 + \frac{1}{2}v_{1_0}^2(t)(1+k_{\mathrm{p}_3}\bar{e}_3)^2 + \frac{1}{2}v_{2_0}^2(t)(1+k_{\mathrm{p}_4}\bar{e}_4)^2 \\
\dot{\bar{\Omega}}_4 = -\bar{\Omega}_1^2 + \bar{\Omega}_2^2 - 2\bar{\Omega}_4 - 1 - \frac{1}{2}v_{1_0}^2(t)(1+k_{\mathrm{p}_3}\bar{e}_3)^2 + \frac{1}{2}v_{2_0}^2(t)(1+k_{\mathrm{p}_4}\bar{e}_4)^2
\end{cases}
\tag{4.26}
$$

where $(\bar{\theta}_1, \bar{\theta}_2, \bar{\theta}_3, \bar{\theta}_4, \bar{\Omega}_1, \bar{\Omega}_2, \bar{\Omega}_3, \bar{\Omega}_4)^T$ is the state vector of the averaged system, representing the fast time-averaged variations of the state vector of the original time-varying system, $(\theta_1, \theta_2, \theta_3, \theta_4, \Omega_1, \Omega_2, \Omega_3, \Omega_4)^T$. The terms $\theta_{\mathrm{d}_i}(t)$, $i \in \{1,2,3,4\}$, are the slowly varying desired trajectories to be followed.

Replacing the averaged coordinates with their desired values in the averaged equations of the unactuated dynamics (the last two equations of (4.26)), one obtains two algebraic equations

for $v_{1_0}(t)$ and $v_{2_0}(t)$:

$$\begin{cases} \ddot{\bar{\theta}}_{\mathrm{d}_3}(t) = \dot{\bar{\theta}}^2_{\mathrm{d}_1}(t) + \dot{\bar{\theta}}^2_{\mathrm{d}_2}(t) - \dot{\bar{\theta}}^2_{\mathrm{d}_3}(t)\sin\bar{\theta}_{\mathrm{d}_4}(t) - 2\dot{\bar{\theta}}_{\mathrm{d}_3}(t) - 4 + \frac{1}{2}\big(v^2_{1_0}(t) + v^2_{2_0}(t)\big) \\ \ddot{\bar{\theta}}_{\mathrm{d}_4}(t) = -\dot{\bar{\theta}}^2_{\mathrm{d}_1}(t) + \dot{\bar{\theta}}^2_{\mathrm{d}_2}(t) - 2\dot{\bar{\theta}}_{\mathrm{d}_4}(t) - 1 - \frac{1}{2}\big(v^2_{1_0}(t) - v^2_{2_0}(t)\big) \end{cases} \tag{4.27}$$

Note that both amplitudes v_{1_0} and v_{2_0} from the inputs u_1 and u_2 respectively are present in the averaged equations of both unactuated coordinates. Solving (4.27) for v_{1_0} and v_{2_0} gives

$$v_{1_0}(t) = \pm\big(3 - 2\dot{\theta}_{\mathrm{d}_4}(t) - \ddot{\theta}_{\mathrm{d}_4}(t) + 2\dot{\theta}_{\mathrm{d}_3}(t) + \dot{\theta}^2_{\mathrm{d}_3}(t)\sin\theta_{\mathrm{d}_4}(t) + \ddot{\theta}_{\mathrm{d}_3}(t) - 2\dot{\theta}^2_{\mathrm{d}_1}(t)\big)^{1/2}$$

and

$$v_{2_0}(t) = \pm\big(5 + 2\dot{\theta}_{\mathrm{d}_4}(t) + \ddot{\theta}_{\mathrm{d}_4}(t) + 2\dot{\theta}_{\mathrm{d}_3}(t) + \dot{\theta}^2_{\mathrm{d}_3}(t)\sin\theta_{\mathrm{d}_4}(t) + \ddot{\theta}_{\mathrm{d}_3}(t) - 2\dot{\theta}^2_{\mathrm{d}_2}(t)\big)^{1/2}$$

Having ensured that the actual and desired unactuated dynamics are consistent, one then seeks values of the control parameters k_{p_1}, k_{p_2}, k_{d_1}, k_{d_2}, k_{p_3} and k_{p_4}.

As discussed at the end of Section 4.3, one may linearize the averaged equations about the slowly varying desired motion to obtain a (slow) time-varying linear system, parameterized by the control gains. Far more tools are available for stability analysis of linear time-invariant systems than for time-varying ones, however. We consider the special case where the desired motion for the averaged system is constant, so that the linearized dynamics are time-invariant. Though we only analyze stability of this time-invariant system, we

do incorporate time-varying desired motions into the simulations.

Suppose that the desired trajectory components are $\theta_{\mathrm{d}_1} = \theta_{\mathrm{d}_2} = \theta_{\mathrm{d}_3} = 0$ and $\theta_{\mathrm{d}_4} = 0.5$. For the nonlinear averaged dynamics (4.26), the corresponding equilibrium points of the averaged system are $\boldsymbol{\theta}_{e_1} = (\frac{-3}{2k_{\mathrm{p}_1}}, 0, 0, 0.5, 0, 0, 0, 0)^T$, $\boldsymbol{\theta}_{e_2} = (\frac{-3}{2k_{\mathrm{p}_1}}, 0, 0, 0.5 + \frac{2}{k_{\mathrm{p}_4}}, 0, 0, 0, 0)^T$, $\boldsymbol{\theta}_{e_3} = (\frac{-3}{2k_{\mathrm{p}_1}}, 0, \frac{2}{k_{\mathrm{p}_3}}, 0.5, 0, 0, 0, 0)^T$, and $\boldsymbol{\theta}_{e_4} = (\frac{-3}{2k_{\mathrm{p}_1}}, 0, \frac{2}{k_{\mathrm{p}_3}}, 0.5 + \frac{2}{k_{\mathrm{p}_4}}, 0, 0, 0, 0)^T$. Note that none of these equilibria exhibits the desired steady value of x; this issue can be addressed by biasing the reference condition. For now, we select and linearize about the equilibrium $\boldsymbol{\theta}_{e_1}$ to obtain the perturbation dynamics $\dot{\boldsymbol{\delta\bar{\theta}}} = \boldsymbol{A}\boldsymbol{\delta\bar{\theta}}$, where the state vector $\boldsymbol{\delta\bar{\theta}} = (\delta\bar{\theta}_1, \delta\bar{\theta}_2, \delta\bar{\theta}_3, \delta\bar{\theta}_4, \delta\bar{\Omega}_1, \delta\bar{\Omega}_2, \delta\bar{\Omega}_3, \delta\bar{\Omega}_4)^T$, and

$$\boldsymbol{A} = \begin{pmatrix} 0 & 0 & 0 & 0 & 1 & 0 & 0 & 0 \\ 0 & 0 & 0 & 0 & 0 & 1 & 0 & 0 \\ 0 & 0 & 0 & 0 & 0 & 0 & 1 & 0 \\ 0 & 0 & 0 & 0 & 0 & 0 & 0 & 1 \\ -k_{\mathrm{p}_1} & 0 & 0 & 5k_{\mathrm{p}_4} & -2 - k_{\mathrm{d}_1} & 0 & 0 & 0 \\ 0 & -k_{\mathrm{p}_2} & 0 & 0 & 0 & -2 - k_{\mathrm{d}_2} & 0 & 0 \\ 0 & 0 & -3k_{\mathrm{p}_3} & -5k_{\mathrm{p}_4} & 0 & 0 & -2 & 0 \\ 0 & 0 & 3k_{\mathrm{p}_3} & -5k_{\mathrm{p}_4} & 0 & 0 & 0 & -2 \end{pmatrix}$$

The characteristic polynomial of the matrix $\boldsymbol{A}$ is

$$P(\lambda) = \big(\lambda^2 + (k_{\mathrm{d}_1} + 2)\lambda + k_{\mathrm{p}_1}\big)\big(\lambda^2 + (k_{\mathrm{d}_2} + 2)\lambda + k_{\mathrm{p}_2}\big)\big(\lambda^4 + 4\lambda^3 + (3k_{\mathrm{p}_3} + 5k_{\mathrm{p}_4} + 4)\lambda^2 + 2(3k_{\mathrm{p}_3} + 5k_{\mathrm{p}_4})\lambda + 30k_{\mathrm{p}_3}k_{\mathrm{p}_4}\big)$$

Applying the Routh-Hurwitz stability criterion (see [Ogata, 2010, Ch. 5]) to each of the constituent polynomials, one finds the following sufficient conditions for stability of the linearized, time-invariant system:

$$k_{\mathrm{p}_1} > 0,\ \ k_{\mathrm{p}_2} > 0,\ \ k_{\mathrm{d}_1} > -2,\ \ k_{\mathrm{d}_2} > -2,\ \ k_{\mathrm{p}_3} > 0,\ \ k_{\mathrm{p}_4} > 0,$$

and

$$9k_{\mathrm{p}_3}^2 + 25k_{\mathrm{p}_4}^2 - 90k_{\mathrm{p}_3}k_{\mathrm{p}_4} + 24k_{\mathrm{p}_3} + 40k_{\mathrm{p}_4} > 0.$$

By Lyapunov's indirect method and the averaging theorem, the original time-varying system is also stable. Of course, different stabilizing values of the control parameters affect the performance of the system (e.g., damping ratio, maximum overshoot, settling time, etc.). One may use other classical control methods, such as the root locus technique, to place the eigenvalues as desired (see [Ogata, 2010, Ch. 6]).

For this example, we have chosen $k_{\mathrm{p}_1} = k_{\mathrm{p}_2} = 50$, $k_{\mathrm{d}_1} = 2$, $k_{\mathrm{d}_2} = 3$, and $k_{\mathrm{p}_3} = k_{\mathrm{p}_4} = 0.5$. With this choice of parameters, the characteristic values of the state matrix $\boldsymbol{A}$ are $-2 \pm 6.78i$, $-2.5 \pm 6.61i$, $-1.75 \pm 1.25i$, and $-0.25 \pm 1.25i$.

The proposed controller effectively stabilizes the closed-loop system to the constant desired trajectory, about which the system was linearized. To illustrate that the controller can track slowly time-varying trajectories, as well, we present simulation results using the following reference signals: $\theta_{d_1}(t) = 0.4 \sin t$, $\theta_{d_2}(t) = -0.3 \sin(0.5t)$, $\theta_{d_3}(t) = 0.5 \sin(0.5t)$, and $\theta_{d_4}(t) = 0.5$. The simulation results, with $\omega = 100$ rad/s and zero initial conditions, are presented in Figures 4.1 and 4.2.

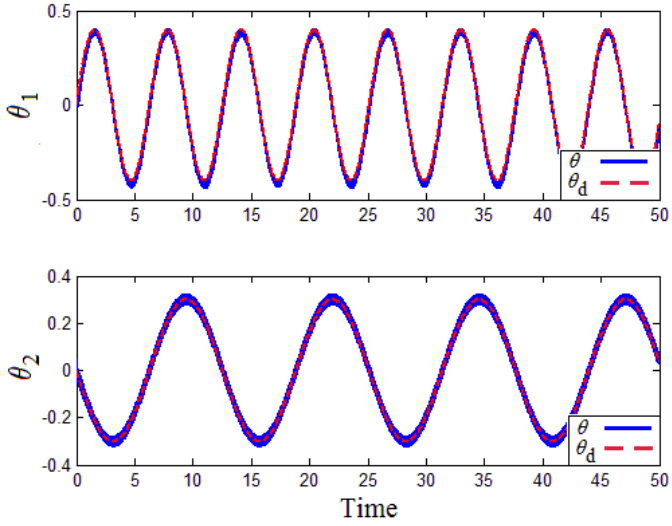

Figure 4.1: Time history of actuated coordinates θ_1 and θ_2

4.6 Example 2: Flapping Plate in Uniform Flow

Consider the 3-DOF device depicted in Figure 4.3. The device consists of a square plate of mass m and width $2a$, with an additional mass m_0 that is rigidly fixed at the top of the plate. The configuration is defined relative to a fixed inertial reference frame $\{\boldsymbol{i}, \boldsymbol{j}, \boldsymbol{k}\}$. The plate is immersed in a uniform flow moving at speed V_∞ in the negative y-direction. A linear

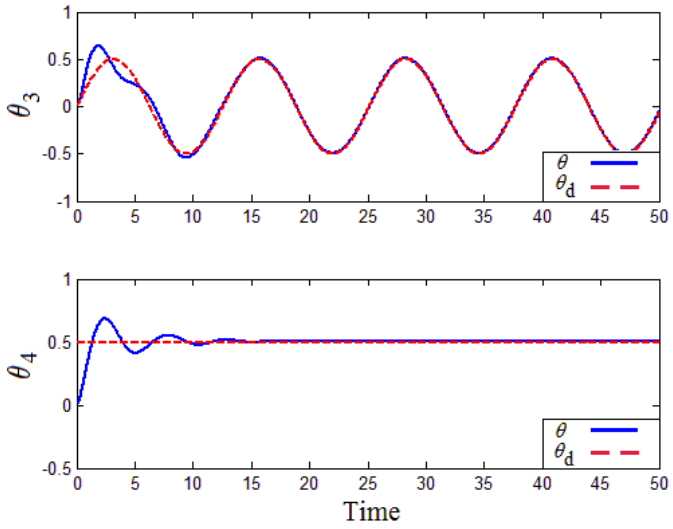

Figure 4.2: Time history of unactuated coordinates θ_3 and θ_4

servo-actuator drives the wing in the direction normal to the flow (the z-direction). The combined motion of the plate in the z and θ directions, which we call "flapping," creates aerodynamic forces which can be used to control the motion of the system in the y direction. The aerodynamic forces are determined using a quasi-steady aerodynamic model. Since the motion of the plate causes acceleration of the fluid in the direction normal to the plate, a parameter γ is included to account for the added mass due to the fluid. Finally, a linear torsional spring (with stiffness k_t) and a linear damper (with damping coefficient b_t) resist the plate's angular motion, as indicated in Figure 4.3.

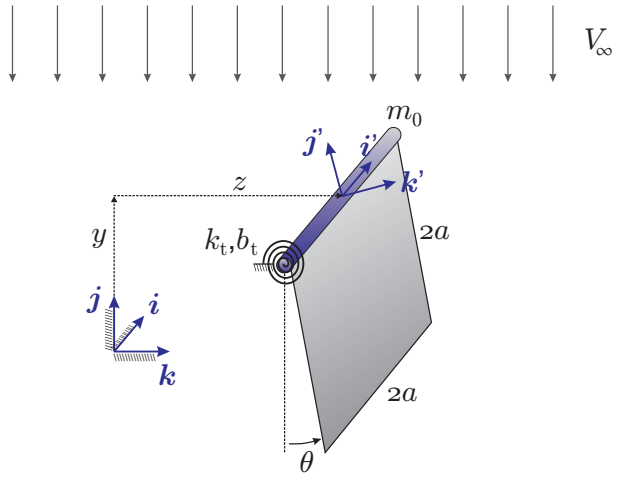

Figure 4.3: Notation for the oscillating wing

4.6.1 Equations of motion and aerodynamic model

Using Lagrange's method (see [Greenwood, 2003, Ch. 2]), one finds that the dynamic model takes the form

$$\boldsymbol{M}(\theta)\begin{pmatrix}\ddot{z}\\ \ddot{\theta}\\ \ddot{y}\end{pmatrix} = \underbrace{\begin{pmatrix}f_z\\ f_\theta\\ f_y\end{pmatrix}}_{\boldsymbol{f}} + \underbrace{\begin{pmatrix}u_z(t)\\ 0\\ 0\end{pmatrix}}_{\boldsymbol{u}(t)} \tag{4.28}$$

where the inertia matrix

$$\boldsymbol{M}(\theta) = \begin{pmatrix} m_0 + m(1+\gamma\cos^2\theta) & ma(1+\gamma)\cos\theta & \frac{1}{2}\gamma m \sin 2\theta \\ ma(1+\gamma)\cos\theta & I_0 + I_p + ma^2(1+\gamma) & ma(1+\gamma)\sin\theta \\ \frac{1}{2}\gamma m \sin 2\theta & ma(1+\gamma)\sin\theta & m_0 + m(1+\gamma\sin^2\theta) \end{pmatrix}$$

and where

$$\boldsymbol{f} = \begin{pmatrix} f_{\text{aero}_z} \\ f_{\text{aero}_\theta} \\ f_{\text{aero}_y} \end{pmatrix} + \begin{pmatrix} -\gamma m\dot{\theta}(\dot{y}\cos 2\theta - \dot{z}\sin 2\theta) + ma(1+\gamma)\dot{\theta}^2 \sin\theta \\ \gamma m\dot{y}\dot{z}\cos 2\theta + \frac{1}{2}\gamma m(\dot{y}^2 - \dot{z}^2)\sin 2\theta - b_t\dot{\theta} - k_t\theta - mga\sin\theta \\ -\gamma m\dot{\theta}(\dot{y}\sin 2\theta + \dot{z}\cos 2\theta) - ma(1+\gamma)\dot{\theta}^2\cos\theta - (m+m_0)g \end{pmatrix}$$

with f_{aero_z} , f_{aero_θ} and f_{aero_y} representing the aerodynamic forces and moment. The term $u_z(t)$ represents the control force in the z direction.

For a symmetric plate in an incompressible flow at a small angle of attack α, there is no aerodynamic moment about the plate. The aerodynamic force, resolved in the wind-relative frame as lift L and drag D, can be assumed to act at the quarter-chord line. It is assumed that the additional mass m_0 does not have any effect on the aerodynamic forces.

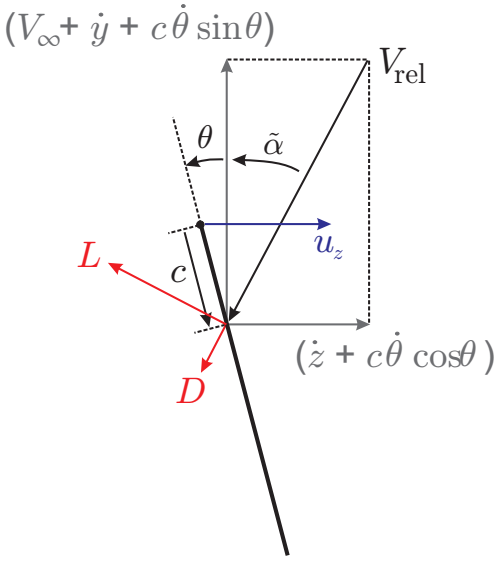

Figure 4.4: Aerodynamic and control forces on the flapping device

Referring to Figure 4.4, the effective angle of attack of the plate at a chord line a distance c

from the leading edge is

$$\alpha = \theta + \arctan\left(\frac{\dot{z} + c\dot{\theta}\cos\theta}{V_\infty + \dot{y} + c\dot{\theta}\sin\theta}\right)$$

We consider a quasisteady aerodynamic model in which the lift and drag forces are well characterized by the instantaneous angle of attack at the quarter-chord $c = a/2$. Assuming that V_∞ is large, we have $\dot{z} + \frac{a}{2}\dot{\theta}\cos\theta \ll V_\infty + \dot{y} + \frac{a}{2}\dot{\theta}\sin\theta$ so that $\alpha \approx \theta + \tilde{\alpha}$ where

$$\tilde{\alpha} = \frac{\dot{z} + \frac{a}{2}\dot{\theta}\cos\theta}{V_\infty + \dot{y} + \frac{a}{2}\dot{\theta}\sin\theta}$$

With these assumptions, the aerodynamic forces in the y and z directions can be written as

$$\begin{aligned} f_{\text{aero}_y} &= L\sin\tilde{\alpha} - D\cos\tilde{\alpha} \qquad &\approx L\tilde{\alpha} - D \\ f_{\text{aero}_z} &= -L\cos\tilde{\alpha} - D\sin\tilde{\alpha} \quad &\approx -L - D\tilde{\alpha} \end{aligned}$$

where L and D represent the lift and drag forces respectively. The moment of the aerodynamic force about the leading edge is

$$\begin{aligned} f_{\text{aero}_\theta} &= -\frac{a}{2}(L\cos\alpha + D\sin\alpha) \\ &\approx -\frac{a}{2}\big(L(\cos\theta - \tilde{\alpha}\sin\theta) + D(\sin\theta + \tilde{\alpha}\cos\theta)\big) \end{aligned}$$

The lift and drag forces can be written as

$$L = C_L(\alpha)(\frac{1}{2}\rho V_{\mathrm{r}}^2)S \quad \text{and} \quad D = C_D(\alpha)(\frac{1}{2}\rho V_{\mathrm{r}}^2)S$$

where ρ is the density of the fluid, S is the surface area of the plate, and V_{r} is the magnitude of relative flow velocity $\boldsymbol{V}_{\mathrm{r}}$ at the point $c = a/2$ aft of the plate's leading edge. Also, under the quasisteady aerodynamics assumption, the lift and drag coefficients take the form

$$C_L = C_{L_\alpha}\alpha$$

$$C_D = C_{D_0} + KC_L^2$$

4.6.2 Closed-loop control

Under the given assumptions, the aerodynamic forces are functions of the velocity and orientation of the plate. Taking $\boldsymbol{q} = (z, \theta, y)^T$, equation (4.28) can be written as

$$\boldsymbol{M}(\boldsymbol{q})\ddot{\boldsymbol{q}} = \boldsymbol{f}(\boldsymbol{q}, \dot{\boldsymbol{q}}) + u(t)$$

or

$$\ddot{\boldsymbol{q}} = \boldsymbol{g}(\boldsymbol{q}, \dot{\boldsymbol{q}}) + \boldsymbol{M}^{-1}(\boldsymbol{q})\boldsymbol{e}_1 u(t) \tag{4.29}$$

where $\boldsymbol{g}(\boldsymbol{q}, \dot{\boldsymbol{q}}) = \boldsymbol{M}^{-1}(\boldsymbol{q})\boldsymbol{f}(\boldsymbol{q}, \dot{\boldsymbol{q}})$ and $\boldsymbol{e}_1 = (1,\ 0,\ 0)^T$. Taking the input to be

$$u_z(t) = k_{\mathrm{p}} e_z(t) + k_{\mathrm{d}} \dot{e}_z(t) + \big(1 + k_y e_y(t)\big) v_z(t)$$

where $e_y(t) = y_{\mathrm{d}}(t) - y(t)$, $e_z(t) = z_{\mathrm{d}}(t) - z(t)$, and $v_z(t) = Z_0(t)\omega \cos \omega t$, one may determine the amplitude $Z_0(t)$ as discussed in Section 4.4. Substituting this input into equation (4.29) one obtains

$$\dot{\boldsymbol{z}} = \boldsymbol{Z}(\boldsymbol{z}, t) + \boldsymbol{Y}(\boldsymbol{z}, t) \left(\frac{1}{\epsilon}\right) \cos\left(\frac{t}{\epsilon}\right) \tag{4.30}$$

where $\boldsymbol{z} = (\boldsymbol{q}^T\ ,\ \dot{\boldsymbol{q}}^T)^T$ and the vector fields

$$\boldsymbol{Z}(\boldsymbol{z}, t) = \begin{pmatrix} \dot{\boldsymbol{q}} \\ \\ \boldsymbol{g}(\boldsymbol{q}, \dot{\boldsymbol{q}}) + \boldsymbol{M}^{-1}(\boldsymbol{q})\boldsymbol{e}_1 (k_{\mathrm{p}} e_z(t) + k_{\mathrm{d}} \dot{e}_z(t)) \end{pmatrix}$$

and

$$\boldsymbol{Y}(\boldsymbol{z}, t) = \begin{pmatrix} \boldsymbol{0}_{3\times 1} \\ \\ \boldsymbol{M}^{-1}(\boldsymbol{q})\boldsymbol{e}_1 Z_0(t)(1 + k_y e_y(t)) \end{pmatrix}$$

If we ignore the induced drag (taking $K = 0$ so that $C_D = C_{D_0}$), then $\boldsymbol{Z}$ and $\boldsymbol{Y}$ in the equation (4.30) are twice differentiable functions and $\boldsymbol{Z}$ contains homogeneous polynomials in $\dot{\boldsymbol{q}}$ of degree two or less. Under these conditions, the averaged form of equation (4.30) takes the form (4.10). (Although we make the simplifying assumption that K = 0 to satisfy the structural requirements, we include induced drag in simulations of the closed-loop system.)

We define the parameters $\rho_m = \frac{m}{S}$ and $\bar{I}_p = \frac{4}{3}\rho_m(1+\gamma)a^4$. Since the plate undergoes almost

periodic oscillations, one can set $\bar{\theta}$ and $\dot{\bar{\theta}}$ to zero. Also setting $\bar{z} = z_{\mathrm{d}}(t)$, $\dot{\bar{z}} = \dot{z}_{\mathrm{d}}(t)$, $\bar{y} = y_{\mathrm{d}}(t)$, $\dot{\bar{y}} = \dot{y}_{\mathrm{d}}(t)$, and $\ddot{\bar{y}} = \ddot{y}_{\mathrm{d}}(t)$ in the averaged equations, we find a single algebraic equation for $Z_0(t)$ from the averaged dynamics of the unactuated coordinate y. Solving this equation gives

$$Z_0(t) = \pm \frac{16l^4\rho_m(1+\gamma)(m_0 + l^2\rho_m(1+\gamma)) + 3I_0(m_0 + 4l^2\rho_m(1+\gamma))}{l(3I_0 + 10l^4\rho_m(1+\gamma))}$$
$$\times \sqrt{\frac{(m_0 + 4l^2\rho_m)(g + \ddot{y}_{\mathrm{d}}(t)) + 2\rho l^2\big(C_{D_0}(V_\infty + \dot{y}_{\mathrm{d}}(t))^2 - C_{L_\alpha}\dot{z}_{\mathrm{d}}^2(t)\big)}{\rho C_{L_\alpha}}}$$

Substituting $Z_0(t)$ into the averaged equations and linearizing at a set point, one may determine a range of values for k_{p}, k_{d}, and k_y that ensure stability of the averaged dynamics. Since the symbolic averaged and linearized systems are complicated, we only present the linearized system for the specific case of hovering flight, i.e., $y_{\mathrm{d}}(t) = z_{\mathrm{d}}(t) = 0$ m. The physical parameters of the system used for simulations are

$$\rho_m = 0.15 \text{ kg/m}^2 \qquad m_0 = 0.1 \text{ kg} \qquad I_0 = 0.005 \text{ kg.m}^2$$
$$a = 0.15 \text{ m} \qquad k_t = 13.6 \text{ N.m/rad} \qquad b_t = 0.5 \text{ N.m.s/rad}$$
$$g = 9.81 \text{ m/s}^2 \qquad \rho = 1 \text{ kg/m}^3 \qquad \gamma = 0.1$$
$$V_\infty = 15 \text{ m/s} \qquad C_{L_\alpha} = 1 \qquad C_{D_0} = 0.1$$
$$K = 0.3 \qquad \omega = 50 \text{ rad/s}$$

The spring stiffness k_t is chosen so that the natural frequency of the plate equals the forcing frequency ω.

For the given physical parameter values, one can show that the origin is the equilibrium point of the nonlinear averaged system. Linearizing the nonlinear averaged dynamics about the origin, one obtains the linear system $\boldsymbol{\delta\dot{\bar{x}}} = \boldsymbol{A}\boldsymbol{\delta\bar{x}}$, where $\boldsymbol{\delta\bar{x}} = (\delta\bar{z}, \delta\bar{\theta}, \delta\bar{y}, \delta\dot{\bar{z}}, \delta\dot{\bar{\theta}}, \delta\dot{\bar{y}})^T$ is the state vector of the linearized system and

$$\boldsymbol{A} = \begin{pmatrix} 0 & 0 & 0 & 1 & 0 & 0 \\ 0 & 0 & 0 & 0 & 1 & 0 \\ 0 & 0 & 0 & 0 & 0 & 1 \\ -8.78k_{\mathrm{p}} & -36.7 - 0.19k_y & 0 & -6.32 - 8.78k_{\mathrm{d}} & 1.32 & 0 \\ 3.59k_{\mathrm{p}} & -2613.1 + 0.08k_y & 0 & -7.64 + 3.59k_{\mathrm{d}} & -93.1 & 0 \\ 0 & 0 & -37.46k_y & 0 & 0 & -1.19 \end{pmatrix}$$

Examining the characteristic polynomial, one can find the range of values of the control parameters to meet the desired stability and performance requirements. In the following simulations we used $k_{\mathrm{p}} = 10$, $k_{\mathrm{d}} = 1$, and $k_y = 2$. For these parameter values, the eigenvalues of $\boldsymbol{A}$ are placed at $-0.59 \pm 8.63i$, $-7.45 \pm 5.66i$, and $-46.7 \pm 21.4i$. The results, using zero initial conditions, are shown in Figure 4.5.

There is an evident steady state error in following the desired trajectory $y_{\mathrm{d}}(t)$. The error can be eliminated by modifying the input to incorporate integral action:

$$u_z(t) = k_{\mathrm{p}}e_z(t) + k_{\mathrm{d}}\dot{e}_z(t) + \big(1 + k_y e_y(t) + k_{y_i}\int_0^t e_y(s)ds + k_{y_d}\dot{e}_y(t)\big)v_z(t)$$

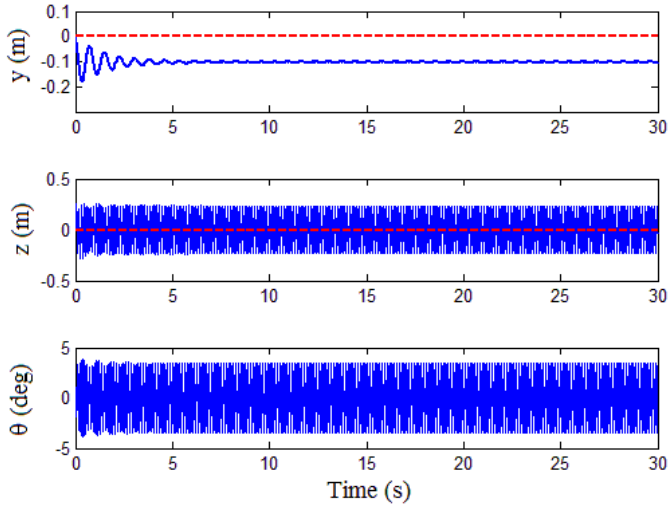

Figure 4.5: Variations of y, z, and θ with respect to time in hovering motion

The result of this modification using $k_{y_i} = 1$ and $k_{y_d} = 0.1$ is shown in Figure 4.6 which shows good convergence to the desired path.

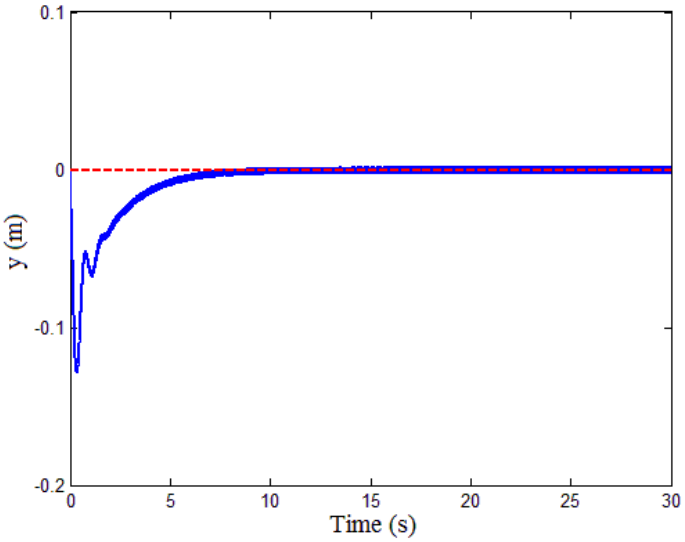

Figure 4.6: Variations of y with respect to time in hovering motion using modified controller

Figure 4.7 shows simulation results for this control law with nominal low frequency trajectories $z_{\mathrm{d}}(t) = 0.5\sin(0.5t)$ m and $y_{\mathrm{d}}(t) = -0.5\sin t$ m. Again, the results indicate effective

tracking of the desired, slowly varying motion on average.

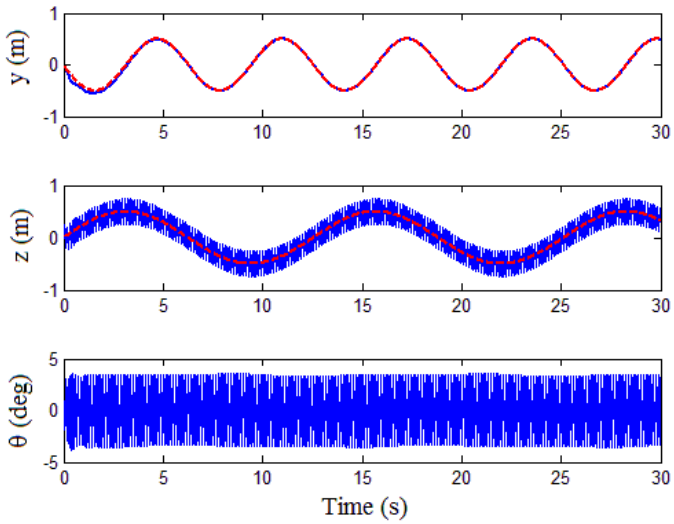

Figure 4.7: Variations of y, z, and θ following a harmonic trajectory with $\omega = 50\,\text{rad/s}$

Note that a variety of simplifying assumptions were made in formulating the control input: small angles, zero induced drag, etc. In the simulations, however, these simplifying assumptions have been removed. The results therefore suggest some degree of robustness to model uncertainty.

To investigate the effect of input frequency on tracking performance, additional simulations were performed with a lower input frequency. Figure 4.8 shows the results with input frequency $\omega = 17\,\text{rad/s}$. (The other parameters, and the desired trajectories, are as defined previously.) Note the larger oscillation amplitude, especially in the actuated z coordinate. For smaller input frequencies, the amplitude of oscillation around the desired trajectory becomes larger, although the system still follows the desired trajectories on average.

When implementing the proposed control method for a real system, the main challenge may

be providing actuators that can generate the required high frequency inputs. As seen in this example, one might be able to use lower frequency inputs, though perhaps at the cost of larger oscillations about the desired trajectory. In any case, the frequencies of vibrational forcing and of the trajectories should be well separated.

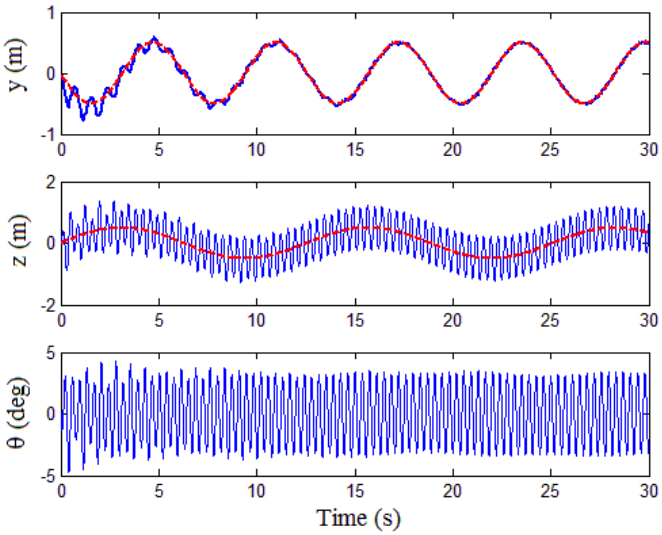

Figure 4.8: Variations of y, z, and θ following a harmonic trajectory with $\omega = 17\,\text{rad/s}$

4.7 Conclusions

This Chapter describes a control technique for approximate trajectory tracking for a class of underactuated mechanical systems using high frequency inputs [Tahmasian and Woolsey, 2015a]. The method, based on multiple scale averaging techniques and vibrational control, allows the system to track slowly varying desired trajectories, on average, in the actuated and unactuated degrees of freedom. Having started with the special case of a single-input, 2-DOF system, the method was extended to the general case of higher dimensional, multi-

input underactuated systems. The work provides explicit conditions defining the class of systems to which the method may be applied. Example applications provided in this section include a 4-DOF system with two inputs and a 3-DOF flapping plate in uniform flow with a single input. In the latter example, the control law was applied to a slightly different model than the one for which it was designed, demonstrating a degree of robustness to uncertainty. This robustness is unsurprising, given that the linearized, averaged dynamics are exponentially stable. The proposed control method may be especially appropriate for high frequency biomimetic systems, such as flapping wing MAVs or robotic fish. A fundamental requirement of the proposed technique is a clear separation between the high frequency of the vibrational forcing and the low frequency associated with the natural dynamics and the slowly varying desired trajectories. If the frequency separation is inadequate, results based on first order averaging are less accurate and higher order averaging may be needed.

4.8 Acknowledgment

The author would like to thank ASME for granting permission to publish this work in this dissertation. This chapter is published in the ASME Journal of Dynamic Systems, Measurement, and Control, 137(7), 2015 [Tahmasian and Woolsey, 2015a].

Chapter 5

Flight Control of Flapping Wing Micro Air Vehicles

This chapter discusses flight control of flapping wing micro air vehicles using a combination of vibrational and state feedback control [Tahmasian et al., 2014; Tahmasian and Woolsey, 2015b]. First a controller is designed to control longitudinal flight using a quasi-steady aerodynamic model and neglecting wing inertial effects. Modulating of the wings' stroke and feather angles controls the vertical and forward motion of the vehicle, respectively. Averaging methods are used to determine the control parameters. Simulations of a system resembling a hawkmoth show that the proposed controller can overcome the disturbances caused by the wing inertia and small parameter uncertainties when following a prescribed trajectory. After introducing the approach through an application to longitudinal flight, the control method is extended to address flight in three-dimensional space.

5.1 Introduction

Bio-inspired engineering involves using examples from nature to solve technical problems [Jenkins, 2011]. For example, inspired by flying insects, researchers are developing flapping wing micro air vehicles (FWMAVs) that can quickly negotiate confined spaces and withstand large disturbances. The engineering design of FWMAVs involves multi-body dynamics, aerodynamics, and control theory. Efforts to mimic insect flight have improved our knowledge of low Reynolds number, unsteady aerodynamics, nonlinear dynamics and control, and the design and manufacture of micro-scale mechanisms.

FWMAVs are generally underactuated systems resembling flying insects, bats, or birds. Underactuated systems contain fewer actuators than degrees of freedom (DOFs), so a vehicle that flaps appendages for propulsion and control is inherently underactuated. Small scale FWMAVs, as opposed to larger ornithopters, use high frequency flapping to generate sufficient aerodynamic forces to overcome gravity and fly. For example the Nano Hummingbird [Keennon et al., 2012] and Harvard Microrobotic Fly [Wood, 2008], two of a few successful FWMAVs, use flapping frequencies of 30 Hz and 110 Hz respectively. Since insects and FWMAVs use periodic aerodynamic forces generated by flapping their wings, they can be modeled as nonlinear time periodic (NLTP) systems. The averaging theorem [Guckenheimer and Holmes, 1983; Sanders and Verhulst, 1985] is often used to construct a nonlinear time invariant (NLTI) approximation of a high frequency NLTP system. If the NLTI system has a hyperbolic equilibrium point, then the NLTP system has a corresponding periodic orbit

with the same stability properties [Guckenheimer and Holmes, 1983].

The aerodynamic forces and moments acting on a FWMAV can be obtained by solving the Navier-Stokes equations with the appropriate boundary conditions, but this approach does not readily support modeling and control design [Ramamurti and Sandberg, 2002]. Typical studies of insect or FWMAV dynamics and control adopt a quasi-steady aerodynamic model whose parameters are determined from experimental studies. Most of these quasi-steady models are based on the blade-element method, in which each wing is divided into spanwise sections over which the flow is assumed to be two-dimensional. Integrating the aerodynamic forces and moments along the span yields an estimate of the total aerodynamic contribution of the wing [Ellington, 1984]. This work adopts the quasi-steady, blade-element aerodynamic model developed in [Deng et al., 2006b].

Early efforts to control a FWMAV's flight were aimed at stabilizing hover. For example, Deng et al. [2006a] used averaging to develop a periodic proportional output feedback control law for hover. Khan and Agrawal [2007] discuss the use of differential flatness to develop a nonlinear controller for the longitudinal dynamics of a FWMAV. In a series of papers, Oppenheimer, Doman, and Sigthorsson describe an approach to three dimensional motion control of a FWMAV by modulating the flapping frequency [Oppenheimer et al., 2009; Doman et al., 2010; Oppenheimer et al., 2011]. The "split-cycle" frequency modulation technique enables an FWMAV to generate non-zero averaged aerodynamic forces, using multiple set of averaged dynamic equations. Later simulations using high-fidelity dynamic and aerodynamic models demonstrated the robustness of the control method to modeling

uncertainties. Another technique, similar to split-cycle control, called "biharmonic amplitude and bias modulation" was developed and tested by Anderson and Cobb [2012, 2014], who also provided a useful summary of the major work on FWMAV.

In other work, closed-loop system robustness was explicitly addressed, as part of the control design objective, for example. Serrani et al. [2010] discussed robust set-point control for the longitudinal motion of a 3-DOF FWMAV and Bhatia et al. [2014] used linear-quadratic regulator theory to address gust resilience. Rifai et al. [2012] discuss the use of bounded state feedback control to regulate a FWMAV's position and attitude, as well as the control system's robustness to model uncertainty. An empirical approach to maneuver control of an insect-scale FWMAV is discussed in [Ma et al., 2013]. By adding adaptive components to the controller to cope with uncertainties, the performance was greatly improved [Chirarattananon et al., 2014]. Other recent work on longitudinal flight control for insect-scale FWMAVs is discussed in [Elzinga et al., 2014]. For recent reviews of dynamic and aerodynamic modeling, stability analysis, and flight control of FWMAVs, see [Taha et al., 2012; Orlowski and Girard, 2012; Sun, 2014].

In this chapter, vibrational control and averaging, based on the method developed in Chapter 4, are used to control the three-dimensional motion of a FWMAV [Bullo, 2002; Bullo and Lewis, 2005]. Under the proposed high-frequency, high-amplitude control law, the dynamics of the closed-loop mechanical system take the form considered in [Bullo, 2002]. Specifically, the closed-loop dynamics are described by the sum of a slowly varying drift vector field and one or more fast-varying input vector fields. Because of the high-frequency, high-amplitude

forcing, the drift vector field is a small perturbation, in comparison with the input vector fields. As recognized in [Bullo, 2002], the structure of the equations suggests the use of the averaging theorem to simplify stability and control analysis. Because the dynamics are averaged over a complete flapping cycle, only one set of averaged equations is needed. The proposed control method is an adaptation of the one developed by [Tahmasian et al., 2013; Tahmasian and Woolsey, 2015a] and discussed in Chapter 4, in which vertical motion is controlled by modulating the stroke amplitude, forward motion is controlled by modulating the feathering angle (the pitch angle of the wing), and lateral motion is controlled by varying these parameters asymmetrically. The pitch attitude is not directly controlled, however it is passively stable if one incorporates a pitch damping contribution due to the body.

This chapter is organized as follows. The equations of longitudinal motion of a FWMAV, including the wing inertia effects, are derived in Section 5.2. By ignoring the wing inertia effects, the equations are transformed to a simpler form that is amenable to the proposed control method. The aerodynamic model is discussed in Section 5.3. In Section 5.4 the proposed control method for control of longitudinal motion is discussed. The performance and robustness of the controller is discussed in Section 5.5, in the context of numerical simulations. Afterward, the method is extended for control of three-dimensional motion of a FWMAV, as discussed in Section 5.6. Section 5.7 reviews the major conclusions from the work and suggests some avenues for continuing research.

5.2 Equations of Longitudinal Motion

The system considered in this work consists of a main body and two wings. To describe the motion of the body and the wings four reference frames are used as shown in Figure 5.1. First an inertial frame $\{x_\mathrm{i}, y_\mathrm{i}, z_\mathrm{i}\}$ is fixed on the ground. Second the body frame $\{x_\mathrm{b}, y_\mathrm{b}, z_\mathrm{b}\}$ is attached to the main body with the origin at its center of mass. The body frame is considered such that the x_b-axis points forward and defines the longitudinal axis of the system, the y_b-axis points to starboard, and z_b is perpendicular to the x_b and y_b axes, forming a right hand coordinate system. A third frame $\{x, y, z\}$ is pinned to the origin of the inertial frame but rotates with the body, such that the x, y and z axes remain parallel to the x_b, y_b and z_b axes, respectively.

In longitudinal flight, the two wings move symmetrically and the y_b-axis remains parallel to the Y axis. In this case, the motion of both wings can be described using a single wing reference frame $\{x_\mathrm{w}, y_\mathrm{w}, z_\mathrm{w}\}$, whose origin is fixed at the joint of the right wing with the y_w axis pointing toward the wing tip. In this work, the motion of each wing is confined to the x_b-y_b plane, as shown in Figure 5.2. Each wing's motion can be described by two angles: the stroke angle β describes the flapping (sweeping) motion of the wing back and forth and the feather angle η describes the rotation of the wing about y_w-axis. Since the velocity of the wings is due mainly to the flapping motion, the wing angle of attack is well approximated by the the feather angle η [Deng et al., 2006a].

To derive the equations of motion of the system when considering the wing inertia effects,

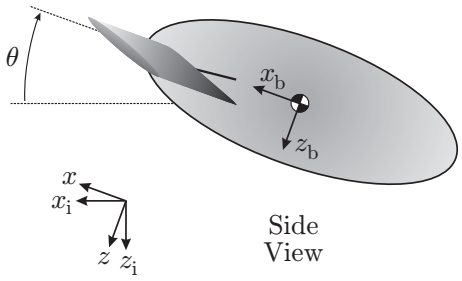

Figure 5.1: The inertial and body coordinate frames (side view)

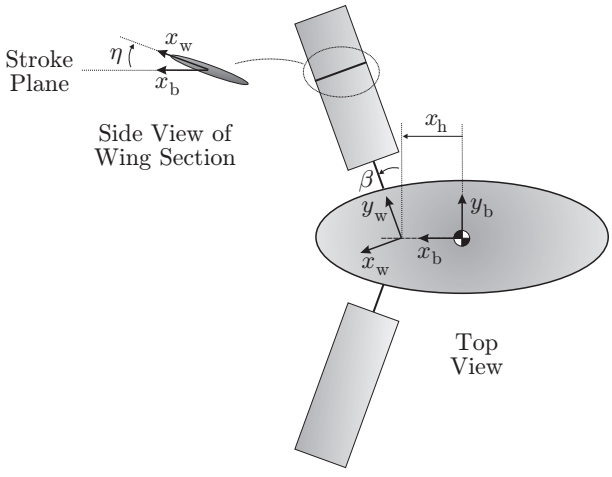

Figure 5.2: The wing angles and wing coordinate frame

we use the principle of virtual power [Greenwood, 2003]. Let $\boldsymbol{i}_{\mathrm{b}}$, $\boldsymbol{j}_{\mathrm{b}}$ and $\boldsymbol{k}_{\mathrm{b}}$ represent the unit vectors defining the body-fixed reference frame. The body translational and rotational velocity in symmetric flight are

$$\boldsymbol{v}_{\mathrm{b}} = u\boldsymbol{i}_{\mathrm{b}} + w\boldsymbol{k}_{\mathrm{b}} \quad \text{and} \quad \boldsymbol{\omega}_{\mathrm{b}} = \dot{\theta}\boldsymbol{j}_{\mathrm{b}}$$

We define the vector of the generalized coordinates of the system as $\boldsymbol{q} = (x\ ,\ z\ ,\ \theta\ ,\ \beta)^T$, where x and z are quasi-coordinates associated with the body velocity components u and w, respectively, and θ is the body pitch angle.

According to the principle of virtual power

$$\sum_i \big(m_i(\dot{\boldsymbol{v}}_i + \ddot{\boldsymbol{\rho}}_{\mathrm{c}_i}) - \boldsymbol{F}_i\big).\frac{\partial \boldsymbol{v}_i}{\partial \dot{\boldsymbol{q}}_j} + \big(\dot{\boldsymbol{h}}_i + m_i\boldsymbol{\rho}_{\mathrm{c}_i} \times \dot{\boldsymbol{v}}_i - \boldsymbol{M}_i\big).\frac{\partial \boldsymbol{\omega}_i}{\partial \dot{\boldsymbol{q}}_j} = 0 \tag{5.1}$$

where the index $i \in \{\mathrm{b}, \mathrm{rw}, \mathrm{lw}\}$ represents the three component rigid bodies (body, right wing, and left wing), the index $j \in \{1, 2, 3, 4\}$ refers to the four degrees of freedom represented by the state vector $\boldsymbol{q}$, and m_i, $\boldsymbol{v}_i$ and $\boldsymbol{\omega}_i$ are the mass, velocity of the center of mass, and angular velocity of the i^{th} rigid body, respectively. The vector $\boldsymbol{\rho}_{\mathrm{c}_i}$ points from the reference point of the i^{th} rigid body to its center of mass. (Since the origin of the body frame is set at the body center of mass, $\boldsymbol{\rho}_{c_{\mathrm{b}}} = \boldsymbol{0}$.) The vector $\boldsymbol{h}_i$ represents the angular momentum of the i^{th} rigid body. The vectors $\boldsymbol{F}_i$ and $\boldsymbol{M}_i$ represent the external force and moment acting on the i^{th} rigid body.

For symmetric flight, the body angular momentum is $\boldsymbol{h}_{\mathrm{b}} = I_y \dot{\theta} \boldsymbol{j}_{\mathrm{b}}$, where I_y is the pitch moment of inertia of the body. Ignoring the aerodynamic effects of the body, the only external force acting on the body is gravity, so $\boldsymbol{F}_{\mathrm{b}} = -mg \sin\theta \boldsymbol{i}_{\mathrm{b}} + mg \cos\theta \boldsymbol{z}_{\mathrm{b}}$ and $\boldsymbol{M}_{\mathrm{b}} = \boldsymbol{0}$.

Each wing has mass m_{w} and mass moments of inertia $I_{x_{\mathrm{w}}}$, $I_{y_{\mathrm{w}}}$ and $I_{z_{\mathrm{w}}}$ about the x_{w}, y_{w} and z_{w} axis, respectively. The translational and rotational velocities are

$$\boldsymbol{v}_{\mathrm{w}} = u\boldsymbol{i}_{\mathrm{b}} + (w - x_{\mathrm{h}}\dot{\theta})\boldsymbol{k}_{\mathrm{b}} \quad \text{and} \quad \boldsymbol{\omega}_{\mathrm{w}} = \dot{\theta}\boldsymbol{j}_{\mathrm{b}} - \dot{\beta}\boldsymbol{k}_{\mathrm{b}}$$

where x_{h} is the longitudinal distance from the origin of the body frame to the origin of the wing frame. The angular velocity vector of the wing can be rewritten in the wing frame as

$$\boldsymbol{\omega}_{\mathrm{w}}^{(\mathrm{w})} = \begin{pmatrix} \omega_1 \\ \omega_2 \\ \omega_3 \end{pmatrix} = \begin{pmatrix} \dot{\beta}\sin\hat{\eta} - \dot{\theta}\cos\hat{\eta}\sin\beta \\ \dot{\theta}\cos\beta \\ -\dot{\beta}\cos\hat{\eta} - \dot{\theta}\sin\hat{\eta}\sin\beta \end{pmatrix}$$

where we define the convenient shorthand:

$$\hat{\eta}(\eta, \dot{\beta}) = \begin{cases} \eta & ; \quad \dot{\beta} \geq 0 \\ \pi - \eta & ; \quad \dot{\beta} < 0 \end{cases}$$

(Both η and $\hat{\eta}$ are used throughout, depending on which is more convenient.)

The position vector pointing from the hinge root to the wing center of mass is $\boldsymbol{\rho}_{\mathrm{c_w}} = -x_{\mathrm{c}}\boldsymbol{i}_{\mathrm{w}} +$

$y_{\mathrm{c}}\boldsymbol{j}_{\mathrm{w}}$. One may compute

$$\ddot{\boldsymbol{\rho}}_{\mathrm{cw}}^{(\mathrm{w})} = \begin{pmatrix} \ddot{\rho}_1 \\ \ddot{\rho}_2 \\ \ddot{\rho}_3 \end{pmatrix} = \begin{pmatrix} x_{\mathrm{c}}(\omega_2^2 + \omega_3^2) - y_{\mathrm{c}}(\dot{\omega}_3 - \omega_1\omega_2) \\ -x_{\mathrm{c}}(\dot{\omega}_3 + \omega_1\omega_2) - y_{\mathrm{c}}(\omega_1^2 + \omega_3^2) \\ x_{\mathrm{c}}(\dot{\omega}_2 - \omega_1\omega_3) + y_{\mathrm{c}}(\dot{\omega}_1 + \omega_2\omega_3) \end{pmatrix}$$

The time derivative of the wing angular momentum can be expressed in the wing frame as

$$\dot{\boldsymbol{h}}_{\mathrm{w}}^{(\mathrm{w})} = \begin{pmatrix} \dot{h}_1 \\ \dot{h}_2 \\ \dot{h}_3 \end{pmatrix} = \begin{pmatrix} I_{x_{\mathrm{w}}}\dot{\omega}_1 + (I_{z_{\mathrm{w}}} - I_{y_{\mathrm{w}}})\omega_2\omega_3 \\ I_{y_{\mathrm{w}}}\dot{\omega}_2 + (I_{x_{\mathrm{w}}} - I_{z_{\mathrm{w}}})\omega_1\omega_3 \\ I_{z_{\mathrm{w}}}\dot{\omega}_3 + (I_{y_{\mathrm{w}}} - I_{x_{\mathrm{w}}})\omega_1\omega_2 \end{pmatrix}$$

The external forces acting on the wings are the gravitational and aerodynamic forces. Since the lateral aerodynamic forces of the two wings are equal and opposite, they cancel. Therefore the vector of the external forces $\boldsymbol{F}_{\mathrm{w}}$ expressed in body frame is

$$\boldsymbol{F}_{\mathrm{w}}^{(\mathrm{b})} = \begin{pmatrix} F_x - m_{\mathrm{w}} g \sin\theta \\ 0 \\ F_z + m_{\mathrm{w}} g \cos\theta \end{pmatrix}$$

where F_x and F_z are the aerodynamic forces acting in x_{b} and z_{b} directions respectively.

The moments applied on the system include the moment due to the weight of the wings, the aerodynamic moment and the control moment acting on the wings. The moment due to gravity is $\boldsymbol{M}_{g_w} = (-d\boldsymbol{i}_{\mathrm{w}} + r_{cg}\boldsymbol{j}_{\mathrm{w}}) \times m_{\mathrm{w}} g \boldsymbol{k}_{\mathrm{I}}$ and the control moment is $\boldsymbol{M}_{\mathrm{c}} = M_\beta \boldsymbol{k}_{\mathrm{b}}$.

Substituting these terms in equation (5.1) and simplifying, the longitudinal equations of motion are

$$\begin{cases} F_x = & m(\dot{u} + w\dot{\theta} + g\sin\theta) + m_{\mathrm{w}}(\ddot{\rho}_1\cos\hat{\eta}\cos\beta + \ddot{\rho}_2\sin\beta + \ddot{\rho}_3\sin\hat{\eta}\cos\beta - x_{\mathrm{h}}\dot{\theta}^2) \\ F_z = & m(\dot{w} - u\dot{\theta} - g\sin\theta) + m_{\mathrm{w}}(\ddot{\rho}_3\cos\hat{\eta} - \ddot{\rho}_1\sin\hat{\eta} - x_{\mathrm{h}}\ddot{\theta}) \\ M_y = & m_{\mathrm{w}}\big(d\dot{u}\sin\hat{\eta} + (d\cos\hat{\eta}\cos\beta - r_{\mathrm{cg}}\sin\beta - x_{\mathrm{h}})\dot{w} + x_{\mathrm{h}}\ddot{\theta}(x_{\mathrm{h}} - d\cos\hat{\eta}\cos\beta + r_{\mathrm{cg}}\sin\beta) \\ & + x_{\mathrm{h}}(\ddot{\rho}_1\sin\hat{\eta} - \ddot{\rho}_3\cos\hat{\eta} + u\dot{\theta} + g\cos\theta) - (d\cos\hat{\eta}\cos\beta - r_{\mathrm{cg}}\sin\beta)(u\dot{\theta} + g) \\ & + d\dot{\theta}(w - x_{\mathrm{h}}\dot{\theta})\sin\hat{\eta}\big) + I_y\ddot{\theta} + \dot{h}_2\cos\beta - \dot{h}_1\cos\hat{\eta}\sin\beta - \dot{h}_3\sin\hat{\eta}\sin\beta \\ M_\beta = & m_{\mathrm{w}}(d\cos\hat{\eta}\sin\beta + r_{\mathrm{cg}}\cos\beta)(\dot{u} + (w - x_{\mathrm{h}}\dot{\theta})\dot{\theta}) + \dot{h}_1\sin\hat{\eta} - \dot{h}_3\cos\hat{\eta} \end{cases} \tag{5.2}$$

where M_y is the aerodynamic moment about the y_{b} axis, and M_β is the stroke control moment applied to the right wing. (In symmetric flight, the left wing moves in unison with the right.)

Rather than use equations (5.2) for control design, one may use simpler equations that omit the mutual inertial effects of the wings and body on one another, such that the motion of the main body can be represented using a conventional fixed-wing aircraft model [Etkin, 1972].

In this case, the equations of motion take the form

$$\begin{cases} \dot{u} &= -qw - g\sin\theta + \frac{1}{m}F_x \\ \dot{w} &= qu + g\cos\theta + \frac{1}{m}F_z \\ \dot{q} &= \frac{1}{I_y}M_y \\ \ddot{\beta} &= \frac{1}{I^{\mathrm{w}}_{z_{\mathrm{b}}}}M_\beta \end{cases} \tag{5.3}$$

where $q = \dot{\theta}$ is the pitch rate of the body and $I^{\mathrm{w}}_{z_{\mathrm{b}}} = I_{x_{\mathrm{w}}}\sin^2\hat{\eta} + I_{z_{\mathrm{w}}}\cos^2\hat{\eta}$ is the mass moment of inertia of the right wing about the z_{b}-axis.

The components of body velocity in the inertial and body frames are related as follows:

$$u = U\cos\theta - W\sin\theta$$

$$w = U\sin\theta + W\cos\theta$$

where $U = \dot{X}$ and $W = \dot{Z}$. Using these transformations, equation (5.3) can be rewritten in the inertial frame as

$$\begin{cases} \dot{U} &= \frac{1}{m}F_X \\ \dot{W} &= g + \frac{1}{m}F_Z \\ \dot{q} &= \frac{1}{I_y}M_y \\ \ddot{\beta} &= \frac{1}{I^{\mathrm{w}}_{z_{\mathrm{b}}}}M_\beta \end{cases} \tag{5.4}$$

where F_X and F_Z are the aerodynamic forces in the X and Z directions respectively.

5.3 Aerodynamic Model

The aerodynamic force and moment are determined using a quasi-steady blade-element model [Deng et al., 2006b,a]. The model includes both the translational and rotational effects of the wing motion. Here, we consider a single wing among a pair that move symmetrically, recognizing that the total contribution will be doubled. We later relax the assumption of symmetric flapping.

The feather (wing pitch) kinematics are prescribed in the following form: $\eta(t) = \eta_0 \text{sgn}(\dot{\beta})$, where sgn represents the signum function. That is, the feather angle remains at constant value η_0 during the forward sweep and reverses sign when the sweep motion reverses. According to Deng *et al.* [Deng et al., 2006b,a], the normal and tangential aerodynamic forces on the wing can be represented as

$$\begin{aligned} F_N &= \frac{1}{2}\rho A_{\text{w}} C_N v_{\text{cp}}^2 \\ F_T &= \frac{1}{2}\rho A_{\text{w}} C_T v_{\text{cp}}^2 \end{aligned} \tag{5.5}$$

where v_{cp} is the velocity of the aerodynamic center of pressure of the wing, ρ is the density of the fluid, A_{w} is the surface area of the wing and C_N and C_T are force coefficients. Since the wings undergo high frequency flapping motion, assuming the body is moving slowly compared to the wings' velocities, almost all of the translational velocity of a blade element of the wing at a distance r from the joint (root) of the wing is due to the flapping motion.(In simulations the induced angle of attack due to the body motion is considered.) So the velocity

of the aerodynamic center of pressure of the wing can be considered as $v_{\rm cp} \approx r_{\rm cp}\dot{\beta}$, where $r_{\rm cp}$ denotes the position of the center of pressure in the $y_{\rm w}$ direction and can be determined using [Deng et al., 2006b]

$$r_{\rm cp} = \sqrt{\frac{\int_0^R c(r) r^2 dr}{A_{\rm w}}} \tag{5.6}$$

where R is the wing length and $c(r)$ is the chord width of the wing at a distance r from the wing joint in the $y_{\rm w}$ direction.

Replacing $v_{\rm cp}$ into (5.5), the normal and tangential forces can be written as

$$\begin{aligned} F_N &= \frac{1}{2}\rho A_{\rm w} C_N r_{\rm cp}^2 \dot{\beta}^2 \\ F_T &= \frac{1}{2}\rho A_{\rm w} C_T r_{\rm cp}^2 \dot{\beta}^2 \end{aligned} \tag{5.7}$$

where using experimental data, the normal and tangential force coefficients C_N and C_T are [Deng et al., 2006b]

$$\begin{aligned} C_N &= \bar{C}_N {\rm sgn}(\dot{\beta}) \sin\eta \\ C_T &= \bar{C}_T {\rm sgn}(\dot{\beta}) \cos^2 2\eta \end{aligned} \tag{5.8}$$

There is another component of the normal force due to feathering (pitching) of the wings:

$$F_{r,N} = \frac{1}{2}\rho A_{\rm w} \bar{C}_r c_{\max} \dot{\eta} v_{\rm cp}$$

where $\bar{C}_r$ is a force coefficient and $c_{\max}$ is the maximum chord of the wing. Since the feather angle η is assumed constant during each half stroke of the wings ($\dot{\eta} = 0$), however, this normal force vanishes. (During stroke transitions, when the feather angle changes sign, the stroke velocity $\dot{\beta}$ goes to zero so that $v_{\text{cp}} \approx 0$.)

To use the aerodynamic forces in the equations of motion, the components of the normal and tangential forces in the body frame can be expressed as

$$\begin{aligned} F_x &= F_T \cos\eta \cos\beta + F_N \sin\eta \cos\beta \\ F_z &= -F_T \sin\eta + F_N \cos\eta \end{aligned} \tag{5.9}$$

Expressed in the inertial frame, the force components are

$$\begin{aligned} F_X &= F_x \cos\theta + F_z \sin\theta \\ F_Z &= -F_x \sin\theta + F_z \cos\theta \end{aligned} \tag{5.10}$$

The aerodynamic moment M_y is the moment of the normal and tangential forces about the center of mass of the body:

$$M_y = r_{\text{cp}}(F_T \sin\eta - F_N \cos\eta)\sin\beta - \frac{1}{4}\bar{c}F_N \text{sgn}(\dot{\beta})\cos\beta \tag{5.11}$$

where $\bar{c}$ is the mean geometric chord of the wing.

Using equations (5.7) through (5.11) and after some calculations, the components of aero-

dynamic force and moment in the inertial frame can be written as

$$F_X = f_X(\theta, \eta, \beta)\dot{\beta}^2$$
$$F_Z = f_Z(\theta, \eta, \beta)\dot{\beta}^2$$
$$M_y = m_y(\theta, \eta, \beta)\dot{\beta}^2 \tag{5.12}$$

where

$$f_X = \frac{1}{2}\rho A_{\mathrm{w}} r_{\mathrm{cp}}^2\big((\bar{C}_N \cos\eta - \bar{C}_T \cos^2 2\eta)\sin\eta\sin\theta + (\bar{C}_N \sin^2\eta + \bar{C}_T \cos\eta\cos^2 2\eta)\cos\beta\cos\theta\big)\mathrm{sgn}(\dot{\beta})$$
$$f_Z = \frac{1}{2}\rho A_{\mathrm{w}} r_{\mathrm{cp}}^2\big((\bar{C}_N \cos\eta - \bar{C}_T \cos^2 2\eta)\sin\eta\cos\theta - (\bar{C}_N \sin^2\eta + \bar{C}_T \cos\eta\cos^2 2\eta)\cos\beta\sin\theta\big)\mathrm{sgn}(\dot{\beta})$$
$$m_y = \frac{1}{2}\rho A_{\mathrm{w}} r_{\mathrm{cp}}^2\big(r_{\mathrm{cp}}(\bar{C}_T \cos^2 2\eta - \bar{C}_N \cos\eta)\mathrm{sgn}(\dot{\beta})\sin\beta - \frac{1}{2}\bar{\mathrm{c}}\bar{\mathrm{C}}_{\mathrm{N}}\cos\beta\big)\sin\eta$$

The aerodynamic force and moment components required to determine the motion of the system are expressed as functions of the body pitch angle θ, and the wing stroke and feather angles β and η. Recall that, because the analysis above concerned a single wing, the force and moment components f_X, f_Z, and m_y in (5.12) are doubled for two wings in symmetric motion.

5.4 Averaging and Control of Longitudinal Flight

Substituting the force and moment components F_X and F_Y and the moment M_y from (5.12) into (5.4), including the contributions from both wings, the dynamic equations of the system

can be written succinctly as follows:

$$\begin{aligned}
\dot{U} &= \frac{1}{m} f_X(\theta, \eta, \beta)\dot{\beta}^2 \\
\dot{W} &= g + \frac{1}{m} f_Z(\theta, \eta, \beta)\dot{\beta}^2 \\
\dot{q} &= \frac{1}{I_y} m_y(\eta, \beta)\dot{\beta}^2 \\
\ddot{\beta} &= \frac{1}{I^{\mathrm{w}}_{z_{\mathrm{b}}}} M_\beta
\end{aligned} \tag{5.13}$$

where the stroke control moment M_β and the feather angle η are the control inputs of the system. The goal is to determine the inputs such that the system follows a slowly varying desired trajectory $(X_{\mathrm{d}}(t), Z_{\mathrm{d}}(t), \theta_{\mathrm{d}}(t))$ on average.

In this work, we use the feather angle η to control the horizontal motion of the vehicle, and adjust the amplitude of stroke angle of the wings to control the vertical motion. If the feather angle η and the wing stroke angle β follow zero-mean, periodic profiles, then the net horizontal force generated during one flapping cycle will be zero. If the feather angle differs slightly when the wing is sweeping forward than when it sweeps back, however, there will be a nonzero net horizontal force which can be used to control the horizontal motion of the vehicle. To control the horizontal motion a proportional-derivative (PD) controller is used to adjust the amplitude of the feather angle of the wing:

$$\eta = \eta_s + k_{p_x}(X_{\mathrm{d}}(t) - X) + k_{d_x}(\dot{X}_{\mathrm{d}}(t) - \dot{X})$$

where $\eta_s = \eta_0 \text{sgn}(\dot{\beta})$, η_0 is a constant acute angle, and k_{p_x} and k_{d_x} are PD control parameters to be selected. Assuming that the change in the feather angle due to PD control is small relative to η_s, then one may use the following approximations when substituting the feather angle into the equations of motion:

$$\begin{aligned} \sin\eta &= \sin(\eta_s) + \eta_x \cos(\eta_s) \\ \cos\eta &= \cos(\eta_s) - \eta_x \sin(\eta_s) \end{aligned} \tag{5.14}$$

where $\eta_x = k_{p_x}(X_{\text{d}}(t) - X) + k_{d_x}(\dot{X}_{\text{d}}(t) - \dot{X})$.

Altitude control can be achieved by adjusting the amplitude of the stroke angle. Using equations (5.4), the simplified dynamic equation for the stroke motion of each wing is

$$\ddot{\beta} = \frac{1}{I^{\text{w}}_{z_{\text{b}}}} M_\beta \tag{5.15}$$

To modulate the stroke amplitude, we choose

$$M_\beta = k_{p_\beta}\beta + k_{d_\beta}\dot{\beta} + B_0(t)\left(1 + k_{p_z}\big(Z_{\text{d}}(t) - Z\big)\right)\omega\cos\omega t \tag{5.16}$$

where $B_0(t)$ is a time varying parameter, and k_{p_β}, k_{d_β} and k_{p_z} are control parameters to be determined. By choosing the control moment M_β as (5.16), the stroke amplitude is adjusted using the altitude tracking error $Z_{\text{d}}(t) - Z$. Defining the state vector $\boldsymbol{x} = (X, Z, \theta, \beta, U, W, q, \omega_\beta)^T$, with $\omega_\beta = \dot{\beta}$, and using equations (5.14) through (5.16), the equa-

tions of motion of the system can be written as

$$\dot{\boldsymbol{x}} = \boldsymbol{f}(\boldsymbol{x}, t) + \boldsymbol{g}(\boldsymbol{x}, t)\omega \cos \omega t \tag{5.17}$$

where

$$\boldsymbol{f}(\boldsymbol{x}, t) = \begin{pmatrix} \dot{X} \\ \dot{Z} \\ q \\ \omega_\beta \\ \frac{1}{m} f_X \omega_\beta^2 \\ g + \frac{1}{m} f_Z \omega_\beta^2 \\ \frac{1}{I_y} m_y \omega_\beta^2 \\ \frac{1}{I_{z_\mathrm{b}}^\mathrm{w}} \left(k_{p_\beta} \beta + k_{d_\beta} \omega_\beta \right) \end{pmatrix}$$

and

$$\boldsymbol{g}(\boldsymbol{x}, t) = \begin{pmatrix} \mathbf{0}_{7\times 1} \\ \frac{B_0(t)}{I_{z_\mathrm{b}}^\mathrm{w}} \left(1 + k_{p_z} (Z_\mathrm{d}(t) - Z) \right) \end{pmatrix}$$

The vector fields $\boldsymbol{f}$ and $\boldsymbol{g}$ contain twice differentiable functions of $\boldsymbol{x}$ (except at the end of each half flapping period, where the feather angle η changes sign) and slowly varying functions of time (relative to the high-frequency flapping motion). Also, $\boldsymbol{f}$ contains homogeneous polynomials in velocity of degree two and less, an important requirement for the control

method being used. Defining the small parameter $\epsilon = \frac{1}{\omega}$, equation (5.17) can be written as

$$\dot{\boldsymbol{x}} = \frac{d\boldsymbol{x}}{dt} = \boldsymbol{f}(\boldsymbol{x}, t) + \boldsymbol{g}(\boldsymbol{x}, t)\left(\frac{1}{\epsilon}\cos\frac{t}{\epsilon}\right) \tag{5.18}$$

The system (5.18) is a mechanical control system with high-frequency, high-amplitude forcing – a vibrational control system. Averaging over the fast time scale $\tau = t/\epsilon$ following Theorem 3.3.1, one may approximate the system (5.18) with the slowly time-varying dynamics

$$\dot{\bar{\boldsymbol{x}}} = \boldsymbol{f}(\bar{\boldsymbol{x}}, t) - \frac{1}{4}\langle \boldsymbol{g} : \boldsymbol{g} \rangle(\bar{\boldsymbol{x}}, t) \tag{5.19}$$

The symmetric product in (5.19) is easily computed using symbolic mathematics software, but the resulting expressions are too large to be shown.

From the structure of the input vector field $\boldsymbol{g}$, one may infer that the input $\cos(\tau)$ does not affect the vertical motion directly, since Z represents an unactuated degree of freedom. However, the component of the symmetric product $\langle \boldsymbol{g} : \boldsymbol{g} \rangle$ corresponding to the Z coordinate is nonzero, resulting in a net vertical force in (5.19). Since the parameter $B_0(t)$ appears in the W component of $\langle \boldsymbol{g} : \boldsymbol{g} \rangle$, the vertical motion may be controlled using the input M_β.

For a system to track a desired trajectory, that trajectory should be dynamically feasible; i.e., it should satisfy the equations of motion. For the FWMAV system to follow some desired, slowly varying time histories $X_\mathrm{d}(t)$, $Z_\mathrm{d}(t)$, and $\theta_\mathrm{d}(t)$ on average, these time histories must be consistent with the averaged dynamic equations. To find the parameter $B_0(t)$, we substitute the desired time histories into the W equation of the averaged dynamics and seek

a time-varying parameter value $B_0(t)$ for which the equation holds identically. To keep the body pitch angle small, we choose $\theta_{\mathrm{d}}(t) = 0$. Also note that, because the wings perform high-frequency, zero-mean periodic motion, $\bar{\beta} \equiv 0$. From the sixth component equation of (5.19), we find that

$$B_0(t) = \frac{I^{\mathrm{w}}_{z_{\mathrm{b}}}}{r_{\mathrm{cp}}} \sqrt{\frac{4m\big(g - \ddot{Z}_{\mathrm{d}}(t)\big)}{2\rho A_{\mathrm{w}}\big(\bar{C}_T(1+\cos 4\eta_0) - 2\bar{C}_N \cos\eta_0\big)\sin\eta_0}} \tag{5.20}$$

Having determined $B_0(t)$, one may substitute it into the averaged equations of motion (5.19) and seek parameters k_{p_β}, k_{d_β}, k_{p_z}, k_{p_x} and k_{d_x} to meet stability and performance requirements. To simplify stability analysis, the nonlinear averaged dynamics (5.19) can be linearized about the slowly varying desired trajectory to obtain a linear, time-varying perturbation system. In cases where the desired trajectory (for the average motion) is constant, the system obtained from linearization will be linear, time-invariant, which considerably simplifies the analysis.

5.5 Simulation and Numerical Results

In this section, the proposed flight control method is applied to a FWMAV with physical parameters resembling those of a hawkmoth. For simplicity, however, the wings are modeled as rectangles with chord length $c = 18.5$ mm and semi-span $R = 52$ mm. The remaining

physical parameters are as defined in [Berman and Wang, 2007; Deng et al., 2006b]:

$$m = 1.6 \times 10^{-3} \text{ kg}, \quad I_y = 10^{-6} \text{ kg.m}^2, \quad I_{z_\text{b}}^\text{w} = 2 \times 10^{-8} \text{ kg.m}^2, \quad \rho = 1.2 \text{ kg/m}^3$$
$$\eta_0 = 40^\circ, \quad x_\text{h} = 0, \quad \omega = 56\pi \text{ rad/s}, \quad \bar{C}_N = -3.4, \quad \bar{C}_T = -0.4$$

We first consider hovering motion: $X_\text{d}(t) = Z_\text{d}(t) = 0$. Replacing the physical parameters and desired trajectories, the averaged equations of motion (5.19) can be simplified to

$$\begin{aligned}
\dot{\bar{X}} &= \bar{U} \\
\dot{\bar{Z}} &= \bar{W} \\
\dot{\bar{\theta}} &= \bar{q} \\
\dot{\bar{U}} &= \big((-8.32 + 18.43P)\cos\bar{\beta}\cos\bar{\theta} + (-9.81 + 4.46P)\sin\bar{\theta}\big)(1 - k_{p_z}\bar{Z})^2 \\
&\quad + \bar{\omega_\beta}^2\big((-9.3 + 20.5P)\cos\bar{\beta}\cos\bar{\theta} + (-10.9 + 5P)\sin\bar{\theta}\big) \times 10^{-4} \\
\dot{\bar{W}} &= 9.81 + \big((-9.81 + 4.46P)\cos\bar{\theta} + (8.32 - 18.43P)\cos\bar{\beta}\sin\bar{\theta}\big)(1 - k_{p_z}\bar{Z})^2 \\
&\quad + \bar{\omega_\beta}^2\big((10.9 + 5P)\cos\bar{\theta} + (9.3 - 20.5P)\cos\bar{\beta}\sin\bar{\theta}\big) \times 10^{-4} \\
\dot{\bar{q}} &= \big((0.95 - 1.13P)\cos\bar{\beta} + (4.73 - 2.15P)\sin\bar{\beta}\big)(1 - k_{p_z}\bar{Z})^2 \\
&\quad + \bar{\omega_\beta}^2\big((1.06 - 1.26P)\cos\bar{\beta} + (5.28 - 2.4P)\sin\bar{\beta}\big) \times 10^{-4} \\
\dot{\bar{\omega}}_\beta &= 2(k_{p_\beta}\bar{\beta} + k_{d_\beta}\bar{\omega_\beta}) \times 10^5
\end{aligned} \tag{5.21}$$

where $P = k_{p_x}\bar{X} + k_{d_x}\bar{U}$, and $\bar{\boldsymbol{x}} = (\bar{X}, \bar{Z}, \bar{\theta}, \bar{\beta}, \bar{U}, \bar{W}, \bar{q}, \bar{\omega_\beta})^T$ is the state vector of the averaged system. The fixed points of the averaged system are $\boldsymbol{x}_{e_1} = (\frac{0.84}{k_{p_x}}, -\frac{0.023}{k_{p_z}}, 0.866, 0, 0, 0, 0, 0)^T$ and $\boldsymbol{x}_{e_2} = (\frac{0.84}{k_{p_x}}, \frac{2.023}{k_{p_z}}, 0.866, 0, 0, 0, 0, 0)^T$. Linearizing equation (5.21) about $\boldsymbol{x}_{e_1}$ one obtains

the linear, time-invariant perturbation system $\boldsymbol{\delta\dot{\bar{x}}} = \boldsymbol{A\delta\bar{x}}$, where $\boldsymbol{\delta\bar{x}}$ is the state vector of the linearized system, and

$$\boldsymbol{A} = \begin{pmatrix} 0 & 0 & 0 & 0 & 1 & 0 & 0 & 0 \\ 0 & 0 & 0 & 0 & 0 & 1 & 0 & 0 \\ 0 & 0 & 0 & 0 & 0 & 0 & 1 & 0 \\ 0 & 0 & 0 & 0 & 0 & 0 & 0 & 1 \\ 16.05k_{p_x} & 0 & -9.81 & 0 & 16.05k_{d_x} & 0 & 0 & 0 \\ -11.68k_{p_x} & 19.18k_{p_z} & 0 & 0 & -11.68k_{d_x} & 0 & 0 & 0 \\ -1.19k_{p_x} & 0 & 0 & 3.07 & -1.19k_{d_x} & 0 & 0 & 0 \\ 0 & 0 & 0 & 2\times 10^5 k_{p_\beta} & 0 & 0 & 0 & 2\times 10^5 k_{d_\beta} \end{pmatrix}$$

Unfortunately, it is not possible to find control parameter values for which the matrix $\boldsymbol{A}$ is Hurwitz. In the best case, $\boldsymbol{A}$ has two conjugate pairs of pure imaginary eigenvalues. One pair is associated with the pitch motion of the body. If a small amount of pitch damping acts on the main body, however, these eigenvalues move into the left half plane. We therefore modify the pitch motion equation in (5.13) to the following:

$$\dot{q} = \frac{1}{I_y}(m_y\omega_\beta^2 - c_{\mathrm{q}}q)$$

where c_{q} is the pitch damping coefficient. For simulations, we take $c_{\mathrm{q}} = 10^{-5}$ Nms/rad. Choosing the control parameters to be

$$k_{p_x} = -10, \quad k_{d_x} = -0.6, \quad k_{p_\beta} = -8 \times 10^{-5}, \quad k_{d_\beta} = -2 \times 10^{-7}, \quad k_{p_z} = -80$$

(omitting units), the eigenvalues of matrix $\boldsymbol{A}$ become $-100 \pm 264.6i$, $-4.8 \pm 11.7i$, $-0.5 \pm 0.7i$, and $\pm 39.2i$. The final conjugate pair of pure imaginary eigenvalues is associated with vertical motion. This pair of eigenvalues can be stabilized by incorporating a derivative term in the control moment M_β as follows

$$M_\beta(t) = k_{p_\beta}\beta + k_{d_\beta}\omega_\beta + B_0(t)\left(1 + k_{p_z}\big(Z_{\mathrm{d}}(t) - Z\big) + k_{d_z}\big(\dot{Z}_{\mathrm{d}}(t) - \dot{Z}\big)\right)\omega\cos\omega t$$

In developing the control method, we assumed that the wing angle of attack is well approximated by η_0. In the simulations, however, the effect of the body's translational motion on the wing angle of attack has been incorporated:

$$\eta = \eta_s + \alpha_{\mathrm{b}} + \eta_x \tag{5.22}$$

where α_{b} represents the angle of attack contribution due to the body's motion:

$$\alpha_{\mathrm{b}} = \tan^{-1}\frac{w - r_{\mathrm{cp}}\dot{\beta}\sin\beta}{V}\mathrm{sgn}(\dot{\beta}) \qquad \text{where} \qquad \mathrm{V} = \sqrt{(\mathrm{r_{cp}}\dot{\beta} + \mathrm{u}\cos\beta)^2 + \mathrm{w}^2} \tag{5.23}$$

Figure 5.3 shows the results of simulations of a FWMAV in feedback-controlled hovering motion, with zero initial conditions and with $k_{d_z} = -1.2$. In Figure 5.3 it can be seen that there is a small, steady-state tracking error in the vertical position of about 0.01 m. This error can be eliminated by incorporating an integral control term in M_β.

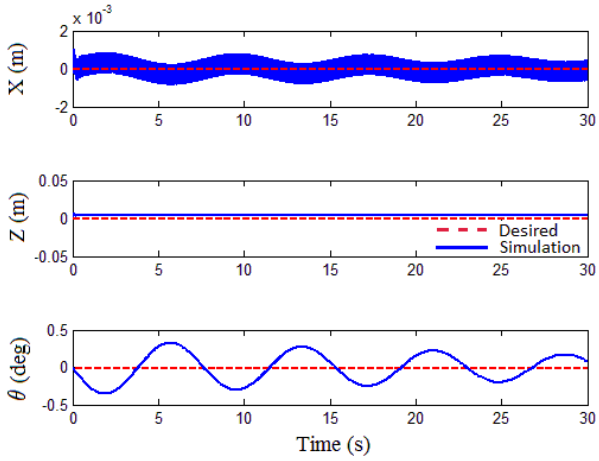

Figure 5.3: Time histories of X, Z and θ for hovering flight without wing inertia effects

Next, the FWMAV was tasked with tracking a circular path in vertical X-Z plane, using the control parameters developed for hovering flight. The simulation results are presented in Figures 5.4 and 5.5. After small deviations at the beginning of motion, the vehicle starts to follow the desired trajectories $X_{\mathrm{d}}(t) = 0.3\sin(t)$ m and $Z_{\mathrm{d}}(t) = -0.3 + 0.3\cos(t)$ m. (Recall that Z is positive downward.)

As evidence of the controller's robustness the simulations were also performed with the inertial effect of the wings incorporated into the model. The physical properties of the wings are

$$m_{\mathrm{w}} = 2 \times 10^{-4} \text{ kg}, \quad I_{xw} = I_{yw} = I_{zw} = 10^{-6} \text{ kg.m}^2$$

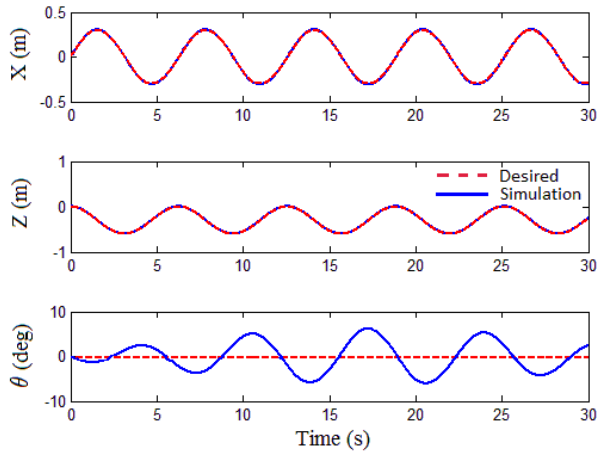

Figure 5.4: Time histories of X, Z and θ for a circular desired trajectory without wing inertia effects

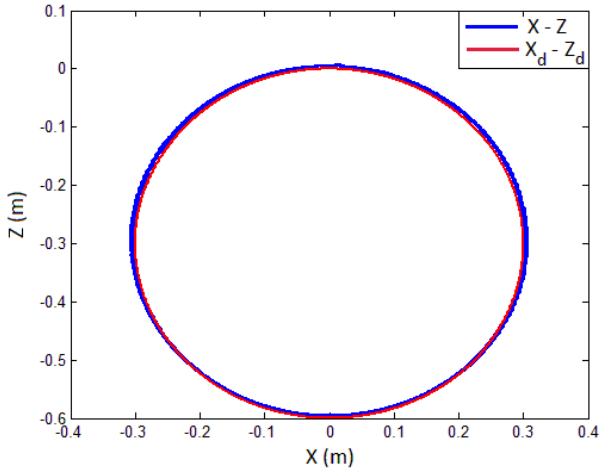

Figure 5.5: X-Z path for a circular desired trajectory without wing inertia effects

with the center of mass of the each wing at its geometric center. The mass and the mass moments of inertia given here were intentionally chosen larger than the values for a hawk-moth, as a further indication of controller robustness. Applying the controller developed for the simpler model, and using equation (5.2), it is evident in Figures 5.6 and 5.7 that the controller performs properly even with this multi-body perturbation in the dynamic model.

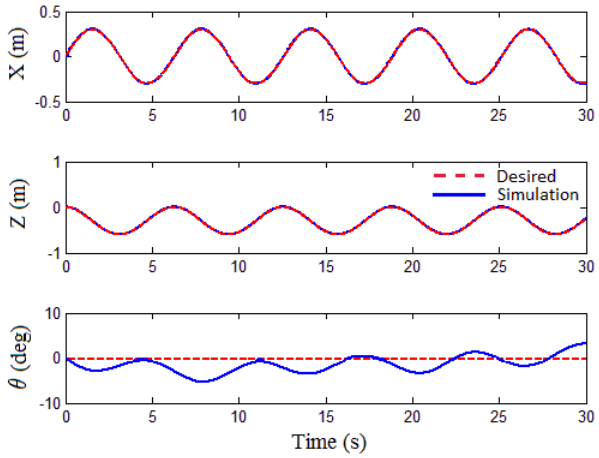

Figure 5.6: Time histories of X, Z and θ following a circular trajectory when considering the wing effects

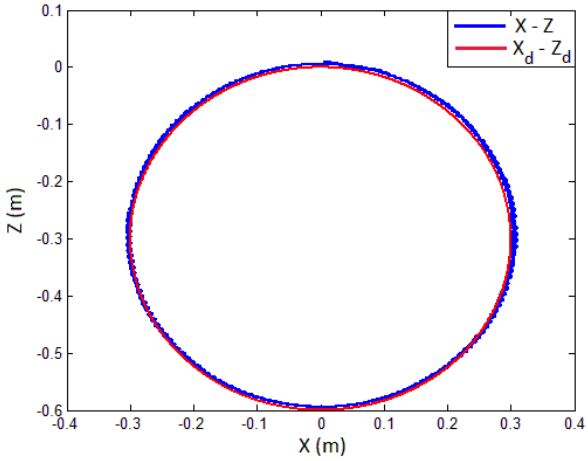

Figure 5.7: The vehicle X-Z path, following a circular trajectory when considering the wing effects

5.6 Control of Three Dimensional Flight

In this section, the controller developed earlier is extended to the problem of three dimensional (3-D) trajectory tracking. In this case, the main body moves in all six degrees of freedom. Rotational motions are parametrized by the roll (ϕ), pitch (θ), and yaw (ψ) angles. For motion in the body longitudinal plane, the method discussed in Section 5.4 is used. To control roll and yaw attitude and lateral translation, we introduce asymmetry into the wing motion. Thus, we define angles $\beta_{\text{rw}}(t)$ and $\beta_{\text{lw}}(t)$ for the stroke angles of the right and left wings, respectively. The two waveforms will have the same frequency but, in general, different amplitudes. Also, the two wings may use different feather angles η_{rw} and η_{lw}. Asymmetric feather angles are used to control the yaw angle (ψ), and thus the inertial direction of forward flight. Since flapping with different wing feather angles also produces a non-zero lateral force, the vehicle deviates from the desired trajectory when undergoing a yaw motion. Lateral motion is controlled by modulating the vehicle's roll angle (ϕ) with differential stroke angle amplitudes.

5.6.1 Equations of three dimensional motion

To simplify control design and analysis, wing inertial effects are neglected when considering the 3-D dynamics. Recall that the multi-body effect of the wings had little impact on the closed-loop performance in the simulations described in the previous section. Let $\boldsymbol{X} = (X, Y, Z)^T$ represent the position of the body frame in the inertial frame and let $\boldsymbol{x} = (x, y, z)^T$

represent the same position vector in a rotating frame pinned at the origin of the inertial frame. The transformation matrix $\boldsymbol{R}$ from the inertial frame to the rotating frame is

$$\boldsymbol{R} = \boldsymbol{R}_{x,\phi}\boldsymbol{R}_{y,\theta}\boldsymbol{R}_{z,\psi}$$

where

$$\boldsymbol{R}_{x,\phi} = \begin{pmatrix} 1 & 0 & 0 \\ 0 & \cos\phi & \sin\phi \\ 0 & -\sin\phi & \cos\phi \end{pmatrix}$$

$$\boldsymbol{R}_{y,\theta} = \begin{pmatrix} \cos\theta & 0 & -\sin\theta \\ 0 & 1 & 0 \\ \sin\theta & 0 & \cos\theta \end{pmatrix}$$

$$\boldsymbol{R}_{z,\psi} = \begin{pmatrix} \cos\psi & \sin\psi & 0 \\ -\sin\psi & \cos\psi & 0 \\ 0 & 0 & 1 \end{pmatrix}$$

Thus, for example, $\boldsymbol{x} = \boldsymbol{R}\boldsymbol{X}$. Let $\boldsymbol{V} = (U, V, W)^T$ represent the translational velocity of the body frame relative to the inertial frame, and expressed in the inertial frame. Let $\boldsymbol{v} = (u, v, w)^T$ represent this same translational velocity, but expressed in the body frame: $\boldsymbol{v} = \boldsymbol{R}\boldsymbol{V}$. Finally, let $\boldsymbol{\omega} = (p, q, r)^T$ represent the angular velocity of the body frame relative to the inertial frame, expressed in the body frame. The rate of change of the roll, pitch, and

yaw angles are related to the body angular velocity components as follows [Etkin, 1972]:

$$\dot{\phi} = p + q\sin\phi\tan\theta + r\cos\phi\tan\theta$$

$$\dot{\theta} = q\cos\phi - r\sin\phi$$

$$\dot{\psi} = (q\sin\phi + r\cos\phi)\sec\theta$$

The dynamic equations for the main body, with the simplified wing dynamic model are

$$\begin{aligned}
F_x &= m(\dot{u} + qw - rv) + mg\sin\theta \\
F_y &= m(\dot{v} + ru - pw) - mg\cos\theta\sin\phi \\
F_z &= m(\dot{w} + pv - qu) - mg\cos\theta\cos\phi \\
M_x &= I_x\dot{p} - I_{zx}(\dot{r} + pq) - (I_y - I_z)qr \\
M_y &= I_y\dot{q} - I_{zx}(r^2 - p^2) - (I_z - I_x)rp \\
M_z &= I_z\dot{r} - I_{zx}(\dot{p} - qr) - (I_x - I_y)pq \\
M_{\beta,\mathrm{rw}} &= I^{\mathrm{w}}_{z_\mathrm{b}}\ddot{\beta}_{\mathrm{rw}} \\
M_{\beta,\mathrm{lw}} &= I^{\mathrm{w}}_{z_\mathrm{b}}\ddot{\beta}_{\mathrm{lw}}
\end{aligned} \tag{5.24}$$

where I_x, I_y and I_z are the mass moments of inertia about the x_b, y_b and z_b axes, respectively, I_{zx} is the product of inertia about z-x axes. The terms F_x, F_y, F_z are the aerodynamic force components and M_x, M_y, M_z are the aerodynamic moment components in the body frame. Finally, $M_{\beta,\mathrm{rw}}$ and $M_{\beta,\mathrm{lw}}$ are the control forces applied on the right and left wings,

respectively.

5.6.2 Control of three dimensional motion

Motion control in 3-D is carried out by decomposing the motion of the wings into symmetric and asymmetric parts. The symmetric part of the wings' motion is used to control the longitudinal degrees of freedom, as discussed in Section 5.4, while the asymmetric part is used to control roll, yaw, and lateral translation.

Suppose the vehicle is to follow a slowly varying yaw angle $\psi_{\mathrm{d}}(t)$. When the wings undergo symmetric motion (as in the case of longitudinal motion), the net aerodynamic moment generated about z_b-axis by the wings is zero. The lateral aerodynamic forces generated along y_b-axis by the two wings are equal and opposite, and therefore cancel each other. If the wings perform slightly asymmetric motions, however, the net aerodynamic moment along z_b-axis and the net lateral force will no longer be zero. The resulting aerodynamic moment and force cause the vehicle to rotate about the z_b-axis (yaw motion) and translate along the y_b-axis (lateral motion). The yaw motion of the vehicle can be controlled by generating a proper aerodynamic moment about the z_b-axis. By using different feather angles η_{rw} and η_{lw} for the two wings, a proper aerodynamic moment can be generated to effect the desired yaw motion. By defining the asymmetric part of the wings' feather angles as

$$\eta_\psi = k_{p_\psi}(\psi_{\mathrm{d}} - \psi) + k_{d_\psi}(\dot{\psi}_{\mathrm{d}} - \dot{\psi})$$

where k_{p_ψ} and k_{d_ψ} are control parameters to be determined, the wings' feather angles can be considered as

$$\eta_{\rm rw} = \eta_s + \eta_x + \eta_\psi$$

$$\eta_{\rm lw} = \eta_s + \eta_x - \eta_\psi$$

The slight difference in the wings' feather angles caused by η_ψ generates an aerodynamic moment about z_b-axis to follow the desired yaw angle $\psi_{\rm d}$. But it also causes a roll motion which generates a lateral force in its turn, causing the vehicle to deviate from its desired trajectory along y_b-axis. The control of the lateral motion of the vehicle can be done by changing the roll angle of the body. A non-zero roll angle of the vehicle causes a non-zero component of the aerodynamic forces along y_b-axis (lateral force). By control of the roll angle, one can control this lateral force to generate lateral motion of the vehicle. To this end, the desired roll angle $\phi_{\rm d}$ at each time is defined as

$$\phi_{\rm d} = k_{p_y}(y_{\rm d} - y) + k_{d_y}(\dot{y}_{\rm d} - \dot{y}) \tag{5.25}$$

where k_{p_y} and k_{d_y} are control parameters and $y_{\rm d}$ is the y component of the desired position vector in the rotating $\{x, y, z\}$ frame. By considering $\boldsymbol{X}_{\rm d} = (X_{\rm d}, Y_{\rm d}, Z_{\rm d})^T$ as the desired position vector in the inertial frame, the desired position vector in the rotating frame $\{x, y, z\}$ can be determined as

$$\boldsymbol{x}_{\rm d} = (x_{\rm d}, y_{\rm d}, z_{\rm d})^T = \boldsymbol{R}^T \boldsymbol{X}_{\rm d}$$

In this work, the control of the roll angle is performed by using different amplitudes for the wings' stroke angles β_{rw} and β_{lw}. Different stroke amplitudes generate different aerodynamic forces at the right and left sides of the body, which cause the rotation of the body about x_b-axis (roll motion). Using the desired roll angle ϕ_{d} defined by (5.25), the asymmetric part of the stroke angle is defined as

$$\beta_\phi = k_\phi(\phi_{\mathrm{d}} - \phi)$$

where k_ϕ is a constant parameter. Using β_ϕ, the control moments applied to the wings are determined as

$$M_{\beta,\mathrm{rw}}(t) = k_{p_{\beta,R}}\beta_{\mathrm{rw}} + k_{d_{\beta,R}}\dot{\beta}_{\mathrm{rw}} + B_0(t)\left(1 + k_{p_z}\left(Z_{\mathrm{d}}(t) - Z\right) + k_{d_z}\left(\dot{Z}_{\mathrm{d}}(t) - \dot{Z}\right) - \beta_\phi\right)\omega\cos\omega t$$

$$M_{\beta,\mathrm{lw}}(t) = k_{p_{\beta,L}}\beta_{\mathrm{lw}} + k_{d_{\beta,L}}\dot{\beta}_{\mathrm{lw}} + B_0(t)\left(1 + k_{p_z}\left(Z_{\mathrm{d}}(t) - Z\right) + k_{d_z}\left(\dot{Z}_{\mathrm{d}}(t) - \dot{Z}\right) + \beta_\phi\right)\omega\cos\omega t$$

Substituting these control moments into equations of motion (5.24), one can transform these equations to the standard averaging form of (5.18) with the averaged approximation of (5.19). Then one may seek control parameter values that enable the system to meet stability and performance requirements.

5.6.3 Numerical results for three dimensional motion

Using the control method described for 3-D motion, the vehicle can turn in hover or during forward motion. In this section the results of following two such trajectories are presented.

The physical parameters are chosen as

$$I_x = 1.5 \times 10^{-6} \text{ kg.m}^2, \quad I_z = 1.2 \times 10^{-6} \text{ kg.m}^2, \quad I_{zx} = -0.02 I_x$$

$$k_{p_\psi} = 1, \quad k_{d_\psi} = 1, \quad k_{p_y} = 0.6, \quad k_{d_y} = 0.4 \quad k_\phi = 20$$

The rest of the physical parameters are the same as Section 5.5. For the simulations, as before, the body's motion was incorporated when computing the wing angle of attack:

$$\eta_{\text{rw}} = \eta_s + \alpha_{\text{b}_{\text{rw}}} + \eta_x + \eta_\psi$$

$$\eta_{\text{lw}} = \eta_s + \alpha_{\text{b}_{\text{lw}}} + \eta_x - \eta_\psi$$

where $\alpha_{\text{b}_{\text{rw}}}$ and $\alpha_{\text{b}_{\text{lw}}}$ are the contributions to wing angle of attack due to the base body translation and rotation.

In the first simulation, the desired trajectory is a concatenation of straight and harmonic ascending and descending flight segments, interspersed with turning maneuvers in hovering flight. The simulation results in Figures 5.8 through 5.10 exhibit effective trajectory following. Since the control of the pitch angle θ is not considered here, in Figure 5.9 the pitch angle is not asymptotically stable and shows deviations from its desired value $\theta_{\text{d}} = 0$. But due to the incorporated pitch damping on the body, the amplitude of the pitch oscillations does not grow beyond a limit.

For the second simulation, the desired trajectory begins with straight forward motion and continues into an ascending helical trajectory. The required yaw angle during the helical

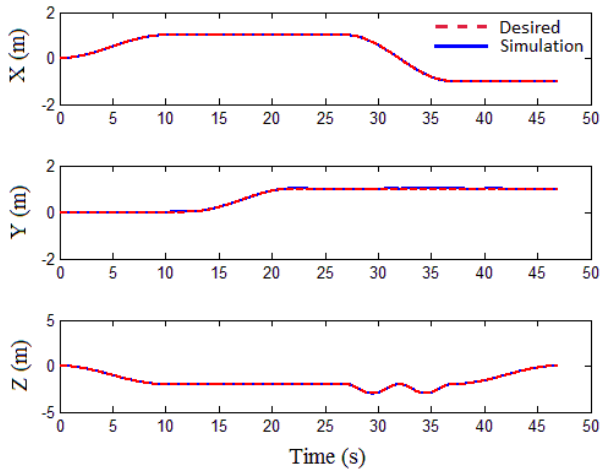

Figure 5.8: Time histories of X, Y and Z following trajectory 1

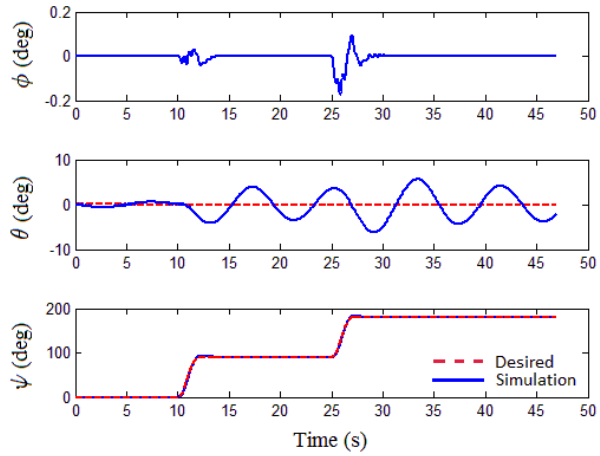

Figure 5.9: Time histories of ϕ, θ and ψ following trajectory 1

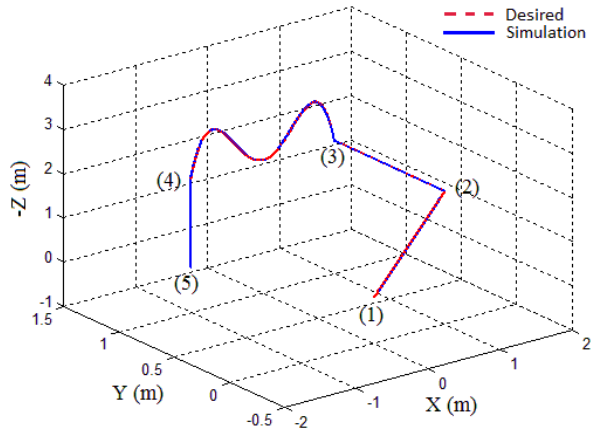

Figure 5.10: The 3-D trajectory 1 of the FWMAV

motion is $\psi_{\mathrm{d}}(t) = \tan^{-1}\frac{v_{\mathrm{d}}(t)}{u_{\mathrm{d}}(t)}$, where u_{d} and v_{d} are the body frame components of the desired translational velocity. Again, Figures 5.11 through 5.13 illustrate effective trajectory following.

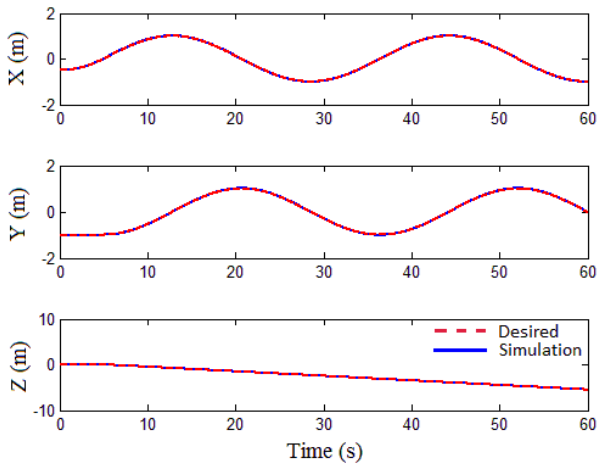

Figure 5.11: Time histories of X, Y and Z following trajectory 2

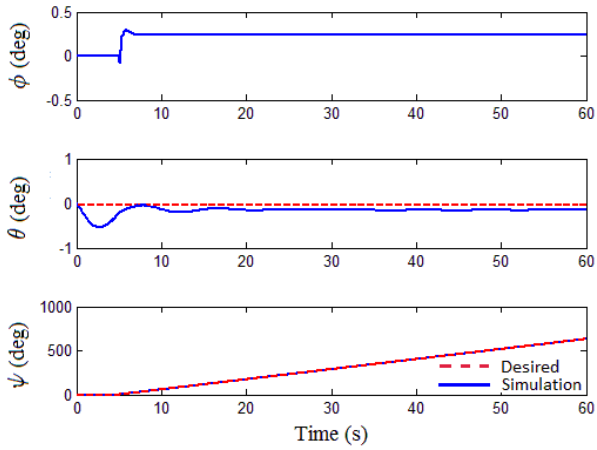

Figure 5.12: Time histories of ϕ, θ and ψ following trajectory 2

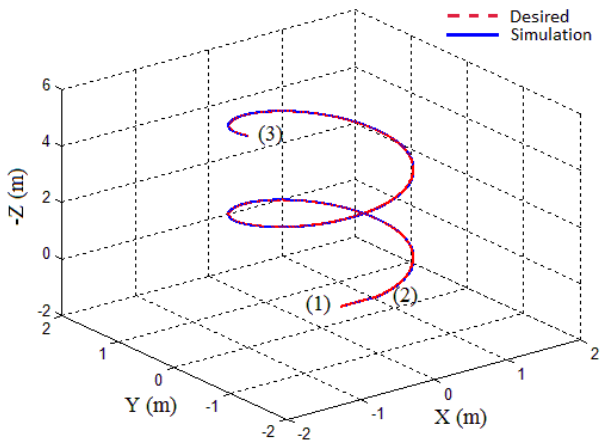

Figure 5.13: The 3-D trajectory 2 of the FWMAV

5.7 Conclusions

An approach to three-dimensional flight control for a FWMAV was developed by treating the vehicle as a vibrational control system – a mechanical system subject to high-frequency, high-amplitude forcing. First, the longitudinal equations of motion were developed and then simplified by omitting the the inertial effects of the wings. Using this simplified model, a trajectory tracking controller was developed using two of the wings' three degrees of freedom: wing stroke (or sweeping) motion and wing feather (or pitching) motion. Modulating the amplitude of the stroke angle enables control of vertical motion while the amplitude of the feather angle allows control of horizontal (forward) motion. The control method was implemented in simulation using the full equations of motion (i.e., including the multi-body mechanics effects) and shown to be effective, suggesting that the proposed controller is robust to model uncertainty. The controller developed for longitudinal flight was then extended to enable three dimensional trajectory tracking. In this case, differential motion of the wings was incorporated to enable control of yaw, roll, and lateral translation. In simulations, the controller enabled turning flight in hover and in forward, climbing flight.

Chapter 6

Input Optimization of Vibrational Control Systems

In this chapter optimization of input amplitudes for mechanical control-affine systems with high-frequency, high-amplitude inputs is discussed. The problem consists of determining the waveform (shape), amplitude, and the relative phase of inputs to minimize their amplitudes while accomplishing some control objective. Using the results of Section 3.4 concerning the effects of the phase shifting of the inputs, and investigating the effects of the waveform of the inputs on the averaged dynamics, the best waveform of the inputs (i.e., the periodic input with smallest possible amplitude) is a square function. Using averaging techniques for control-affine systems, the problem of input optimization is then transformed into a constrained optimization problem. The constraints are algebraic nonlinear equalities in terms of the amplitudes of the inputs and their relative phase. The constrained optimization problem

may be solved using analytical or numerical methods. The method is used for input optimization of two 3-DOF systems with three and two inputs. The use of averaging techniques for selection of physical parameters in input optimization of the mechanical control systems is also discussed.

6.1 Introduction

The actuators for mechanical control systems provide the necessary forces and moments to generate desired motions. The mass of the actuators often comprise a considerable part of the total mass of the systems (global mass). The size and mass of an actuator scales with its maximum output. Using control forces with larger amplitudes, one needs to use bigger actuators which increases the global mass of the system. Therefore besides studying the optimization of consumed energy or time by the system [Bobrow et al., 1985; Berman and Wang, 2007; Gregory et al., 2012], using smaller actuators with less mass to reduce the total mass of the system has always been a design objective in robotics [Chedmail and Gautier, 1990]. For some mechanical control systems, such as flying or swimming robots, the mass of the system is critical for its operation. For biomimetic systems such as flapping wing micro air vehicles (FWMAV), decreasing the global mass of the system is an important goal of the design [Karpelson et al., 2008].

In this chapter using averaging technique and the results obtained in Section 3.4, optimization of the inputs' amplitudes for a class of mechanical control systems with high-frequency, high-

amplitude zero-mean inputs is addressed. We show that for a mechanical control system, of all zero-mean, periodic inputs (e.g., square, sine, triangular, etc. waveforms), which generate the same averaged dynamics for the system, the periodic square input uses the minimum amplitude possible. The main contributions of this work is to show that the amplitudes of the inputs will be minimum if using zero-mean, periodic square inputs, and to transform the optimization problem into a classical constrained optimization one [Bertsekas, 1982; Burns, 2014]. A set of algebraic nonlinear equality constraints with independent parameters are derived which must be satisfied by the optimum inputs. The independent parameters are the amplitudes of the square inputs, and their relative phases. Solving the constrained optimization problem one gets the necessary amplitude of each square input and the phase shift between the inputs which result in smallest amplitudes. Also the physical design parameters selection for input optimization of mechanical control systems is discussed.

This chapter is organized as follows. In Section 6.2 the effect of the shape of waveform of the input is addressed and the optimization problem for a 1-DOF system is solved. Input optimization of higher-dimensional systems, along with two examples, is presented in Section 6.3. In Section 6.4 selection of design parameters for input optimization of mechanical control systems using averaging is addressed. Finally in Section 6.5, the results and conclusions are mentioned in brief.

6.2 Input Optimization of 1-DOF Control-Affine Systems

In this section the optimization of the input amplitude for a 1-DOF mechanical control-affine system is discussed. Consider the 1-DOF control affine system with one input

$$\ddot{q} = f(q, \dot{q}) + g(q)u_1(t), \quad q(0) = q_0,\ \dot{q}(0) = v_0 \tag{6.1}$$

Suppose that f and g contain twice differentiable polynomials in q, and the polynomials in f are homogeneous in $\dot{q}$ of degree two or less. System (6.1) is the special form of (3.10) for $m = n = 1$.

Using $\boldsymbol{x} = (q,\ \dot{q})^T$ as the state vector and the input $u_1(t) = \omega v_1(\omega t)$, where $v_1(t)$ is a T-periodic, zero-mean function, the first order system can be written as

$$\dot{\boldsymbol{x}} = \boldsymbol{Z}(\boldsymbol{x}) + \boldsymbol{Y}(\boldsymbol{x})\omega v_1(\omega t), \quad \boldsymbol{x}(0) = \boldsymbol{x}_0 = (q_0, v_0)^T \tag{6.2}$$

where $\boldsymbol{Z}(\boldsymbol{x}) = (\dot{q},\ f(q, \dot{q}))^T$ and $\boldsymbol{Y}(\boldsymbol{x}) = (0,\ g(q))^T$. The goal is to find the signal $v_1(t)$ with the minimum possible amplitude for the system (6.2) to have a stable periodic orbit in a $O(\epsilon)$ neighborhood of a point $\boldsymbol{x}_{\mathrm{e}} = (q_{\mathrm{e}},\ 0)$, where $\epsilon = \frac{1}{\omega}$.

As mentioned in Section 3.3, for any two T-periodic, zero-mean functions $v_i(t)$ and $v_j(t)$, we

define the input parameters κ_i, λ_{ij}, and μ_{ij} as

$$\kappa_i = \frac{1}{T}\int_0^T \int_0^t v_i(\tau)d\tau dt \tag{6.3}$$

$$\lambda_{ij} = \frac{1}{T}\int_0^T \left(\int_0^t v_i(\tau)d\tau\right)\left(\int_0^t v_j(\tau)d\tau\right) dt \tag{6.4}$$

and

$$\mu_{ij} = \frac{1}{2}(\lambda_{ij} - \kappa_i\kappa_j). \tag{6.5}$$

Using Theorem 3.3.1, the average dynamics of (6.2) can be written as

$$\dot{\bar{\boldsymbol{x}}} = \boldsymbol{Z}(\bar{\boldsymbol{x}}) - \mu_{11}\langle \boldsymbol{Y} : \boldsymbol{Y}\rangle(\bar{\boldsymbol{x}}), \quad \bar{\boldsymbol{x}}(0) = \bar{\boldsymbol{x}}_0 = \boldsymbol{x}_0 + \kappa_1 \boldsymbol{Y}(\boldsymbol{x}_0) \tag{6.6}$$

where κ_1 and μ_{11} are determined using (6.3) through (6.5). According to averaging theorem, if the averaged dynamics (6.6) has a stable equilibrium point $\boldsymbol{x}_{\mathrm{e}}$, then the original system (6.2) has a stable periodic orbit about that point. Therefore the point $\boldsymbol{x}_{\mathrm{e}}$ must be an equilibrium point of the averaged dynamics (6.6), i.e.,

$$\boldsymbol{Z}(\boldsymbol{x}_{\mathrm{e}}) - \mu_{11}\langle \boldsymbol{Y} : \boldsymbol{Y}\rangle(\boldsymbol{x}_{\mathrm{e}}) = \boldsymbol{0} \tag{6.7}$$

The set of equations (6.7) consists of two algebraic equations where the first one is satisfied

for $\bar{\boldsymbol{x}} = \boldsymbol{x}_{\mathrm{e}}$. The second of these equations can be shown as

$$f(q_{\mathrm{e}}, 0) - \mu_{11} h(q_{\mathrm{e}}) = 0 \tag{6.8}$$

where $h(\boldsymbol{x}) = \boldsymbol{e}_2 \cdot \langle \boldsymbol{Y} : \boldsymbol{Y} \rangle(\boldsymbol{x})$, and $\boldsymbol{e}_i$ is the i^{th} unit vector of the standard basis of Euclidean space. In other words, $h(\boldsymbol{x})$ is the second element of the symmetric product $\langle \boldsymbol{Y} : \boldsymbol{Y} \rangle(\boldsymbol{x})$. Therefore for the averaged dynamics to have an equilibrium point $\boldsymbol{x}_{\mathrm{e}}$, the input $v(t)$ must be chosen such that

$$\mu_{11} = \frac{f(q_{\mathrm{e}}, 0)}{h(q_{\mathrm{e}})} \tag{6.9}$$

Evidently there are infinite number of T-periodic, zero-mean functions $v_1(t)$ with different waveforms and amplitudes which satisfy (6.9). Figure 6.1 shows three of such functions $v_1(t)$, namely square, sine, and triangular, with $T = 1$ and $\mu_{11} = 1$. From Figure 6.1 it is evident that the square function generates the same input parameter $\mu_{11} = 1$ with smaller amplitude compared to the other two functions. In the following two theorems it is shown that this is always correct.

Theorem 6.2.1 *: For any T-periodic, zero mean function $v(t)$, there exists a phase $0 \leq \phi_0 \leq T$ such that for the function $w(t) = v(t + \phi_0)$,*

$$\kappa_s = \frac{1}{T} \int_0^T \int_0^t w(\tau) d\tau dt = 0.$$

Proof: See Appendix C.

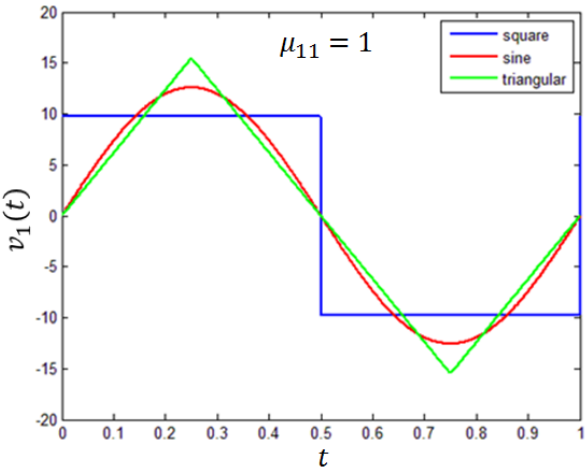

Figure 6.1: Three T-periodic, zero-mean functions with different amplitudes and the input parameter $\mu_{11} = 1$

Remark 6.2.2 *: According to Theorem 3.4.1, for any value of ϕ_0, the input parameters μ and μ_s determined using* (6.5) *for $v(t)$ and $w(t) = v(t + \phi_0)$ respectively, are equal (i.e., $\mu = \mu_s$). One consequence of Theorem 6.2.1 is that for the time-periodic system* (6.2)*, one can always determine a phase shifted input $w_1(t) = v_1(t + \phi_0)$ such that when applying that input, the averaged dynamics* (6.6) *starts from the same initial conditions as the system* (6.2) *itself. Note that the initial conditions of the averaged dynamics* (6.6) *are $\bar{\boldsymbol{x}}_0 = \boldsymbol{x}_0 + \kappa_1 \boldsymbol{Y}(\boldsymbol{x}_0)$.*

Theorem 6.2.3 *: Of all T-periodic, zero-mean functions $v(t)$ with the same amplitude B, the T-periodic square function*

$$S_B(t) = \begin{cases} B & ; \quad 0 \leq t \leq \frac{T}{2} \\ -B & ; \quad \frac{T}{2} < t \leq T \end{cases}$$

results in the largest value μ, as determined using (6.5)*.*

Proof: According to Theorem 6.2.1, all T-periodic, zero-mean functions $v(t)$ with the same amplitude B can be shifted by an amount ϕ, with $0 \leq \phi \leq T$, such that $\kappa_s = 0$ (where κ_s is the value of κ for the phase-shifted function) without affecting the value of μ. That is, $\mu = \mu_s = \frac{1}{2}\lambda_s$. (Note that the amount of phase shift ϕ required to make $\kappa_s = 0$ depends on the particular choice of function $v(t)$.) Rather than consider each function $v(t)$, comparing its value of μ, one may consider the phase-shifted functions $w(t) = v(t + \phi)$ and compare values of λ_s. Defining $A_s(t) = \int_0^t w(\tau)d\tau$, and using equation (6.4), one obtains

$$\lambda_s = \int_0^T A_s^2(t)dt$$

The magnitude of the zero-mean square function $S_B(t)$ is maximum for all $t \in \mathbb{R}$, except at isolated times. Thus, for all T-periodic, zero-mean functions $v(t)$ with the same amplitude B, the square function $S_B(t)$ has the maximum absolute area $A(t)$ under the curve t-$v(t)$ for any $t \in [0, T]$, and so has maximum $A_s^2(t)$. Of all functions $v(t)$ with equal amplitude, the square function $S_B(t)$ has the maximum λ_s, and therefore has the maximum $\mu_s = \mu$. □

Remark 6.2.4 *: Theorem 6.2.3 may be restated as follows: Of all T-periodic, zero-mean functions with equal values of μ determined using* (6.5)*, the T-periodic square function $S_B(t)$ has the minimum possible amplitude B.*

Therefore using Theorem 6.2.3 and Remark 6.2.4, for all T-periodic, zero-mean functions $v_1(t)$ which satisfy (6.9), the square function $S_B(t)$ has the minimum amplitude. For function $S_B(t)$ with period T and amplitude B, one can determine the input parameter $\mu_{square} = \frac{T^2B^2}{96}$.

For any other T-periodic, zero-mean function with the same amplitude B, $\mu_{11} < \mu_{square}$.

Note that in the system (6.10) if the amplitude of the input $v_1(t)$ is B_1, the total amplitude of the input $u_1(t)$ is ωB_1. The effect of the frequency ω is in the error of the response of the averaged dynamics compared to the response of the original time-periodic system.

6.3 Input Optimization of Higher-Dimensional Systems

Consider the n-DOF ($n > 1$) mechanical control-affine system with m independent inputs

$$\ddot{\boldsymbol{q}} = \boldsymbol{f}(\boldsymbol{q}, \dot{\boldsymbol{q}}) + \sum_{i=1}^{m} \boldsymbol{g}_i(\boldsymbol{q}) u_i(t) \tag{6.10}$$

with the high-frequency, high-amplitude inputs $u_i(t) = \omega v_i(t)$, and its first order form

$$\dot{\boldsymbol{x}} = \boldsymbol{Z}(\boldsymbol{x}) + \sum_{i=1}^{m} \boldsymbol{Y}_i(\boldsymbol{x}) \left(\frac{1}{\epsilon}\right) v_i\left(\frac{t}{\epsilon}\right) \tag{6.11}$$

as mentioned in Section 3.3. The goal is to determine inputs $v_i(t)$, $i \in \{1, \ldots, m\}$, with amplitudes B_i, for the system to have a stable periodic orbit about a point $\boldsymbol{x}_{\mathrm{e}} = (\boldsymbol{q}_{\mathrm{e}}^T, \boldsymbol{0}_{1\times n})^T$ while minimizing the cost function $J = \sum_{i=1}^{m} B_i^2$. For the system (6.11) to have a stable periodic orbit about the point $\boldsymbol{x}_{\mathrm{e}}$, the point must be a stable equilibrium point of its averaged dynamics. As discussed in Section 3.3, the averaged dynamics of the system 6.11 is in the

form

$$\dot{\bar{\boldsymbol{x}}} = \boldsymbol{Z}(\bar{\boldsymbol{x}}) - \sum_{i,j=1}^{m} \mu_{ij} \langle \boldsymbol{Y}_i : \boldsymbol{Y}_j \rangle (\bar{\boldsymbol{x}}) \tag{6.12}$$

with μ_{ij} determined using (6.3) through (6.5). Therefore $\boldsymbol{x}_{\mathrm{e}}$ must satisfy

$$\boldsymbol{Z}(\boldsymbol{x}_{\mathrm{e}}) - \sum_{i,j=1}^{m} \mu_{ij} \langle \boldsymbol{Y}_i : \boldsymbol{Y}_j \rangle (\boldsymbol{x}_{\mathrm{e}}) = \boldsymbol{0}_{2n\times 1} \tag{6.13}$$

The first n equations of the $2n$ equations (6.13) are satisfied automatically, based on the structure of the system, and the last n equations can be written as

$$\sum_{i,j=1}^{m} \mu_{ij} \boldsymbol{h}_{ij}(\boldsymbol{q}_{\mathrm{e}}) - \boldsymbol{f}(\boldsymbol{q}_{\mathrm{e}}, \boldsymbol{0}) = \boldsymbol{0}_{n\times 1} \tag{6.14}$$

where $\boldsymbol{h}_{ij}(\boldsymbol{q}_{\mathrm{e}})$ is the $n \times 1$ vector of the last n components of $\langle \boldsymbol{Y}_i : \boldsymbol{Y}_j \rangle (\boldsymbol{x}_{\mathrm{e}})$. Note that due to the structure of the system considered, the first n components of the symmetric product $\langle \boldsymbol{Y}_i : \boldsymbol{Y}_j \rangle (\boldsymbol{x})$ are zero.

Since $\mu_{ij} = \mu_{ji}$, $i, j \in \{1, \ldots, m\}$, (see (3.15)), apparently the set of equations (6.14) consists of n algebraic equations and $\frac{m(m+1)}{2}$ unknowns μ_{ij}, $i, j \in \{1, \ldots, m\}$, $i \leq j$. But the unknowns μ_{ij}, $i \leq j$, are not all independent. Each of the parameters μ_{ii}, $i \in \{1, \ldots, m\}$, depends on the waveform and amplitude of the input $v_i(t)$ and are independent (therefore, m unknowns). But besides waveform and amplitude, parameters μ_{ij}, $i < j$, depend on the relative phase between $v_i(t)$ and $v_j(t)$ also.

The relative phases of the inputs are not all independent. For example, if the relative phase

of the inputs $v_1(t)$ and $v_2(t)$ is ϕ_{21}, and that of the inputs $v_1(t)$ and $v_3(t)$ is ϕ_{31}, the relative phase of the inputs $v_2(t)$ and $v_3(t)$ is determined as $\phi_{32} = \phi_{31} - \phi_{21}$, and is not independent. In general, if the relative phases of all the inputs $v_i(t)$, $i \in \{2, \ldots, m\}$, with $v_1(t)$ are known, the relative phase of any two inputs $v_i(t)$ and $v_j(t)$, $i, j \in \{2, \ldots, m\}$, are also known. And therefore there are only $m-1$ independent μ_{ij}, $i < j$ to be determined from (6.14). So, in total there are $2m-1$ independent parameters μ_{ij} to be determined. We assume $2m-1 > n$ such that (6.14) has more than one set of solutions (in general, infinite sets of solutions).

From the definition of symmetric product (see (3.16)) it is evident that $\boldsymbol{h}_{ij} = \boldsymbol{h}_{ji}$, $i, j \in \{1, \ldots, m\}$. Also from the structure of the class of systems considered in (6.10), the vector fields of the symmetric products $\langle \boldsymbol{Y}_i : \boldsymbol{Y}_j \rangle$, are only functions of the generalized coordinates $\boldsymbol{q}$ (and not the velocities $\dot{\boldsymbol{q}}$). Therefore the vector fields $\boldsymbol{h}_{ij}$ are also functions of the generalize coordinates only. Defining

$$\boldsymbol{a}_{ij} = \begin{cases} \boldsymbol{h}_{ij}(\boldsymbol{q}_{\mathrm{e}}) \ ; \ i = j \\ 2\boldsymbol{h}_{ij}(\boldsymbol{q}_{\mathrm{e}}) \ ; \ i \neq j \end{cases}$$

and $\boldsymbol{b} = -\boldsymbol{f}(\boldsymbol{q}_{\mathrm{e}}, \boldsymbol{0})$, the set of equations (6.14) can be rewritten in the form

$$\sum_{i,j=1 \ (i \leq j)}^{m} \boldsymbol{a}_{ij}\mu_{ij} + \boldsymbol{b} = \boldsymbol{0} \tag{6.15}$$

Suppose that μ_{ij}^*, $i, j \in \{1, \ldots, m\}$, $i \leq j$, are a set of solutions of equation (6.15). Consider a set of T-periodic, zero-mean functions $v_i(t)$ which generate $\mu_{ij} = \mu_{ij}^*$, i.e., defining $A_i(t) =$

$\int_0^t v_i(\tau)d\tau$

$$\frac{1}{2}\left(\frac{1}{T}\int_0^T A_i^2(t)dt - \left(\frac{1}{T}\int_0^T A_i(t)dt\right)^2\right) = \mu_{ii}^* \ , \ i \in \{1,\ldots,m\}$$

and

$$\frac{1}{2}\left(\frac{1}{T}\int_0^T A_i(t)A_j(t)dt - \left(\frac{1}{T}\int_0^T A_i(t)dt\right)\left(\frac{1}{T}\int_0^T A_j(t)dt\right)\right) = \mu_{ij}^* \ , \ i,j \in \{1,\ldots,m\}, i<j$$

According to Theorem 6.2.3, if one chooses $v_i(t)$ as T-periodic zero-mean square function $S_{B_i}(t)$ with an amplitude of $B_i = \frac{\sqrt[4]{6\mu_{ii}^*}}{T}$, then the amplitude B_i is less than the amplitude of any other T-periodic zero-mean function chosen as $v_i(t)$. In addition, choosing the inputs $v_i(t)$ as square functions allows the biggest possible range to be chosen for μ_{ij}, $i \neq j$, by phase shifting between the inputs. To make this last statement precise, we present the following theorem.

Theorem 6.3.1 *For all T-periodic, zero-mean functions $v_1(t)$ and $v_2(t)$ with a certain $\mu_{11} \geq 0$ and $\mu_{22} \geq 0$*

1. $|\mu_{12}| \leq \sqrt{\mu_{11}\mu_{22}}$,

2. *the square functions $S_{B_1}(t)$ and $S_{B_2}(t)$ allow the greatest freedom to adjust μ_{12} by modulating the relative phase of $v_1(t)$ and $v_2(t)$.*

Proof: See Appendix D.

The optimization goal can be restated as to minimize $J = \sum_{i=1}^{m} B_i^2$ under n constraints (6.15),

therefore a constrained optimization problem [Bertsekas, 1982; Burns, 2014]. The problem may be solved using the method of Lagrange multipliers and redefining the cost function ψ as

$$\psi = \sum_{i=1}^{m} B_i^2 + \sum_{k=1}^{n} \zeta_k \left(\sum_{i,j=1\ (i\leq j)}^{m} a_{ij_k}\mu_{ij} + b_k \right) \tag{6.16}$$

where a_{ij_k} and b_k are the k^{th} elements of the vectors $\boldsymbol{a}_{ij}$, and $\boldsymbol{b}$ respectively, and ζ_k, $k \in \{1, \ldots, n\}$, are the Lagrange multipliers.

Using Theorems 6.2.3 and 6.3.1 it is evident that choosing all the inputs as square functions has two advantages. First it results in smaller amplitudes, and second it provides the biggest possible range for μ_{ij}, $i, j \in \{1, \ldots, m\}$, $i < j$, to be chosen by phase shifting between inputs. (It should be noted that square phase functions may introduce practical challenges related to the discontinuity of the input signals, excitation of unmodeled dynamic modes, etc.) Therefore we choose $v_i(t)$, $i \in \{1, \ldots, m\}$, as square functions with amplitudes B_i, and try to find their relative phases to minimize $\sum_{i=1}^{m} B_i^2$.

The cost function ψ in (6.16) may be rewritten as

$$\psi = \sum_{i=1}^{m} B_i^2 + \sum_{k=1}^{n} \zeta_k \left(\sum_{i=1}^{m} a_{ii_k}\mu_{ii} \right) + \sum_{k=1}^{n} \zeta_k \left(\sum_{i,j=1\ (i<j)}^{m} a_{ij_k}\mu_{ij} + b_k \right) \tag{6.17}$$

Since for T-periodic square function with an amplitude of B_i, $\mu_{ii} = \frac{T^2}{96} B_i^2$, the cost func-

tion (6.17) may be expressed as

$$\psi = \sum_{i=1}^{m} \left(1 + \sum_{k=1}^{n} c_{i_k}\zeta_k\right) B_i^2 + \sum_{k=1}^{n} \zeta_k \left(\sum_{i,j=1\ (i<j)}^{m} a_{ij_k}\mu_{ij} + b_k\right) \tag{6.18}$$

where $c_{i_k} = \frac{T^2}{96} a_{ii_k}$, and $|\mu_{ij}| \leq \frac{T^2}{96} |B_i B_j|$, $i, j \in \{1, \ldots, m\}$, $i < j$.

As mentioned earlier the parameters μ_{ij}, $i, j \in \{1, \ldots, m\}$, $i < j$, are not all independent. To replace the dependent parameters μ_{ij} with independent ones, they may be replaced by the relative phases of the inputs. Suppose that the phase of each input $v_i(t)$, $i \in \{1, \ldots, m\}$ with $v_1(t)$ is ϕ_i (and so $\phi_1 = 0$). Then the relative phase of $v_j(t)$ and $v_i(t)$ is $\phi_{ij} = \phi_j - \phi_i$, $i, j \in \{1, \ldots, m\}$. For two T-periodic square functions $v_i(t)$ and $v_j(t)$with amplitudes B_i and B_j respectively, and a relative phase of $0 \leq \phi_{ij} \leq \frac{T}{2}$, it can be shown that

$$\mu_{ij} = \frac{T^2 B_i B_j}{96}(32\phi_{ij}^3 - 24\phi_{ij}^2 + 1) \tag{6.19}$$

Therefore using $\phi_{ij} = \phi_j - \phi_i$ in (6.19) and replacing μ_{ij} in (6.18), the cost function ψ may be written in terms of $n + 2m - 1$ independent variables B_i, $i \in \{1, \ldots, m\}$, ϕ_j, $j \in \{2, \ldots, m\}$, and the Lagrange multipliers ζ_k, $k \in \{1, \ldots, n\}$ as

$$\begin{aligned}\psi = &\sum_{i=1}^{m} \left(1 + \sum_{k=1}^{n} c_{i_k}\zeta_k\right) B_i^2 \\ &+ \sum_{k=1}^{n} \zeta_k \left(\sum_{i,j=1\ (i<j)}^{m} \frac{T^2}{96} a_{ij_k} B_i B_j \left(32(\phi_j - \phi_i)^3 - 24(\phi_j - \phi_i)^2 + 1\right) + b_k\right)\end{aligned} \tag{6.20}$$

where $\phi_1 = 0$. The extrema of the cost function are its stationary points which may be found using $n + 2m - 1$ equations

$$\begin{cases} \frac{\partial \psi}{\partial B_i} = 0 \ , \ i \in \{1, \ldots, m\} \\ \frac{\partial \psi}{\partial \phi_i} = 0 \ , \ i \in \{2, \ldots, m\} \\ \frac{\partial \psi}{\partial \zeta_k} = 0 \ , \ k \in \{1, \ldots, n\} \end{cases} \tag{6.21}$$

Note that the set of equations (6.21) may not have a solution inside the boundaries, or the solutions may be the local extrema only, not the global ones. To find the global extrema one should also check for possible solutions on the boundaries. Since the solutions on the boundaries, if they exist, usually are not local extrema, they will not be a solution of (6.21).

6.3.1 Example 1: Input optimization of a 3-DOF system

Consider the 3-DOF system with three inputs

$$\begin{cases} \ddot{q}_1 = & -0.5\dot{q}_1^2 + \dot{q}_2^2 + 0.5\dot{q}_3^2 - 2\dot{q}_1\dot{q}_2 - 2.5\dot{q}_1\dot{q}_3 + 0.5\dot{q}_2\dot{q}_3 - 3.5\dot{q}_1 - \dot{q}_2 + \dot{q}_3 - 5q_1 - 0.02 \\ & +(q_1 + q_2 + q_3 - 1)u_1(t) \\ \ddot{q}_2 = & 1.5\dot{q}_1^2 + 1.5\dot{q}_3^2 - 0.5\dot{q}_1\dot{q}_2 - 1.5\dot{q}_1\dot{q}_3 - 2\dot{q}_2\dot{q}_3 + \dot{q}_1 - 3.5\dot{q}_2 + \dot{q}_3 - 5q_2 - 0.3 \\ & +(q_1 - q_2 + q_3 - 1)u_2(t) \\ \ddot{q}_3 = & \dot{q}_1^2 + 0.5\dot{q}_2^2 + 1.5\dot{q}_3^2 - 0.5\dot{q}_1\dot{q}_2 + 1.5\dot{q}_1\dot{q}_3 + 0.5\dot{q}_2\dot{q}_3 - \dot{q}_1 - 4.5\dot{q}_3 - 5q_3 - 0.15 \\ & +(q_1 + q_2 + 2q_3 + 1)u_3(t) \end{cases} \tag{6.22}$$

where $u_i(t) = \omega v_i(\omega t)$, $i \in \{1, 2, 3\}$, are high-frequency, high-amplitude periodic inputs. The goal is for the system to have a stable periodic orbit in an $O(\epsilon) = O(\frac{1}{\omega})$ neighborhood of the origin, when using inputs with the minimum possible amplitudes.

Defining the state vector $\boldsymbol{x} = (q_1, q_2, q_3, \dot{q}_1, \dot{q}_2, \dot{q}_3)^T$, the dynamic equations (6.22) can be written as six first order equations.

Considering $v_i(t)$, $i \in \{1, 2, 3\}$, as T-periodic, square functions with amplitudes of B_i and using Theorem 3.3.1, the averaged dynamics of (6.22) can be determined. Since the averaged equations are complicated, they are not shown here. For the original system to have a stable periodic orbit around the origin, the origin must be an equilibrium point of the averaged

system. Setting $\boldsymbol{x} = \mathbf{0}$ in the averaged dynamics, the three constraint equations may be determined as

$$\begin{cases} B_1^2 + 2B_2^2 + B_3^2 - 64\Delta_{22}B_1B_2 + 96\Delta_{33}B_1B_3 - \Delta_{23}B_2B_3 - 1.92 = 0 \\ 3B_1^2 - 2B_2^2 + 3B_3^2 + 32\Delta_{22}B_1B_2 + 96\Delta_{33}B_1B_3 + 2\Delta_{23}B_2B_3 - 28.8 = 0 \\ 2B_1^2 + B_2^2 - B_3^2 - 32\Delta_{22}B_1B_2 - 32\Delta_{33}B_1B_3 + \Delta_{23}B_2B_3 - 14.4 = 0 \end{cases} \tag{6.23}$$

where

$$\Delta_{22} = (\phi_2 - 0.68)(\phi_2 - 0.25)(\phi_2 + 0.18)$$

$$\Delta_{33} = (\phi_3 - 0.68)(\phi_3 - 0.25)(\phi_3 + 0.18)$$

$$\Delta_{23} = 1 - 24(\phi_2 - \phi_3)^2 - 32(\phi_2 - \phi_3)^3.$$

Using the constraint equations (6.23),the cost function ψ can be determined from (6.20). Now one may use mathematical software and numerical methods to find the global minimum of the determined cost function when $0 \leq \phi_i \leq \frac{T}{2}$, $i \in \{2, 3\}$. Also using the linearization of the averaged dynamics about the origin, one must check the stability of the origin for the optimum solution. For this example, using both Mathematica and *fmincon* of Matlab, and using $T = 1$, the optimum solution was determined as $B_1 = 2.876$, $B_2 = 0.675$, $B_3 = 1.88$, $\phi_2 = 0.09$, and $\phi_3 = 0.33$. For these optimum values the origin is a stable equilibrium point for the averaged dynamics. The simulation results of the original and averaged dynamics using the optimum inputs are shown in Figure 6.2. The

initial conditions of the simulations are $\boldsymbol{x}(0) = (0.2, 0.2, -0.2, 0, 0, 0)^T$ and the frequency is $\omega = 3\pi$. Note that the initial conditions of the averaged dynamics are different (in this case $\bar{\boldsymbol{x}}(0) = (0.2, 0.2, -0.2, -0.575, -0.131, -0.15)^T$).

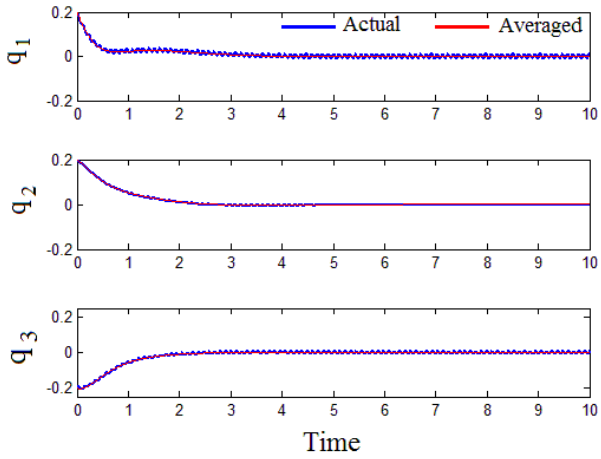

Figure 6.2: Time histories of the original and averaged systems when using the optimum inputs

Remark 6.3.2 *: The equilibrium point $\boldsymbol{x}_e$ of the averaged dynamics may be unstable for the determined optimum parameter. In that case the requirements for the stability of the equilibrium point may be considered as extra inequality constraints in the optimization problem.*

6.3.2 Example 2: Planar two-link mechanism on a cart

Consider the planar two-link mechanism on a cart, as depicted in Figure 6.3. Each link is a uniform bar with mass m_i, $i \in \{1, 2\}$, length l_i, and mass moment of inertia $I_i = \frac{1}{12} m_i l_i^2$ about its center of mass. The system is a 3-DOF system with two inputs and moves in a horizontal

plane, therefore gravity does not affect the motion. The inputs are the force $F(t)$ acting on the cart and the torque $\tau(t)$ acting on the first link. We assume the system is subject to linear damping with coefficients of k_{d_1} and k_{d_2} in the first and second joints, respectively. Considering $\boldsymbol{q} = (x, \theta_1, \theta_2)^T$ as the vector of the generalized coordinates, the goal is for the system to have a periodic orbit in a $O(\epsilon)$ neighborhood of a desired configuration $\boldsymbol{q}_{\mathrm{d}} = (x_{\mathrm{d}}, \theta_{d_1}, \theta_{d_2})^T$, while using inputs with minimum possible amplitudes.

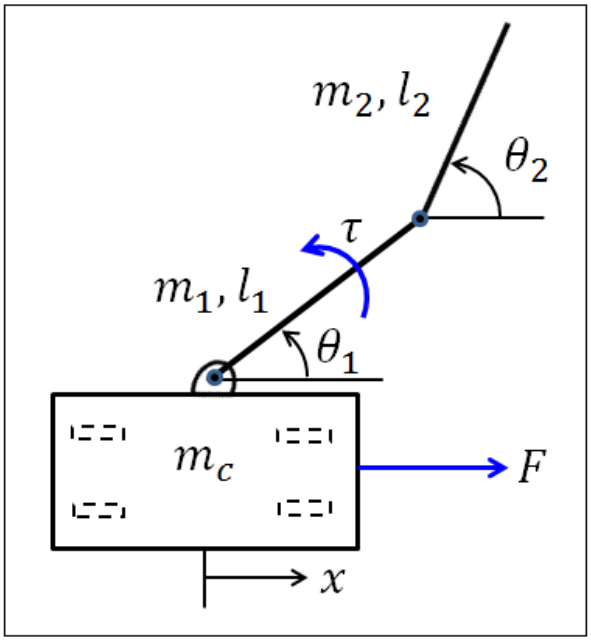

Figure 6.3: Two-link mechanism on a cart

Using Euler-Lagrange equations [Greenwood, 2003], the dynamic equations of the system can be written in the form of

$$\boldsymbol{M}(\boldsymbol{q})\ddot{\boldsymbol{q}} = \boldsymbol{f}(\boldsymbol{q}, \dot{\boldsymbol{q}}) + \boldsymbol{F}_c(t) \tag{6.24}$$

where considering m_c as the mass of the cart, the generalized inertia matrix $\boldsymbol{M}$ is

$$\boldsymbol{M} = \begin{pmatrix} m_c + m_1 + m_2 & -\frac{1}{2}(m_1 + 2m_2)l_1 \sin\theta_1 & -\frac{1}{2}m_2 l_2 \sin\theta_2 \\ -\frac{1}{2}(m_1 + 2m_2)l_1 \sin\theta_1 & I_1 + \frac{1}{4}(m_1 + 4m_2)l_1^2 & \frac{1}{2}m_2 l_1 l_2 \cos(\theta_1 - \theta_2) \\ -\frac{1}{2}m_2 l_2 \sin\theta_2 & \frac{1}{2}m_2 l_1 l_2 \cos(\theta_1 - \theta_2) & I_2 + \frac{1}{4}m_2 l_2^2 \end{pmatrix} \tag{6.25}$$

and

$$\boldsymbol{f} = \begin{pmatrix} \frac{1}{2}\big((m_1 + 2m_2)l_1\dot{\theta}_1^2 \cos\theta_1 + m_2 l_2 \dot{\theta}_2^2 \cos\theta_2\big) \\ -\frac{1}{2}m_2 l_1 l_2 \dot{\theta}_2^2 \sin(\theta_1 - \theta_2) - k_{d_1}\dot{\theta}_1 + k_{d_2}(\dot{\theta}_2 - \dot{\theta}_1) \\ \frac{1}{2}m_2 l_1 l_2 \dot{\theta}_1^2 \sin(\theta_1 - \theta_2) - k_{d_2}(\dot{\theta}_2 - \dot{\theta}_1) \end{pmatrix}$$

and the vector of inputs

$$\boldsymbol{F}_c(t) = \begin{pmatrix} F(t) \\ \tau(t) \\ 0 \end{pmatrix}.$$

Consider the inputs as

$$\begin{aligned} F(t) &= -k_p(x - x_{\mathrm{d}}) - k_{\mathrm{d}}\dot{x} + \omega v_1(\omega t) \\ \tau(t) &= \tau_s - k_{p_1}(\theta_1 - \theta_{d_1}) + \omega v_2(\omega t) \end{aligned} \tag{6.26}$$

where $v_1(t)$ and $v_2(t)$ are T-periodic, zero-mean functions with amplitudes of F_0 and τ_0 respectively, k_p, k_{p_1}, and k_{d} are control parameters, and τ_s is a nonzero constant. (The purpose of using the parameter τ_s will be explained in Section 7.1.)

Using the state vector $\boldsymbol{x} = (\boldsymbol{q}^T, \dot{\boldsymbol{q}}^T)^T$, one may transform the equations of motion of the system into (6.11) with $m = 2$, and determine the averaged dynamics using Theorem 3.3.1. The averaged dynamics is in the form of

$$\dot{\bar{\boldsymbol{x}}} = \boldsymbol{Z}(\bar{\boldsymbol{x}}) - \sum_{i,j=1}^{2} \mu_{ij} \langle \boldsymbol{Y}_i : \boldsymbol{Y}_j \rangle (\bar{\boldsymbol{x}}) \tag{6.27}$$

where $\boldsymbol{Y}_i$ is the i^{th} column of $\boldsymbol{M}^{-1}$, and

$$\boldsymbol{Z}(\boldsymbol{x}) = \begin{pmatrix} \dot{\boldsymbol{q}} \\ \boldsymbol{M}^{-1}(\boldsymbol{q})\big(\boldsymbol{f}(\boldsymbol{q}, \dot{\boldsymbol{q}}) + \boldsymbol{g}(\boldsymbol{q}, \dot{\boldsymbol{q}})\big) \end{pmatrix}$$

where

$$\boldsymbol{g} = \begin{pmatrix} -k_p(x - x_{\text{d}}) - k_{\text{d}}\dot{x} \\ \tau_s - k_{p_1}(\theta_1 - \theta_{d_1}) \\ 0 \end{pmatrix}.$$

Using the inputs (6.26), the system may possess stable periodic orbit in $O(\frac{1}{\omega})$ neighborhood of $\boldsymbol{q}_{\text{d}}$. This happens if the point $\boldsymbol{x}_{\text{e}} = (\boldsymbol{q}_{\text{d}}^T, \boldsymbol{0}_{1\times 3})^T$ is a stable equilibrium point of the averaged dynamics. For the point $\boldsymbol{x}_{\text{e}}$ to be an equilibrium point of the averaged system, it must satisfy

$$\boldsymbol{Z}(\boldsymbol{x}_{\text{e}}) - \sum_{i,j=1}^{2} \mu_{ij} \langle \boldsymbol{Y}_i : \boldsymbol{Y}_j \rangle (\boldsymbol{x}_{\text{e}}) = \boldsymbol{0} \tag{6.28}$$

The set of algebraic equations (6.28) contains six equations, the first three being satisfied automatically because of the system structure. So for the point $\boldsymbol{q}_{\text{d}}$ to be an equilibrium

point of the averaged dynamics, one needs to satisfy the last three equations of (6.28).

To drive the system to the desired coordinates $\boldsymbol{q}_{\mathrm{d}}$ one should choose a value for τ_s, and find μ_{ij}, $i,j \in \{1,2\}$, to satisfy equations (6.28). Depending on the physical parameters of the system, for some values of τ_s there may be no acceptable solution for μ_{ij} (note that $\mu_{ii} > 0$).

One important observation is that only two of the last three equations of (6.28) are independent and need to be satisfied. Therefore there is a set of two independent equations and three unknowns μ_{ij}, $i,j \in \{1,2\}$ (note that $\mu_{ij} = \mu_{ji}$), and therefore there is a one-parameter family of solutions. There is thus parametric freedom available for further optimization.

Consider the case where the links have mass per unit length ρ_m. For the physical parameters

$$m_c = 1 \text{ kg},\ \rho_m = 1 \text{ kg/m},\ l_1 = 0.8 \text{ m},\ l_2 = 1 \text{ m}$$

$$k_p = 5,\ k_{\mathrm{d}} = 2,\ k_{p_1} = 10,\ k_{d_1} = 2,\ k_{d_2} = 1$$

and for $x_{\mathrm{d}} = 0$, $\theta_{d_1} = -\frac{\pi}{9}$ rad, $\theta_{d_2} = \frac{\pi}{9}$ rad, and $\tau_s = 1$ N.m, the set of equations (6.28) to be satisfied are

$$\begin{cases} 0.2271\mu_{11} - 0.6111\mu_{12} - 1.5465\mu_{22} &= -0.4727 \\ 1.0179\mu_{11} - 3.1218\mu_{12} - 5.9772\mu_{22} &= -2.3732 \\ 1.4390\mu_{11} - 3.0137\mu_{12} - 11.9323\mu_{22} &= -2.4241 \end{cases} \tag{6.29}$$

Since the last set of equations contain only two independent equations and three unknowns,

there are infinite number of solutions for the inputs $v_1(t)$ and $v_2(t)$ to be chosen. Using $F_0^2 + \tau_0^2$ as the cost function to be minimized, according to Theorem 6.2.3 one must choose the inputs as T-periodic, zero-mean square functions with amplitudes of F_0 and τ_0, and a relative phase of ϕ. Considering square inputs and $T = 2\pi$ s, and using the optimization procedure discussed in Section 6.3 one determines $F_0 = 4.336$ N, $\tau_0 = 1.202$ N.m, and $\phi = 0$ as the optimum inputs. The averaged system is then linearized about the desired equilibrium point $\boldsymbol{x}_e$, and the control parameters are sought to stabilize the resulting linear system. The simulation results using the optimum inputs determined and $\omega = 50$ rad/s with initial conditions of $x_0 = 0.2$ m, $\theta_{1_0} = \frac{\pi}{6}$ rad, $\theta_{2_0} = \frac{\pi}{3}$ rad, and zero initial velocities are presented in Figures 6.4 through 6.6.

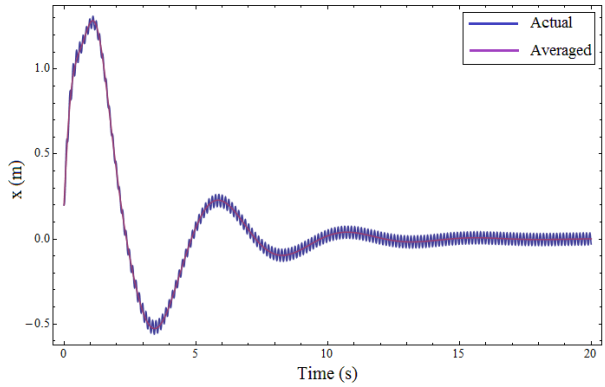

Figure 6.4: Time histories of $x(t)$ of the two-link mechanism on a cart

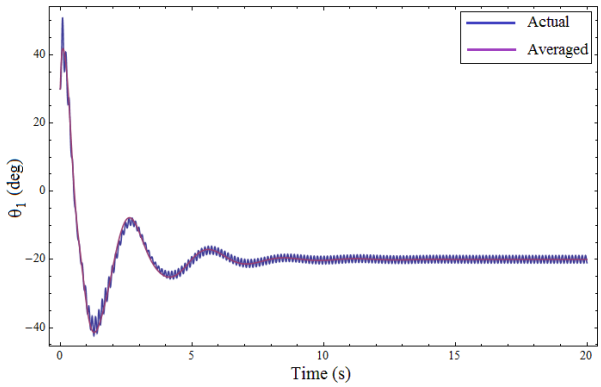

Figure 6.5: Time histories of $\theta_1(t)$ of the two-link mechanism on a cart

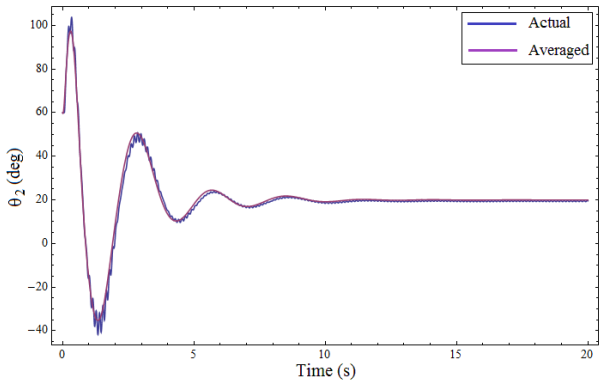

Figure 6.6: Time histories of $\theta_2(t)$ in the two-link mechanism on a cart

6.4 Selection of Design Parameters for Input Optimization

In this section the determination of optimum design parameters to minimize the amplitudes of high-frequency inputs in mechanical control-affine systems is discussed. Consider the n-DOF control system (3.10) with high-frequency inputs $u_i = \omega v_i(\omega t)$, $i \in \{1, \ldots, m\}$

$$\ddot{\boldsymbol{q}} = \boldsymbol{f}(\boldsymbol{q}, \dot{\boldsymbol{q}}; \boldsymbol{p}) + \sum_{i=1}^{m} \boldsymbol{g}_i(\boldsymbol{q}; \boldsymbol{p}) \omega v_i(\omega t), \quad \boldsymbol{q}(0) = \boldsymbol{q}_0, \ \dot{\boldsymbol{q}}(0) = \boldsymbol{v}_0 \tag{6.30}$$

where $\boldsymbol{p} = (p_1, \ldots, p_l)$ is the vector of design parameters, and $v_i(t)$ are zero-mean, T-periodic functions with amplitudes B_i. Using the state vector $\boldsymbol{x} = (\boldsymbol{q}^T, \dot{\boldsymbol{q}}^T)^T$ system (6.30) can be written in the first order form of (6.11) with the initial conditions of $\boldsymbol{x}(0) = \boldsymbol{x}_0 = (\boldsymbol{q}_0^T, \boldsymbol{v}_0^T)^T$. The goal is to determine the design parameters $\boldsymbol{p}$ in their acceptable ranges to minimize $\sum_{i=1}^{m} B_i^2$, while the system possesses a stable periodic orbit around a point $\boldsymbol{x}_\mathrm{e}$.

Using the first order form of system (6.30), its averaged dynamics is

$$\dot{\bar{\boldsymbol{x}}} = \boldsymbol{Z}(\bar{\boldsymbol{x}}; \boldsymbol{p}) - \sum_{i,j=1}^{m} \mu_{ij} \langle \boldsymbol{Y}_i : \boldsymbol{Y}_j \rangle (\bar{\boldsymbol{x}}; \boldsymbol{p}) \tag{6.31}$$

with the initial conditions of $\bar{\boldsymbol{x}}(0) = \bar{\boldsymbol{x}}_0 = \boldsymbol{x}_0 + \sum_{i=1}^{m} \kappa_i \boldsymbol{Y}_i(\boldsymbol{x}_0; \boldsymbol{p})$, and with $\boldsymbol{Z}$, $\boldsymbol{Y}_i$, and μ_{ij} defined as in (6.11) through (3.15). Following the procedure as discussed in Section 6.3, for the time-periodic system to have a periodic orbit about the point $\boldsymbol{x}_\mathrm{e}$, the point must be an

equilibrium point of the averaged dynamics (6.31), and therefore satisfies constraints in the form of

$$\sum_{i,j=1\ (i\leq j)}^{m} \boldsymbol{a}_{ij}(\boldsymbol{p})\mu_{ij} + \boldsymbol{b}(\boldsymbol{p}) = \boldsymbol{0} \tag{6.32}$$

where $\boldsymbol{a}_{ij}$ and $\boldsymbol{b}$ are as defined in (6.15). To determine the optimum parameters $\boldsymbol{p}$ to minimize $\sum_{i=1}^{m} B_i^2$, one may form the cost function ψ_{p} as

$$\psi_{\mathrm{p}} = \sum_{i=1}^{m} B_i^2 + \sum_{k=1}^{n} \zeta_k \left(\sum_{i=1}^{m} a_{ii_k}(\boldsymbol{p})\mu_{ii} \right) + \sum_{k=1}^{n} \zeta_k \left(\sum_{i,j=1\ (i<j)}^{m} a_{ij_k}(\boldsymbol{p})\mu_{ij} + b_k(\boldsymbol{p}) \right) \tag{6.33}$$

where ζ_k, $k \in \{1, \ldots, n\}$ are the Lagrange multipliers. With the discussions made in Section 6.3 one may choose $v_i(t)$ as square functions, and rewrite the cost function (6.33) as

$$\begin{aligned} \psi_{\mathrm{p}} = & \sum_{i=1}^{m} \left(1 + \sum_{k=1}^{n} c_{i_k}\zeta_k \right) B_i^2 \\ & + \sum_{k=1}^{n} \zeta_k \left(\sum_{i,j=1\ (i<j)}^{m} \frac{T^2}{96} a_{ij_k}(\boldsymbol{p}) B_i B_j \left(32(\phi_j - \phi_i)^3 - 24(\phi_j - \phi_i)^2 + 1 \right) + b_k(\boldsymbol{p}) \right) \end{aligned} \tag{6.34}$$

with c_{i_k} and ϕ_i defined as in (6.20). Therefore the optimum solution can be determined by

solving the set of equations

$$\begin{cases} \frac{\partial \psi_{\mathrm{p}}}{\partial B_i} = 0 \ , \ i \in \{1, \ldots, m\} \\ \\ \frac{\partial \psi_{\mathrm{p}}}{\partial \phi_i} = 0 \ , \ i \in \{2, \ldots, m\} \\ \\ \frac{\partial \psi_{\mathrm{p}}}{\partial p_j} = 0 \ , \ j \in \{1, \ldots, l\} \\ \\ \frac{\partial \psi_{\mathrm{p}}}{\partial \zeta_k} = 0 \ , \ k \in \{1, \ldots, n\} \end{cases} \tag{6.35}$$

together with checking for possible solutions on the boundaries of the parameters $\boldsymbol{p}$ and the phases ϕ_i.

Example: Consider the 2-DOF system with two high-frequency inputs and design parameters $0 < a \leq 5$ and $0 < b \leq 5$

$$\begin{cases} \ddot{q}_1 = \dot{q}_1^2 - \dot{q}_2^2 + 2a\dot{q}_1\dot{q}_2 - 2\dot{q}_1 - 3q_1 - 0.4 + (q_1 + b^2 q_2 - 1)\omega v_1(\omega t) \\ \\ \ddot{q}_2 = 2\dot{q}_1^2 - 3\dot{q}_2^2 + 0.5b\dot{q}_1\dot{q}_2 - 2.5\dot{q}_2 - 3q_2 - 0.3 + (a^2 q_1 - q_2 - 1)\omega v_2(\omega t) \end{cases} \tag{6.36}$$

where $v_1(t)$ and $v_2(t)$ are T-periodic, zero-mean functions with amplitudes B_1 and B_2 respectively. The goal is to find the design parameters a and b for the system to possess a stable periodic orbit around the origin while minimizing $B_1^2 + B_2^2$.

For the system to have a stable periodic orbit around the origin, its averaged dynamics must have a stable equilibrium point at the origin. Considering the inputs $v_1(t)$ and $v_2(t)$ as square functions with a period of $T = 1$ and a relative phase of ϕ_2, and averaging the system, one

determines the following two constraint equations for the origin to be an equilibrium point of the averaged system.

$$\begin{cases} 2B_1^2 - B_2^2 + (2a + b^2)(32\phi_2^3 - 24\phi_2^2 + 1)B_1B_2 - 19.2 & = 0 \\ 2B_1^2 - 4B_2^2 + (a^2 + 0.5b)(32\phi_2^3 - 24\phi_2^2 + 1)B_1B_2 - 14.4 & = 0 \end{cases} \tag{6.37}$$

Using numerical methods one may seek the parameters $0 < a \leq 5$, $0 < b \leq 5$, and $0 \leq \phi_2 \leq 0.5$, to minimize the cost function $\psi = B_1^2 + B_2^2$ under constraints (6.37). Using *fmincon* of Matlab the solution of the optimization problem was determined as $B_1 = 0.8218$, $B_2 = 0.6544$, $\phi_2 = 0.5$, $a = 5$, and $b = 4.8974$, which is a solution on the boundaries. For these values the origin is a stable equilibrium point of the averaged system.

6.5 Conclusions

Using averaging methods, optimization of input amplitudes for high-frequency mechanical control systems was discussed. Using properties of the shape of inputs on the averaged dynamics, it was shown that when using periodic square inputs, one needs smaller input amplitudes, and therefore smaller actuators. Using the equations of averaged dynamics, the problem of input optimization simplified into a constrained optimization problem, where the amplitude of each input and their relative phases can be determined to minimize the amplitudes of the inputs. As an example of a mechanical system, vibrational control and input optimization of a planar two-link mechanism on a cart with two inputs was presented. Fi-

nally, the problem of selection of design parameters for input optimization of high-frequency mechanical control systems was discussed, and an example of a 2-DOF system with two inputs and two design parameters was presented.

Chapter 7

Summary and Future Work

In this dissertation vibrational control and input optimization of mechanical control-affine systems is considered. Using high-frequency oscillations of actuated coordinates of a dynamic system, one may influence the system's behavior in unintuitive ways. Using this fact, a control method for trajectory tracking of a class of mechanical underactuated systems is developed. In the control law, a carefully chosen combination of high-frequency, zero-mean oscillatory inputs and state feedback is used, and the controller is robust against disturbances. For the selection of control parameters averaging techniques and linearization are used. Using high-frequency, high-amplitude inputs and state feedback, the control law is defined such that the closed-loop dynamics is in a proper form for averaging. Using the controller both actuated and unactuated coordinates track slowly varying desired trajectories on average. As a future work, one may try to extend the method for control of classes of electrical and electronic systems which use high-frequency signals. Also one may try to extend the

averaging method used for averaging of control-affine systems, to mechanical systems whose drift vector fields are homogeneous functions in velocities of degrees more than two.

Flapping wing micro-air vehicles are underactuated mechanical systems which use high-frequency flapping of their wings for hovering and flight. Using reasonable approximations and assumptions in their aerodynamics model, they are of the same class of systems for which a control method is developed in this thesis. The control method developed here is used for altitude control of FWMAVs using the flapping (sweeping) angle of the wings as the inputs. Also adding feathering (pitch) angle of the wings as another input, the longitudinal flight of FWMAVs is controlled when using symmetric flapping. Considering non-symmetric flapping of the wings, the control method is then extended for control of three-dimensional flight of FMVAVs. As future work one may use the same control strategy for motion control of other high-frequency biomimetic systems such as robotic fish. Also design and manufacture of a physical model of such systems can be very useful in verifying the effectiveness of the proposed control strategy. For example one may use a flapping plate mounted on a frictionless cart moving on horizontal plane to control the position of the cart. Besides verifying the effectiveness of the developed control method, the device can be an ideal test bed for further investigation of the unsteady aerodynamics of flapping. Both rigid and flexible plates with different shapes may be used to determine the effects of the wings' stiffness and shape on the aerodynamics of the flapping.

One useful mathematical tool for analysis of dynamics of time-periodic systems is averaging. Averaging theorem and higher-order averaging tools provide well developed techniques for

transforming time-periodic dynamical systems to time-invariant ones. In this dissertation using the available techniques for averaging of high-frequency, high-amplitude mechanical control systems, more properties of the averaged dynamics of such systems are revealed. The effects of the waveform (shape) of the inputs and their relative phase on the averaged dynamics are investigated. Using the results, the problem of inputs amplitudes minimization for mechanical control-affine systems is solved. It is shown that the mentioned problem can be stated as a constrained optimization problem, which may be solved analytically or numerically. Also it is shown that the zero-mean, periodic square waveform is the ideal waveform for minimization of input amplitudes. In addition, selection of the design parameters of mechanical control systems for input optimization of mechanical control systems is investigated. As future work one may try to use the same strategy for optimization of other cost functionals, such as the consumed energy, of high-frequency mechanical control systems. Also, design optimization of mechanical control systems using the method suggested in this thesis can be studied much further. There is a great potential of the suggested method for design optimization of high-frequency biomimetic systems, and studying of biolocomotion systems.

As another future work, further investigation of the vibrational control of the two-link mechanism on a cart presented in Section 6.3.2 is suggested. In the following section the results obtained in this dissertation for two cases of motion in horizontal and vertical planes are discussed and further work on the problem is suggested.

7.1 Vibrational Control of a Two-Link Mechanism on a Cart

Consider the planar two-link mechanism as depicted in Figure 7.1. Each link is a uniform bar with mass m_i, $i \in \{1, 2\}$, length l_i, and mass moment of inertia $I_i = \frac{1}{12} m_i l_i^2$ about its center of mass. The links move in a horizontal plane, therefore gravity does not affect the motion. The system is a 2-DOF system with one input $\tau(t)$ acting on the first link. We assume the system is subject to linear damping with coefficients of k_{d_1} and k_{d_2} in the lower and upper joints, respectively. Defining $\boldsymbol{q} = (\theta_1, \theta_2)^T$ as the vector of generalized coordinates and using

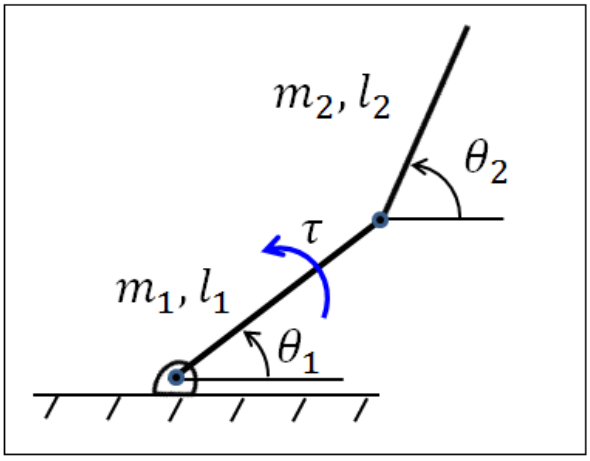

Figure 7.1: Two-link mechanism

Euler-Lagrange equations [Greenwood, 2003], the dynamic equations of the system can be written in the form of

$$\boldsymbol{M}(\boldsymbol{q})\ddot{\boldsymbol{q}} = \boldsymbol{f}(\boldsymbol{q}, \dot{\boldsymbol{q}}) + \boldsymbol{F}_c(t) \tag{7.1}$$

where the inertia matrix $\boldsymbol{M}$ is

$$\boldsymbol{M} = \begin{pmatrix} I_1 + \frac{1}{4}(m_1 + 4m_2)l_1^2 & \frac{1}{2}m_2 l_1 l_2 \cos(\theta_1 - \theta_2) \\ \frac{1}{2}m_2 l_1 l_2 \cos(\theta_1 - \theta_2) & I_2 + \frac{1}{4}m_2 l_2^2 \end{pmatrix}$$

and

$$\boldsymbol{f} = \begin{pmatrix} -\frac{1}{2}m_2 l_1 l_2 \dot{\theta}_2^2 \sin(\theta_1 - \theta_2) - k_{d_1}\dot{\theta}_1 + k_{d_2}(\dot{\theta}_2 - \dot{\theta}_1) \\ \frac{1}{2}m_2 l_1 l_2 \dot{\theta}_1^2 \sin(\theta_1 - \theta_2) - k_{d_2}(\dot{\theta}_2 - \dot{\theta}_1) \end{pmatrix}$$

and the input vector

$$\boldsymbol{F}_c(t) = \begin{pmatrix} \tau(t) \\ 0 \end{pmatrix}.$$

Consider the input as

$$\tau(t) = -k_{p_1}(\theta_1 - \theta_{d_1}) + \omega v(\omega t) \tag{7.2}$$

where $v(t)$ is a T-periodic, zero-mean function with an amplitude of τ_0, k_{p_1} is control parameter, and θ_{d_1} is the desired equilibrium configuration of the first link. Multiplying equation (7.1) by $\boldsymbol{M}^{-1}$, and using the state vector $\boldsymbol{x} = (\theta_1, \theta_2, \dot{\theta}_1, \dot{\theta}_2)^T$, equations of motion of the system can be written in the form of

$$\dot{\boldsymbol{x}} = \boldsymbol{Z}(\boldsymbol{x}) + \boldsymbol{Y}(\boldsymbol{x})\omega v(\omega t)$$

where the vector fields $\boldsymbol{Z}(\boldsymbol{x})$ and $\boldsymbol{Y}(\boldsymbol{x})$, and the input $v(t)$, satisfy the necessary conditions of Theorem 3.3.1. Therefore one may determine the averaged dynamics of the system using

Theorem 3.3.1 as (3.17). Since the equations of averaged dynamics are complicated, we do not present them here. Using the equations of the averaged dynamics and the input defined as (7.2), it can be shown that any point $\boldsymbol{q}_{\mathrm{e}} = (\theta_{d_1}, \theta_{d_1} \pm \frac{\pi}{2})^T$ is a stable equilibrium point of the averaged system. Therefore the original system possesses a stable periodic orbit in $O(\frac{1}{\omega})$ neighborhood of that equilibrium point. In fact, for this system, the only stable configurations (equilibria) which the system can be driven to using vibrational control, are the cases where the links are perpendicular to each other. The problem of vibrational control of a two-link mechanism using the concept of averaged potential is discussed in [Bullo, 2002] and [Bullo and Lewis, 2005, Ch. 12]. The responses of the actual and averaged systems for $\theta_{d_1} = -\frac{\pi}{6}$ rad, initial conditions $\boldsymbol{x}_0 = (\frac{\pi}{6}, \frac{\pi}{2}, 0, 0)^T$, and $v(t) = \tau_0 \cos t$ are shown in Figure 7.2. The physical parameters used for simulations are $m_1 = 0.8$ kg, $m_2 = 1$ kg, $l_1 = 0.8$ m, $l_2 = 1$ kg, $\tau_0 = 1$ N.m, $k_{p_1} = 1$, $k_{d_1} = k_{d_2} = 0.5$, and $\omega = 30$ rad/s.

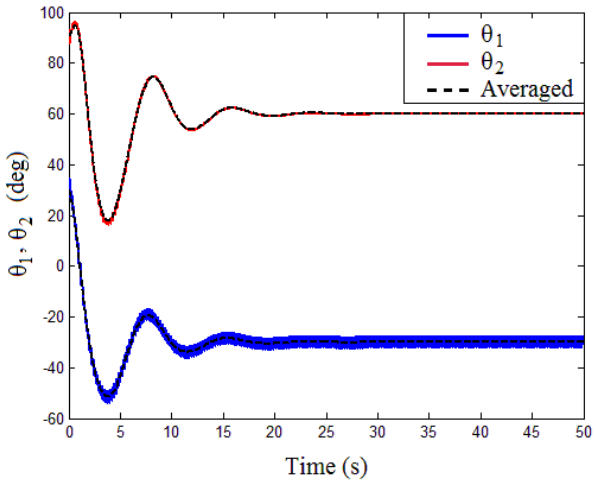

Figure 7.2: Time histories of the actual and averaged dynamics of the two-link mechanism

7.1.1 Two-link mechanism on a cart without gravity

Consider the system of two-link mechanism on a cart presented in Section 6.3.2 and depicted in Figure 6.3. The equations of motion of the system are in the form of (7.1), with the inertia matrix $\boldsymbol{M}$ and the vector $\boldsymbol{f}$ defined as in Section 6.3.2, and the input vector $\boldsymbol{F}_c(t) = (F(t), \tau(t), 0)^T$. As discussed, to steer the system to a desired configuration, one may use vibrational control with the inputs

$$\begin{aligned} F(t) &= -k_p(x - x_{\mathrm{d}}) - k_{\mathrm{d}}\dot{x} + \omega v_1(\omega t) \\ \tau(t) &= \tau_s - k_{p_1}(\theta_1 - \theta_{d_1}) + \omega v_2(\omega t) \end{aligned} \tag{7.3}$$

where $v_1(t)$ and $v_2(t)$ are T-periodic, zero-mean functions with amplitudes of F_0 and τ_0 respectively, k_p, k_{p_1}, and k_{d} are control parameters, and τ_s is a constant. The case of $\tau_s \neq 0$ along with numerical results is discussed in Section 6.3.2. Here we present the results we have already obtained for the special case of $\tau_s = 0$. But this special case still needs further discussion.

As mentioned, the goal is to drive the system to a desired configuration $\boldsymbol{q}_{\mathrm{d}} = (x_{\mathrm{d}}, \theta_{d_1}, \theta_{d_2})^T$ using the inputs (7.3). The role of the parameter τ_s is very important to drive the second link to its desired configuration θ_{d_2}. By choosing $\tau_s = 0$, equations (6.28) will be a set of three dependent linear homogeneous algebraic equations (two independent homogeneous equations). The trivial solution $F_0 = 0$ and $\tau_0 = 0$ of the homogeneous equations, which means there is no oscillatory input (vibrational control), is not admissible. However nonzero

solutions may also exist. But these nonzero solutions do not drive the unactuated link to the desired configuration. In fact using the nonzero solutions, the averaged dynamics does not represent the original time-varying system, and the original system does not have any periodic orbit in the neighborhood of the equilibrium points of the averaged dynamics.

Consider the two-link mechanism on a cart with the same parameters and desired configuration as in the example presented in Section 6.3.2. Using $\tau_s = 0$ for this case, equations (6.29) take the linear homogeneous form

$$\begin{cases} 0.2271\mu_{11} - 0.6111\mu_{12} - 1.5465\mu_{22} & = 0 \\ 1.0179\mu_{11} - 3.1218\mu_{12} - 5.9772\mu_{22} & = 0 \\ 1.4390\mu_{11} - 3.0137\mu_{12} - 11.9323\mu_{22} & = 0 \end{cases} \tag{7.4}$$

Since only two of these equations are dependent, besides the trivial zero solution, there may be infinite set of nonzero admissible solutions (note that $\mu_{ii} > 0$). Suppose that one tries to use $v_1(t) = F_0 \cos t$ and $v_2(t) = \tau_0 \cos(t + \phi)$ as the oscillatory inputs. Therefore equations (7.4) take the form

$$\begin{cases} 0.0568F_0^2 - 0.3866\tau_0^2 - 0.1528F_0\tau_0 \cos\phi & = 0 \\ 0.2545F_0^2 - 1.4943\tau_0^2 - 0.7804F_0\tau_0 \cos\phi & = 0 \\ 0.3597F_0^2 - 2.9831\tau_0^2 - 0.7534F_0\tau_0 \cos\phi & = 0 \end{cases} \tag{7.5}$$

It is evident that $F_0 = 0$ and $\tau_0 = 0$ are trivial solutions which are not admissible. Choosing

$\tau_0 = 1$ N.m, one determines $F_0 = 3.675$ N and $\phi = 0.8271$ rad as a set of "apparently" admissible solution. (Note that for all nonzero solutions for F_0 and τ_0, one always determines the same value for ϕ. In this case $\phi = k\pi \pm 0.8271$ rad, $k \in \mathbb{Z}$.) The responses of the actual and averaged dynamics using the cosine oscillatory inputs determined and the same initial conditions as before are shown in Figures 7.3 through 7.5.

From the figures it is evident that in both actual and averaged dynamics, the actuated coordinates x and θ_1 are converging to their desired values. But this is not the case for the unactuated coordinate θ_2. Though in the averaged dynamics, the coordinate converges to its desired value quickly, in the actual dynamics it approaches to a different value than the desired one. This means that in this case the averaged dynamics does not represent the actual one.

Investigation on the behavior of the actual and averaged systems shows that as $\tau_s \to 0$, the amplitudes of the oscillatory inputs $v_1(t)$ and $v_2(t)$, i.e., F_0 and τ_0, also approach zero ($F_0 \to 0$ and $\tau_0 \to 0$). Moreover, at least one of the eigenvalues of the state matrix of the LTI system obtained by linearization of the averaged system about its desired equilibrium point $\boldsymbol{x}_{\mathrm{e}}$ also approaches zero. This means that when $\tau_s = 0$, the desired equilibrium point of the averaged dynamics is not hyperbolically stable. Therefore, according to the averaging theorem, one cannot expect the averaged dynamics represents the actual one for all $t \geq 0$. As is evident from Figure 7.5, the responses of the averaged and actual dynamics stay close to each other for a small time interval only.

Further investigation of the system may reveal more information about the behavior of the

system for the case of $\tau_s = 0$. Also one may try to find other vibrational control systems which show similar behaviors. Anyway, further analysis of the special case of this problem, where $\tau_s = 0$, is a potential future work.

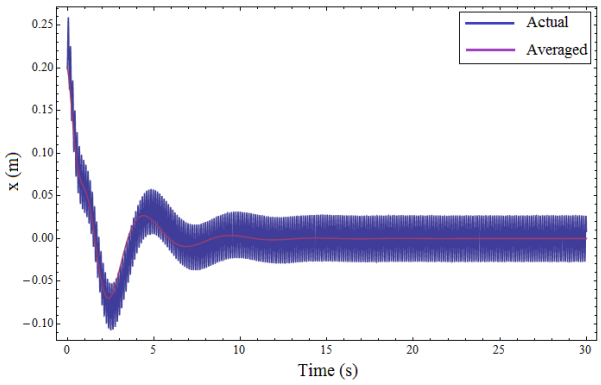

Figure 7.3: Time histories of $x(t)$ of the two-link mechanism on a cart

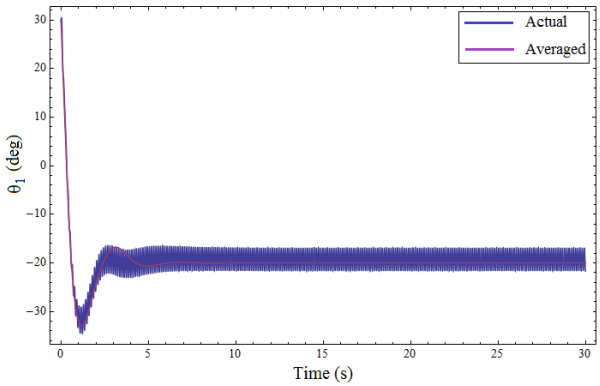

Figure 7.4: Time histories of $\theta_1(t)$ of the two-link mechanism on a cart

7.1.2 Two-link mechanism on a cart with gravity

Vibrational control can also be used to control the described system of two-link mechanism on a cart with two inputs when the links move in vertical plane as depicted in Figure 7.6. Therefore, in this case the weight of the links are also present. It is well known that inverted

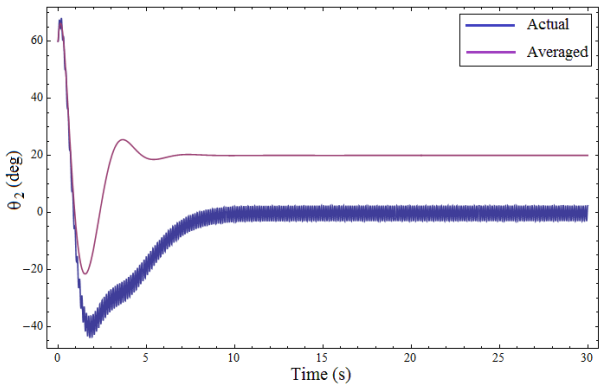

Figure 7.5: Time histories of $\theta_2(t)$ in the two-link mechanism on a cart

single or double pendulum on a cart can be stabilized in their upper equilibrium positions ($\theta_1 = \theta_2 = \frac{\pi}{2}$) using linear state feedback or nonlinear control methods [Furuta et al., 1978]. But using vibrational control the links can be stabilized in non-vertical orientations also. Though the results obtained in this dissertation show the effectiveness of the proposed vibrational control law, the problem and its applications still may be discussed further.

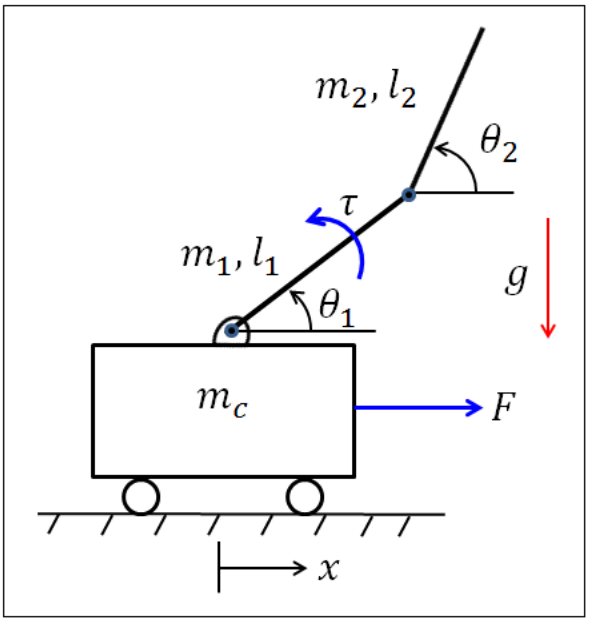

Figure 7.6: Two-link mechanism on a cart with gravity

The dynamic equations of the system can be written as (7.1), where the inertia matrix $\boldsymbol{M}$ is the same as (6.25), and the vector $\boldsymbol{f}(\boldsymbol{q}, \dot{\boldsymbol{q}})$ is

$$\boldsymbol{f} = \begin{pmatrix} \frac{1}{2}\big((m_1 + 2m_2)l_1\dot{\theta}_1^2 \cos\theta_1 + m_2 l_2 \dot{\theta}_2^2 \cos\theta_2\big) \\ -\frac{1}{2}m_2 l_1 l_2 \dot{\theta}_2^2 \sin(\theta_1 - \theta_2) - \frac{1}{2}(m_1 + 2m_2)g l_1 \cos\theta_1 - k_{d_1}\dot{\theta}_1 + k_{d_2}(\dot{\theta}_2 - \dot{\theta}_1) \\ \frac{1}{2}m_2 l_1 l_2 \dot{\theta}_1^2 \sin(\theta_1 - \theta_2) - m_2 g l_2 \cos\theta_2 - k_{d_2}(\dot{\theta}_2 - \dot{\theta}_1) \end{pmatrix}$$

Choosing the inputs as

$$\begin{aligned} F(t) &= -k_p(x - x_{\mathrm{d}}) - k_{\mathrm{d}}\dot{x} + \omega v_1(\omega t) \\ \tau(t) &= \tau_s - k_{p_1}(\theta_1 - \theta_{d_1}) + \frac{1}{2}g\big((m_1 + 2m_2)l_1 \cos\theta_1 + \omega v_2(\omega t) \end{aligned} \tag{7.6}$$

the equations of motion of the system can again be written in the proper form for averaging. After determining the averaged dynamics, one can linearize it about a desired equilibrium point $\boldsymbol{q}_{\mathrm{d}} = (x_{\mathrm{d}}, \theta_{d_1}, \theta_{d_2})^T$ and try to stabilize the linearized system. The results using $\tau_s = -8$ N.m, $k_p = 10$, $k_{\mathrm{d}} = 2$, $k_{p_1} = 15$, $k_{d_1} = 1$, and $k_{d_2} = 2$, a desired equilibrium point of $x_{\mathrm{d}} = 0$, $\theta_{d_1} = \frac{\pi}{9}$ rad, and $\theta_{d_2} = \frac{5\pi}{6}$ rad, and cosine inputs with amplitudes of $F_0 = 7.52$ N and $\tau_0 = 4.54$ N.m and a phase difference of $\phi = \frac{8\pi}{9}$ rad are shown in Figures 7.7 through 7.9. The rest of physical parameters are the same as used in Section 6.3.2, and the initial conditions are $x_0 = 0.1$ m, $\theta_{1_0} = 0$, $\theta_{2_0} = \frac{3\pi}{4}$ rad, with zero initial velocities. One may also try to find optimum inputs and physical parameters using the procedure presented in Chapter 6. The results presented here are not for optimum inputs. In this case the optimum inputs are

square functions with a phase difference of $\phi = \pi$.

Just as the case of motion in horizontal plane, in this case also for special value(s) of τ_s one may determine solutions which are not admissible. The difference is that in the case of motion in vertical plane it may happen for nonzero value(s) of τ_s. Further studying of these special cases, and trying to find ranges of physical parameters of the system and τ_s where the system is vibrationally controllable are potential future work.

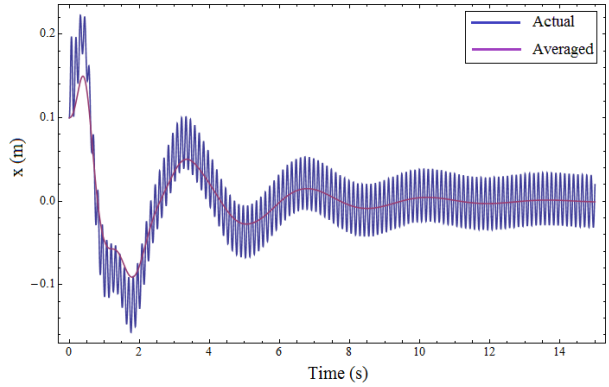

Figure 7.7: Time histories of $x(t)$ in the two-link mechanism on a cart with gravity

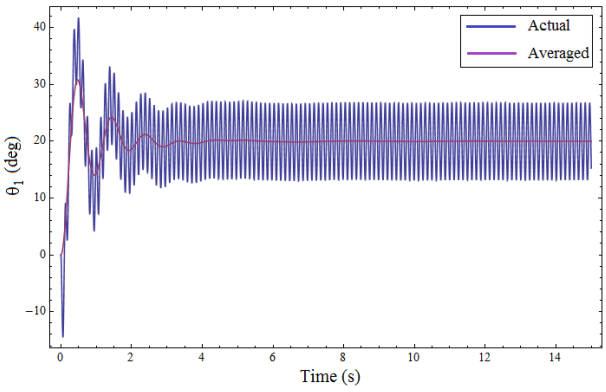

Figure 7.8: Time histories of $\theta_1(t)$ in the two-link mechansim on a cart with gravity

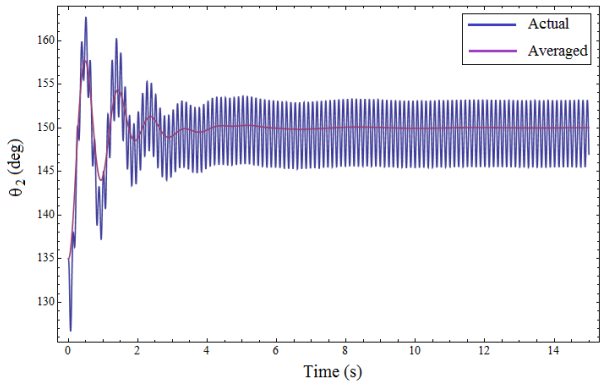

Figure 7.9: Time histories of $\theta_2(t)$ in the two-link mechanism on a cart with gravity

7.2 Conclusions

In this dissertation a number of problems concerning vibrational control and optimization of mechanical control systems were addressed. But the subject is still far from being over. As is usual in science, solving a problem brings new problems into attention. As mentioned in this chapter, there are different opportunities, both theoretical and experimental, to continue or verify the research done in this dissertation. Verifying the performance of the control method proposed in Chapter 4 by a real physical system, applying the controller developed in Chapter 5 to control a real FWMAV, using the optimization technique developed in Chapter 6 for design and input optimization of biomimetic systems and biolocomotion studies, and further investigation on the vibrational control of the two-link mechanism on a cart introduced in Section 6.3.2 and analyzed in the current chapter, are examples of these opportunities for future work.

Appendix A

Proof of Theorem 3.4.1

Since $v_i(t)$, $i \in \{1, \ldots, m\}$, are zero-mean, T-periodic functions, $w_i(t)$ are also zero-mean, T-periodic. For $w_i(t)$ and $w_j(t)$, $i, j \in \{1, \ldots, m\}$ we define

$$\kappa_{s_i} = \frac{1}{T} \int_0^T \int_0^t w_i(\tau) d\tau dt \tag{A.1}$$

$$\lambda_{s_{ij}} = \frac{1}{T} \int_0^T \left(\int_0^t w_i(\tau) d\tau \right) \left(\int_0^t w_j(\tau) d\tau \right) dt \tag{A.2}$$

and

$$\mu_{s_{ij}} = \frac{1}{2} (\lambda_{s_{ij}} - \kappa_{s_i} \kappa_{s_j}). \tag{A.3}$$

Therefore the averaged dynamics of (3.20) is

$$\dot{\bar{\boldsymbol{y}}} = \boldsymbol{Z}(\bar{\boldsymbol{y}}) - \sum_{i,j=1}^{m} \mu_{s_{ij}} \langle \boldsymbol{Y}_i : \boldsymbol{Y}_j \rangle (\bar{\boldsymbol{y}})$$

with initial conditions of $\bar{\boldsymbol{y}}(0) = \boldsymbol{x}_0 + \sum_{i=1}^{m} \kappa_{s_i} \boldsymbol{Y}_i(\boldsymbol{x}_0)$.

For any $0 \leq \phi_0 \leq T$, we show that $\mu_{s_{ij}} = \mu_{ij}$. Using $w_i(t) = v_i(t + \phi_0)$, $\mu_{s_{ij}}$ can be written as

$$\begin{aligned}\mu_{s_{ij}} =& \frac{1}{2T} \int_0^T \left(\int_0^t v_i(\tau + \phi_0) d\tau \right) \left(\int_0^t v_j(\tau + \phi_0) d\tau \right) dt \\ & - \frac{1}{2T^2} \left(\int_0^T \int_0^t v_i(\tau + \phi_0) d\tau dt \right) \left(\int_0^T \int_0^t v_j(\tau + \phi_0) d\tau dt \right)\end{aligned} \tag{A.4}$$

Using $s = \tau + \phi_0$, equation (A.4) can be written as

$$\begin{aligned}\mu_{s_{ij}} =& \frac{1}{2T} \int_0^T \left(\int_{\phi_0}^{t+\phi_0} v_i(s) ds \right) \left(\int_{\phi_0}^{t+\phi_0} v_j(s) ds \right) dt \\ & - \frac{1}{2T^2} \left(\int_0^T \int_{\phi_0}^{t+\phi_0} v_i(s) ds dt \right) \left(\int_0^T \int_{\phi_0}^{t+\phi_0} v_j(s) ds dt \right)\end{aligned}$$

which can be expanded to

$$\begin{aligned}\mu_{s_{ij}} = & \frac{1}{2T} \int_0^T \left(\int_0^{t+\phi_0} v_i(s) ds - \int_0^{\phi_0} v_i(s) ds \right) \left(\int_0^{t+\phi_0} v_j(s) ds - \int_0^{\phi_0} v_j(s) ds \right) dt \\ & - \frac{1}{2T^2} \left(\int_0^T \left(\int_0^{t+\phi_0} v_i(s) ds - \int_0^{\phi_0} v_i(s) ds \right) dt \right) \left(\int_0^T \left(\int_0^{t+\phi_0} v_j(s) ds - \int_0^{\phi_0} v_j(s) ds \right) dt \right)\end{aligned} \tag{A.5}$$

After some math, expression (A.5) simplifies to

$$\begin{aligned}\mu_{s_{ij}} =&\frac{1}{2T}\int_0^T \left(\int_0^{t+\phi_0} v_i(s)ds\right)\left(\int_0^{t+\phi_0} v_j(s)ds\right)dt \\ &- \frac{1}{2T^2}\left(\int_0^T\int_0^{t+\phi_0} v_i(s)dsdt\right)\left(\int_0^T\int_0^{t+\phi_0} v_j(s)dsdt\right)\end{aligned} \tag{A.6}$$

Using change of variable $r = t + \phi_0$, equation (A.6) can be written as

$$\begin{aligned}\mu_{s_{ij}} =&\frac{1}{2}\left(\frac{1}{T}\int_{\phi_0}^{T+\phi_0}\left(\int_0^r v_i(s)ds\right)\left(\int_0^r v_j(s)ds\right)dr\right. \\ &\left.-\left(\frac{1}{T}\int_{\phi_0}^{T+\phi_0}\int_0^r v_i(s)dsdr\right)\left(\frac{1}{T}\int_{\phi_0}^{T+\phi_0}\int_0^r v_j(s)dsdr\right)\right)\end{aligned}$$

But since $v_i(t)$, $i \in \{1,\ldots,m\}$, and therefore $\int v_i(t)dt$, are T-periodic, and for any T-periodic function $v(t)$, $\int_\phi^{T+\phi} v_i(t)dt = \int_0^T v_i(t)dt$, therefore $\mu_{s_{ij}}$ can be written as

$$\begin{aligned}\mu_{s_{ij}} =&\frac{1}{2}\left(\frac{1}{T}\int_0^T\left(\int_0^r v_i(s)ds\right)\left(\int_0^r v_j(s)ds\right)dr\right. \\ &\left.-\left(\frac{1}{T}\int_0^T\int_0^r v_i(s)dsdr\right)\left(\frac{1}{T}\int_0^T\int_0^r v_j(s)dsdr\right)\right)\end{aligned}$$

which is the same as μ_{ij}. □

Appendix B

Proof of Proposition 4.4.1

Proof of Proposition 4.4.1: According to [Bullo, 2002] the $(n+k)^{\text{th}}$ element of the symmetric product vector $\langle \boldsymbol{Y}_a(\boldsymbol{q},t) : \boldsymbol{Y}_b(\boldsymbol{q},t) \rangle$ can be written as

$$\langle \boldsymbol{Y}_a : \boldsymbol{Y}_b \rangle_{n+k} = \sum_{r,s=1}^{n} \left(\frac{\partial Y_{a_{n+k}}}{\partial q_r} Y_{b_{n+r}} + \frac{\partial Y_{b_{n+k}}}{\partial q_r} Y_{a_{n+r}} - \frac{\partial^2 Z_{n+k}}{\partial \dot{q}_r \partial \dot{q}_s} Y_{a_{n+r}} Y_{b_{n+s}} \right) \tag{B.1}$$

where Y_{a_i} is the i^{th} element of $\boldsymbol{Y}_a$. For $\boldsymbol{Y}_a = \boldsymbol{Y}_b = \boldsymbol{Y}$, the expression (B.1) simplifies to

$$\langle \boldsymbol{Y} : \boldsymbol{Y} \rangle_{n+k} = -\sum_{r,s=1}^{n} \left(\frac{\partial^2 Z_{n+k}}{\partial \dot{q}_r \partial \dot{q}_s} Y_{n+s} - 2 \frac{\partial Y_{n+k}}{\partial q_r} \right) Y_{n+r} \tag{B.2}$$

Substituting (B.2) into (4.21), the $(n+k)^{\text{th}}$, $k \in \{1, \ldots, n\}$, equation of (4.21) can be written as

$$\ddot{\bar{q}}_k = Z_{n+k}(\bar{\boldsymbol{q}}, \dot{\bar{\boldsymbol{q}}}, t) + \frac{1}{4}\sum_{r,s=1}^{n}\left(\frac{\partial^2 Z_{n+k}(\bar{\boldsymbol{q}}, \dot{\bar{\boldsymbol{q}}}, t)}{\partial \dot{\bar{q}}_r \partial \dot{\bar{q}}_s} Y_{n+s}(\bar{\boldsymbol{q}}, t) - 2\frac{\partial Y_{n+k}(\bar{\boldsymbol{q}}, t)}{\partial \bar{q}_r}\right) Y_{n+r}(\bar{\boldsymbol{q}}, t) \tag{B.3}$$

From (4.19), it is easy to show that for $k \in \{1, \ldots, n\}$,

$$\frac{\partial^2 Z_{n+k}(\boldsymbol{q}, \dot{\boldsymbol{q}}, t)}{\partial \dot{q}_l \partial \dot{q}_r} = \frac{\partial^2 g_k(\boldsymbol{q}, \dot{\boldsymbol{q}})}{\partial \dot{q}_l \partial \dot{q}_r} \quad \text{and} \quad Z_{n+k}(\boldsymbol{q}_{\mathrm{d}}, \dot{\boldsymbol{q}}_{\mathrm{d}}, t) = g_k(\boldsymbol{q}_{\mathrm{d}}, \dot{\boldsymbol{q}}_{\mathrm{d}}) \tag{B.4}$$

Define

$$C_i(\boldsymbol{q}, t) = v_{0_i}(t)\big(1 + k_{\mathrm{u}_i}\big(q_{\mathrm{d}_j}(t) - q_j(t)\big)\big)$$

for $i \in \{1, \ldots, m\}$ and $j \in \{m+1, \ldots, n\}$. According to (4.20),

$$Y_{n+k}(\boldsymbol{q}, t) = \sum_{i=1}^{m} C_i(\boldsymbol{q}, t) h_{i_k}(\boldsymbol{q}) \quad \text{and} \quad Y_{n+k}(\boldsymbol{q}_{\mathrm{d}}, t) = \sum_{i=1}^{m} v_{0_i}(t) h_{i_k}(\boldsymbol{q}_{\mathrm{d}}) \tag{B.5}$$

Using (B.5) one obtains

$$\frac{\partial Y_{n+k}(\boldsymbol{q}, t)}{\partial q_r} = \sum_{i=1}^{m}\left(\frac{\partial C_i(\boldsymbol{q}, t)}{\partial q_r} h_{i_k}(\boldsymbol{q}) + C_i(\boldsymbol{q}, t)\frac{\partial h_{i_k}(\boldsymbol{q})}{\partial q_r}\right)$$

But

$$\frac{\partial C_i(\boldsymbol{q}, t)}{\partial q_r} = -v_{0_i}(t) k_{\mathrm{u}_i} \delta_{rj}$$

Therefore

$$\frac{\partial Y_{n+k}(\boldsymbol{q},t)}{\partial q_r} = \sum_{i=1}^{m}\left(-v_{0_i}(t)k_{\mathrm{u}_i}h_{i_k}(\boldsymbol{q})\delta_{rj} + C_i(\boldsymbol{q},t)\frac{\partial h_{i_k}(\boldsymbol{q})}{\partial q_r}\right) \tag{B.6}$$

Using (B.4), (B.5), and (B.6), equation (B.3) can be written as

$$\begin{aligned}\ddot{\bar{q}}_k =& Z_{n+k}(\bar{\boldsymbol{q}},\dot{\bar{\boldsymbol{q}}},t) + \frac{1}{4}\sum_{r,s=1}^{n}\sum_{i,l=1}^{m}\Big(\frac{\partial^2 g_k(\bar{\boldsymbol{q}},\dot{\bar{\boldsymbol{q}}})}{\partial\dot{\bar{q}}_r\partial\dot{\bar{q}}_s}C_l(\bar{\boldsymbol{q}},t)h_{l_s}(\bar{\boldsymbol{q}}) \\ &+ 2v_{0_l}(t)k_{\mathrm{u}_l}h_{l_k}(\bar{\boldsymbol{q}})\delta_{rp} - 2C_l(\bar{\boldsymbol{q}},t)\frac{\partial h_{l_k}(\bar{\boldsymbol{q}})}{\partial\bar{q}_r}\Big)C_i(\bar{\boldsymbol{q}},t)h_{i_r}(\bar{\boldsymbol{q}})\end{aligned} \tag{B.7}$$

For $\bar{\boldsymbol{q}} = \boldsymbol{q}_{\mathrm{d}}$, using (B.4) and noting that $C_i(\boldsymbol{q}_{\mathrm{d}},t) = v_{0_i}(t)$, equation (B.7) can be simplified as

$$\begin{aligned}\ddot{q}_{\mathrm{d}_k}(t) =& g_k(\boldsymbol{q}_{\mathrm{d}},\dot{\boldsymbol{q}}_{\mathrm{d}}) + \frac{1}{4}\sum_{i,l=1}^{m}v_{0_i}(t)v_{0_l}(t)\sum_{r,s=1}^{n}\Bigg(\frac{\partial^2 g_k(\bar{\boldsymbol{q}},\dot{\bar{\boldsymbol{q}}})}{\partial\dot{\bar{q}}_r\partial\dot{\bar{q}}_s}h_{l_s}(\bar{\boldsymbol{q}}) \\ &+2k_{\mathrm{u}_l}h_{l_k}(\bar{\boldsymbol{q}})\delta_{rp} - 2\frac{\partial h_{l_k}(\bar{\boldsymbol{q}})}{\partial\bar{q}_r}\Bigg)\Big|_{\bar{\boldsymbol{q}}=\boldsymbol{q}_{\mathrm{d}}}h_{i_r}(\boldsymbol{q}_{\mathrm{d}})\end{aligned}$$

So for $\bar{\boldsymbol{q}} = \boldsymbol{q}_{\mathrm{d}}$, the parameter $v_{0_i}(t)$ will appear in the averaged dynamics of q_k (i.e., the k^{th} component of equation (4.21)), provided there exists an $l \in \{1,\ldots,m\}$ such that

$$\sum_{r,s=1}^{n}\left(\frac{\partial^2 g_k(\boldsymbol{q},\dot{\boldsymbol{q}})}{\partial\dot{q}_r\partial\dot{q}_s}h_{l_s}(\boldsymbol{q}) + 2k_{\mathrm{u}_l}h_{l_k}(\boldsymbol{q})\delta_{rp} - 2\frac{\partial h_{l_k}(\boldsymbol{q})}{\partial q_r}\right)\Big|_{\boldsymbol{q}=\boldsymbol{q}_{\mathrm{d}}}h_{i_r}(\boldsymbol{q}_{\mathrm{d}}) \neq 0$$

or

$$\sum_{r,s=1}^{n}\left(\frac{\partial^2 g_k(\boldsymbol{q},\dot{\boldsymbol{q}})}{\partial\dot{q}_r\partial\dot{q}_s}h_{i_s}(\boldsymbol{q}) + 2k_{\mathrm{u}_i}h_{i_k}(\boldsymbol{q})\delta_{rj} - 2\frac{\partial h_{i_k}(\boldsymbol{q})}{\partial q_r}\right)\Big|_{\boldsymbol{q}=\boldsymbol{q}_{\mathrm{d}}}h_{l_r}(\boldsymbol{q}_{\mathrm{d}}) \neq 0$$

□

Appendix C

Proof of Theorem 6.2.1

Using integration by parts, κ_s can be written as

$$\kappa_s = \frac{1}{T}\left(t\int_0^t w(\tau)d\tau\Big|_0^T - \int_0^T tw(t)dt \right)$$

Since $v(t)$ is T-periodic and zero-mean, so $w(t)$ is also T-periodic and zero mean. Therefore $\int_0^T w(t)dt = 0$, and κ_s simplifies to

$$\kappa_s = -\frac{1}{T}\int_0^T tw(t)dt$$

Replacing $w(t) = v(t+\phi)$ in the last equation one gets

$$\kappa_s = -\frac{1}{T}\int_0^T tv(t+\phi)dt$$

which using $\tau = t + \phi$ can be written as

$$\kappa_s = -\frac{1}{T}\int_{\phi}^{T+\phi}(\tau - \phi)v(\tau)d\tau = -\frac{1}{T}\int_{\phi}^{T+\phi}\tau v(\tau)d\tau + \frac{\phi}{T}\int_{\phi}^{T+\phi}v(\tau)d\tau$$

But $\int_{\phi}^{T+\phi} v(\tau)d\tau = \int_0^T v(\tau)d\tau = 0$. Therefore

$$\kappa_s = -\frac{1}{T}\int_{\phi}^{T+\phi} tv(t)dt$$

So ϕ_0 is the solution of

$$F(\phi_0) = \int_{\phi_0}^{T+\phi_0} tv(t)dt = 0$$

which we will show always exists. $F(\phi)$ can be written as

$$F(\phi) = \int_0^{T+\phi} tv(t)dt - \int_0^{\phi} tv(t)dt = \int_0^T tv(t)dt + \int_T^{T+\phi} tv(t)dt - \int_0^{\phi} tv(t)dt$$

Using change of variable $\tau = t - T$ for the second integral in the right hand side of the expression above

$$F(\phi) = \int_0^T tv(t)dt + \int_0^{\phi}(\tau + T)v(\tau + T)d\tau - \int_0^{\phi} tv(t)dt$$

which using $v(\tau + T) = v(\tau)$ simplifies to

$$F(\phi) = T\int_0^{\phi} v(t)dt + \int_0^T tv(t)dt$$

Using the result of integration by parts at the beginning of proof, $F(\phi)$ can be shown as

$$F(\phi) = T \int_0^{\phi} v(t)dt - \int_0^T \int_0^t v(\tau)d\tau dt$$

Defining the constant $M = -\int_0^T \int_0^t v(\tau)d\tau dt$, and $A(t) = \int_0^t v(\tau)d\tau$, the function $F(\phi)$ can be written as

$$F(\phi) = T\, A(\phi) - \int_0^T A(t)dt = T\, A(\phi) + M$$

Without loss of generality suppose that $M > 0$. Since $A(0) = A(T) = 0$, therefore $F(0) = F(T) = M > 0$. Though $v(t)$ may be a piecewise continuous function, $A(\phi)$ is continuous everywhere (it is the area under t-$v(t)$ curve). Therefore it is enough to show that there exists $0 \leq \phi \leq T$ such that $F(\phi) \leq 0$. Also since $A(\phi)$ is continuous and $A(0) = A(T) = 0$, so $A(\phi)$ has at least one minimum at $\phi = \phi_{\mathrm{m}}$ and $A(\phi_{\mathrm{m}}) \leq 0$. Consider $F(\phi_{\mathrm{m}}) = TA(\phi_{\mathrm{m}}) - \int_0^T A(t)dt$. Since $A(t)$ is continuous, using first mean value theorem for integrals [Olmsted, 1961], there exists $0 \leq \phi^* \leq T$ such that

$$\int_0^T A(t)dt = T\, A(\phi^*)$$

Therefore

$$F(\phi_{\mathrm{m}}) = T\, A(\phi_{\mathrm{m}}) - T\, A(\phi^*) = T\big(A(\phi_{\mathrm{m}}) - A(\phi^*)\big)$$

But since $A(\phi_{\mathrm{m}})$ is the minimum of $A(\phi)$ and T is positive, $F(\phi_{\mathrm{m}}) \leq 0$, and so there exist $0 \leq \phi_0 \leq T$ such that $F(\phi_0) = 0$ which results in $\kappa_s = 0$. $\square$

Appendix D

Proof of Theorem 6.3.1

Using equation (6.5)

$$\mu_{11}\mu_{22} - \mu_{12}^2 = \frac{1}{4}\left((\lambda_{11} - \kappa_1^2)(\lambda_{22} - \kappa_2^2) - (\lambda_{12} - \kappa_1\kappa_2)^2\right)$$

which using (6.3) and (6.4), and defining $A_i(t) = \int_0^t v_i(t)dt$, can be written as

$$\begin{aligned}\mu_{11}\mu_{22} - \mu_{12}^2 =& \frac{1}{4T^2}\left[\left(\int_0^T A_1^2(t)dt - \frac{1}{T}\left(\int_0^T A_1(t)dt\right)^2\right)\left(\int_0^T A_2^2(t)dt - \frac{1}{T}\left(\int_0^T A_2(t)dt\right)^2\right)\right. \\ & \left. - \left(\int_0^T A_1(t)A_2(t)dt - \frac{1}{T}\left(\int_0^T A_1(t)dt\right)\left(\int_0^T A_2(t)dt\right)\right)^2\right] \qquad \text{(D.1)}\end{aligned}$$

For two integrable functions $f, g : [0, T] \to \mathbb{R}$, $T \in \mathbb{R}$, consider Cauchy-Bunyakovsky-Schwarz theorem [Mitrinovic et al., 1993, Ch. 4]

$$\left(\int_0^T f^2(x)dx\right)\left(\int_0^T g^2(x)dx\right) \geq \left(\int_0^T f(x)g(x)dx\right)^2 \tag{D.2}$$

Replacing $f(x)$ with $f(x) - \frac{1}{T}\int_0^T f(x)dx$, and $g(x)$ with $g(x) - \frac{1}{T}\int_0^T g(x)dx$ in (D.2) and after some math, one gets

$$\left(\int_0^T f^2(x)dx - \frac{1}{T}\left(\int_0^T f(x)dx\right)^2\right)\left(\int_0^T g^2(x)dx - \frac{1}{T}\left(\int_0^T g(x)dx\right)^2\right) \geq \left(\int_0^T f(x)g(x)dx - \frac{1}{T}\left(\int_0^T f(x)dx\right)\left(\int_0^T g(x)dx\right)\right)^2 \tag{D.3}$$

Comparing the right hand side of expression (D.1) with inequality (D.3) it is evident that the right hand side of (D.1) is always positive, so $\mu_{11}\mu_{22} \geq \mu_{12}^2$.

For the case when $v_1(t)$ and $v_2(t)$ are square functions with amplitudes B_1 and B_2 respectively, using (6.3) through (6.5) it is easy to show that $\mu_{11} = \frac{T^2B_1^2}{96}$ and $\mu_{22} = \frac{T^2B_2^2}{96}$. Also if the phase between the two square functions is zero, $\mu_{12} = \sqrt{\mu_{11}\mu_{22}} = \frac{T^2B_1B_2}{96}$ and is maximum, and if the phase between them is $\frac{T}{2}$, then $\mu_{12} = -\sqrt{\mu_{11}\mu_{22}} = -\frac{T^2B_1B_2}{96}$ and is minimum, and for a phase shift of $\frac{T}{4}$, $\mu_{12} = 0$. For any other phase, according to the first part of the theorem $|\mu_{12}| < \sqrt{\mu_{11}\mu_{22}}$. So using square functions S_{B_1} and S_{B_2} and depended on the phase difference between them, μ_{12} may have any value in its maximum possible range. Note that one may choose other waveforms, such as sine or triangular ones, to generate μ_{12} in the same

range as the square functions, but those other waveforms need bigger amplitudes than the square ones. □

Bibliography

M. L. Anderson and R. G. Cobb. Toward flapping wing control of micro air vehicles. *Journal of Guidance, Control, and Dynamics*, 35(1):296–308, 2012.

M. L. Anderson and R. G. Cobb. Implementation of a flapping wing micro air vehicle control technique. *Journal of Guidance, Control, and Dynamics*, 37(1):290–300, 2014.

J. Baillieul. Stable average motions of mechanical systems subject to periodic forcing. In M. J. Enos, editor, *Dynamics and Control of Mechanical Systems: The Falling Cat and Related Problems*, pages 1–23. American Mathematical Society, 1993.

J. Baillieul. The geometry of controlled mechanical systems. In J. Baillieul and J. C. Willems, editors, *Mathematical Control Theory*, pages 322–354. Springer, 1999.

J. Baillieul. Averaging methods for force controlled and acceleration controlled Lagrangian systems. In *Proc. IEEE Conference on Decision and Control*, pages 1266–1272, Sydney, Australia, December 2000.

R. Bellman, J. Bentsman, and S. M. Meerkov. Stability of fast periodic systems. *IEEE Transactions on Automatic Control*, AC-30(3):289–291, 1985.

R. E. Bellman, J. Bentsman, and S. M. Meerkov. Vibrational control of nonlinear systems: Vibrational stabilizability. *IEEE Transactions on Automatic Control*, AC-31(8):710–716, 1986a.

R. E. Bellman, J. Bentsman, and S. M. Meerkov. Vibrational control of nonlinear systems: Vibrational controllability and transient behavior. *IEEE Transactions on Automatic Control*, AC-31(8):717–724, 1986b.

J. Bentsman. Vibrational control of a class of nonlinear systems by nonlinear multiplicative vibrations. *IEEE Transactions on Automatic Control*, AC-32(8):711–716, 1987.

G. J. Berman and Z. J. Wang. Energy-minimizing kinematics in hovering insect flight. *Journal of Fluid Mechanics*, 582:153–168, 2007.

D. P. Bertsekas. *Constrained Optimization and Lagrange Multiplier Methods*. Computer Science and Applied Mathematics. Academic Press, New York, NY, 1982.

M. Bhatia, M. Patil, C. Woolsey, B. Stanford, and P. Beran. Stabilization of flapping-wing micro-air vehicles in gust environments. *Journal of Guidance, Control, and Dynamics*, 37 (2):592–607, 2014.

A. M. Bloch, P. S. Krishnaprasad, J. E. Marsden, and R. M. Murray. Nonholonomic me-

chanical systems with symmetry. *Archive for Rational Mechanics and Analysis*, 136(1): 21–99, 1996.

J. E. Bobrow, S. Dubowsky, and J. S. Gibson. Time-optimal control of robotic manipulators along specified paths. *The International Journal of Robotics Research*, 4(3):3–17, 1985.

N. N. Bogoliubov and Y. A. Mitropolsky. *Asymtotic methods in the theory of non-linear oscillations*. Hindustan Publishing Corporation, Delhi, India, 1961.

R. W. Brockett. System theory on group manifolds and coset spaces. *SIAM Journal on Control*, 10(2):265–284, 1972.

R. W. Brockett. Asymptotic stability and feedback stabilization. In R. W. Brockett, R. S. Millman, and H. J. Sussmann, editors, *Differential Geometric Control Theory*, pages 181–191. Birkhäuser, 1983.

R. W. Brockett. On the rectification of vibratory motion. *Sensors and Actutaors*, 20(1-2): 91–96, 1989.

F. Bullo. Averaging and vibrational control of mechanical systems. *SIAM Journal on Control and Optimization*, 41(2):542–562, 2002.

F. Bullo. Trajectory design for mechanical control systems: from geometry to algorithms. *European Journal of Control*, 10(5):397–410, 2004.

F. Bullo and A. D. Lewis. Kinematic controllability and motion planning for the snakeboard. *IEEE Transactions on Robotics and Automation*, 19(3):494–498, 2003.

F. Bullo and A. D. Lewis. *Geometric Control of Mechanical Systems*. Texts in Applied Mathematics. Springer, New York, NY, 2005.

F. Bullo, N. E. Leonard, and A. D. Lewis. Controllability and motion algorithms for underactuated Lagrangian systems on lie groups. *IEEE Transactions on Automatic Control*, 45 (8):1437–1454, 2000.

J. A. Burns. *Introduction to the Calculus of Variations and Control with Modern Applications*. Chapman and Hall/CRC Applied Mathematics and Nonlinear Science. CRC Press, Boca Raton, FL, 2014.

P. Chedmail and M. Gautier. Optimum choice of robot actuators. *ASME Journal of Engineering for Industry*, 112:361–367, 1990.

P. Chirarattananon, K. Y. Ma, and R. J. Wood. Adaptive control of a millimeter-scale flapping-wing robot. *Bioinspiration and Biomimetics*, 9(2), 2014.

J. Cortes and S. Martinez. Configuration controllability of mechanical systems underactuated by one control. *SIAM Journal on Control and Optimization*, 41(6):1901–1921, 2003.

P. E. Crouch. Geometric structures in systems theory. *IEE Proceedings D (Control Theory and Applications)*, 128(5):242–252, 1981.

X. Deng, L. Schenato, and S. S. Sastry. Flapping flight for biomimetic robotic insects, part 2: Flight control design. *IEEE Transactions on Robotics*, 22(4):789–803, 2006a.

X. Deng, L. Schenato, W. C. Wu, and S. S. Sastry. Flapping flight for biomimetic robotic insects, part 1: System modeling. *IEEE Transactions on Robotics*, 22(4):776–788, 2006b.

D. B. Doman, M. W. Oppenheimer, and D. O. Sigthorsson. Wingbeat shape modulation for flapping-wing micro-air-vehicle control during hover. *Journal of Guidance, Control, and Dynamics*, 33(3):724–739, 2010.

C. P. Ellington. The aerodynamics of the hovering insect flight. i. the quasi-steady analysis. *Philosophical Transactions of the Royal Society, B. Biological Sciences*, 305(1122):1–15, 1984.

M. J. Elzinga, F. van Breugel, and M. H. Dickinson. Strategies for the stabilization of longitudinal forward flapping flight revealed using a dynamically-scaled robotic fly. *Bioinspiration and Biomimetics*, 9(2), 2014.

B. Etkin. *Dynamics of Atmospheric Flight*. John Wiley and Sons, Inc., New York, 1972.

I. Fantoni and R. Lozano. *Non-linear Control for Underactuated Mechanical Systems*. Communication and Control Engineering. Springer, London, 2002.

K. Furuta, T. Okutani, and H. Sone. Computer control of a double inverted pendulum. *Computers and Electrical Engineering*, 5(1):67–84, 1978.

D. T. Greenwood. *Advanced Dynamics*. Cambridge University Press, Cambridge, UK, 2003.

J. Gregory, A. Olivares, and E. Staffetti. Energy-optimal trajectory planning for robot

manipulators with holonomic constraints. *Systems and Control Letters*, 61(2):279–291, 2012.

J. Guckenheimer and P. Holmes. *Nonlinear Oscillations, Dynamical Systems, and Bifurcations of Vector Fields*. Applied Mathematical Sciences. Springer-Verlag, New York, NY, 1983.

L. Gurvits. Averaging approach to nonholonomic motion planning. In *Proc. IEEE International Conference on Robotics and Automation*, pages 2541–2546, Nice, France, May 1992.

P. Hartman. *Ordinary Differential Equations*. John Wiley and Sons, Inc., New York, NY, 1964.

R. Hermann and A. J. Krener. Nonlinear controllability and observability. *IEEE Transactions on Automatic Control*, AC-22(5):728–740, 1977.

K. S. Hong. An open-loop control for underactuated manipulators using oscillatory inputs: Steering capability of an unactuated joint. *IEEE Transactions on Control Systems Technology*, 10(3):469–480, 2002.

K. S. Hong, K. R. Lee, and K. I. Lee. Vibrational control of underactuated mechanical systems: control design through averaging analysis. *KSME International Journal*, 13(1): 1–10, 1999.

C. Jenkins. *Bio-inspired Engineering*. Momentum Press, New York, 2011.

V. Jurdjevic. *Geometric Control Theory*. Cambridge Studies in Advanced Mathematics. Cambridge University Press, Cambridge, UK, 1997.

M. Karpelson, G. Wei, and R. J. Wood. A review of actuation and power electronics options for flapping-wing robotic insects. In *Proc. IEEE International Conference on Robotics and Automation*, pages 779–786, Pasadena, CA, May 2008.

M. Keennon, K. Klingebiel, H. Won, and A. Andriukov. Development of the nano hummingbird: A tailless flapping wing micro air vehicle. In *Proc. AIAA Aerospace Science Meeting*, Nashville, TN, January 2012.

H. K. Khalil. *Nonlinear Systems*. Prentice-Hall, Inc., New Jersey, 1996.

Z. A. Khan and S. K. Agrawal. Control of longitudinal flight dynamics of a flapping-wing micro air vehicle using time-averaged model and differential flatness based controller. In *Proc. American Control Conference*, pages 5284–5289, New York City, NY, July 2007.

P. V. Kokotovic. Applications of singular perturbation techniques to control problems. *SIAM Review*, 26(4):501–550, 1984.

P. V. Kokotovic, J. J. Allemong, J. R. Winkelman, and J. H. Chow. Singular perturbation and iterative separation of time scales. *Automatica*, 16(1):23–33, 1980.

I. Kolmanovsky and N. H. McClamroch. Developments in nonholonomic control problems. *IEEE Control Systems Magazine*, 15(6):20–36, 1995.

P. S. Krishnaprasad and D. P. Tsakiris. Oscillations, se(2)-snakes and motion control. In *Proc. Conference on Decision and Control*, pages 2806–2811, New Orleans, LA, December 1995.

E. Lalish, K. Morgansen, and T. Tsukamaki. Oscillatory control for constant-speed unicycle-type vehicles. In *Proc. IEEE Conference on Decision and Control*, pages 5246–5251, New Orleans, LA, December 2007.

N. E. Leonard and P. S. Krishnaprasad. Motion control of drift-free left-invariant systems on lie groups. *IEEE Transactions on Automatic Control*, 40(9):1539–1554, 1995.

A. D. Lewis and R. M. Murray. Configuration controllability of simple mechanical control systems. *SIAM Journal on Control and Optimization*, 35(3):766–790, 1997.

P. Liljeback, K. Y. Pettersen, O. Stavdahl, and J. T. Gravdahl. Stability analysis of snake robot locomotion based on averaging theory. In *Proc. IEEE Conference on Decision and Control*, pages 1977–1984, Atlanta, GA, December 2010.

K. Y. Ma, P. Chirarattananon, S. B. Fuller, and R. J. Wood. Controlled flight of a biologically inspired insect-scale robot. *Science*, 340:603–607, 2013.

V. Manikonda and P. S. Krishnaprasad. Controllability of a class of underactuated mechanical systems with symmetry. *Automatica*, 38(11):1837–1850, 2002.

S. Martinez, J. Cortes, and F. Bullo. Analysis of oscillatory control systems. In *Proc. 15th IFAC Triennial World Congress*, pages 288–293, Barcelona, Spain, July 2002.

S. Martinez, J. Cortes, and F. Bullo. Analysis and design of oscillatory control systems. *IEEE Transactions on Automatic Control*, 48(7):1164–1177, 2003a.

S. Martinez, J. Cortes, and F. Bullo. Motion planning and control problems for underactuated robots. In A. Bicchi, H. I. Christensen, and D. Prattichizzo, editors, *Control Problems in Robotics*, volume 4, pages 59–74. Springer, 2003b.

S. M. Meerkov. Averaging of trajectories of slow dynamic systems. *Journal of Differential Equations*, 9(11):1239–1245, 1973.

S. M. Meerkov. Vibrational control theory. *Journal of The Franklin Institute*, 303(2):117–128, 1977.

S. M. Meerkov. Principle of vibrational control: Theory and applications. *IEEE Transactions on Automatic Control*, AC-25(4):755–762, 1980.

S. M. Meerkov. Condition of vibrational stabilizability for a class of nonlinear systems. *IEEE Transactions on Automatic Control*, AC-27(2):485–487, 1982.

S. Mitrinovic, J. E. Pecaric, and A. M. Fink. *Classical and New Inequalities in Analysis*. Mathematics and Its Applications. Kluwer Academic Publishers, Dordrecht, The Netherlands, 1993.

Y. A. Mitropolsky. Averaging method in non-linear mechanics. *Int. Journal of Nonlinear Mechanics*, 2(1):69–96, 1967.

K. A. Morgansen, V. Duindam, R. J. Mason, J. W. Burdick, and R. M. Murray. Nonlinear control methods for planar carangiform robot fish locomotion. In *Proc. IEEE International Conference on Robotics and Automation*, pages 427–434, Seoul, Korea, May 2001.

K. A. Morgansen, P. A. Vela, and J. W. Burdick. Trajectory stabilization for a planar carangiform robot fish. In *Proc. IEEE International Conference on Robotics and Automation*, pages 756–762, Washington, DC, May 2002.

K. A. Morgansen, B. I. Triplett, and D. J. Klein. Geometric methods for modeling and control of free-swimming fin-actuated underwater vehicles. *IEEE Transactions on Robotics*, 23(6): 1184–1199, 2007.

Y. Nakamura, T. Suzuki, and M. Koinuma. Nonlinear behavior and control of a nonholonomic free-joint manipulator. *IEEE Transactions on Robotics and Automation*, 13(6): 853–862, 1997.

H. Nijmeijer and A. J. van der Schaft. *Nonlinear Dynamical Control Systems*. Springer-Verlag, New York, NY, 1990.

K. Ogata. *Modern Control Engineering*. Prentice Hall, New Jersey, 2010.

J. M. H. Olmsted. *Advanced Calculus*. Prentice Hall, New York, NY, 1961.

M. W. Oppenheimer, D. B. Doman, and D. O. Sigthorsson. Dynamics and control of a minimally actuated biomimetic vehicle: Part ii - control. In *Proc. AIAA Guidance, Navigation, and Control Conference*, Chicago, IL, August 2009. AIAA 2009-6161.

M. W. Oppenheimer, D. B. Doman, and D. O. Sigthorsson. Dynamics and control of a biomimetic vehicle using biased wingbeat forcing functions. *Journal of Guidance, Control, and Dynamics*, 34(1):204–217, 2011.

C. T. Orlowski and A. R. Girard. Dynamics, stability, and control analyses of flapping wing micro-air vehicles. *Progress in Aerospace Sciences*, 51:18–30, 2012.

R. Ramamurti and W. C. Sandberg. A three-dimensional computational study of the aerodynamic mechanisms of insect flight. *Journal of Experimental Biology*, 205(10):1507–1518, 2002.

H. Rifai, N. Marchand, and G. Poulin-Vittrant. Bounded control of an underactuated biomimetic aerial vehicle- validation with robustness tests. *Robotics and Autonomous Systems*, 60(9):1165–1178, 2012.

V. R. Saksena, J. O'Reilly, and P. V. Kokotovic. Singular perturbation and time-scale methods in control theory: Survey 1976-1983. *Automatica*, 20(3):273–293, 1984.

J. A. Sanders and F. Verhulst. *Averaging Methods in Nonlinear Dynamical Systems*. Applied Mathematical Sciences. Springer-Verlag, New York, NY, 1985.

A. K. Sanyal, A. M. Bloch, and N. H. McClamroch. Control of mechanical systems with cyclic coordinates using higher order averaging. In *Proc. IEEE Conference on Decision and Control*, pages 6835–6840, Seville, Spain, December 2005.

A. Sarychev. Stability criteria for time-periodic systems via high-order averaging techniques.

In M. Thoma, F. Allgower, and M. Morari, editors, *Nonlinear control in the year 2000*, pages 365–377. Springer, 2001a.

A. V. Sarychev. Lie- and chronologico-algebraic tools for studying stability of time-varying systems. *Systems and Control Letters*, 43(1):59–76, 2001b.

S. Sastry. *Nonlinear Systems: Analysis, Stability, and Control*. Interdisciplinary Applied Mathematics. Springer, New York, NY, 1999.

L. Schenato. *Analysis and Control of Flapping Flight: From Biological to Robotic Insects*. PhD thesis, University of California at Berkeley, Berkeley, CA, 2003.

A. Serrani, B. E. Keller, M. A. Bolender, and D. B. Doman. Robust control of a 3-dof flapping wing micro air vehicle. In *Proc. AIAA Guidance, Navigation, and Control Conference*, Toronto, Canada, August 2010.

M. Sun. Insect flight dynamics: Stability and control. *Reviews of Modern Physics*, 86: 615–646, 2014.

H. J. Sussmann. Lie brackets and local controllability: A sufficient condition for scalar-input systems. *SIAM Journal on Control and Optimization*, 21(5):686–713, 1983.

H. J. Sussmann. A general theorem on local controllability. *SIAM Journal on Control and Optimization*, 25(1):158–194, 1987.

H. J. Sussmann and V. Jurdjevic. Controllability of nonlinear systems. *Journal of Differential Equations*, 12(1):95–116, 1972.

H. J. Sussmann and W. Liu. Limits of highly oscillatory controls and the approximation of general paths by admissible trajectories. In *Proc. Conference on Decision and Control*, pages 437–442, Brighton, England, December 1991.

T. Suzuki and Y. Nakamura. Control of manipulators with free joints via the averaging method. In *Proc. IEEE International Conference on Robotics and Automation*, pages 2998–3005, Albuquerque, NM, April 1997.

H. E. Taha, M. R. Hajj, and A. H. Nayfeh. Flight dynamics and control of flapping-wing mavs: a review. *Nonlinear Dynamics*, 70(2):907–939, 2012.

H. E. Taha, S. Tahmasian, C. A. Woolsey, A. H. Nayfeh, and M. R. Hajj. The need for higher-order averaging in the stability analysis of hovering, flapping-wing flight. *Bioinspiration and Biomimetics*, 10, 2015.

S. Tahmasian and C. A. Woolsey. A control design method for underactuated mechanical systems using high frequency inputs. *ASME Journal of Dynamic Systems, Measurement, and Control*, 137(7), 2015a.

S. Tahmasian and C. A. Woolsey. Flight control of flapping wing micro air vehicles using vibrational control and averaging. *IEEE Transactions on Control Systems Technology*, (under review), 2015b.

S. Tahmasian, H. E. Taha, and C. A. Woolsey. Control of underactuated mechanical systems using high frequency input. In *Proc. IEEE American Control Conference*, pages 603–608, Washington, DC, June 2013.

S. Tahmasian, C. A. Woolsey, and H. E. Taha. Longitudinal flight control of flapping wing micro air vehicles. In *Proc. AIAA SciTech*, National Harbor, MD, January 2014.

K. S. Tsakalis and P. A. Ioannou. *Linear Time-Varying Systems*. Prentice-Hall, New Jersey, 1993.

P. A. Vela. *Averaging and Control of Nonlinear Systems (with Application to Biomimetic Locomotion)*. PhD thesis, California Institute of Technology, Pasadena, CA, 2003.

P. A. Vela and J. W. Burdick. A general averaging theory via series expansions. In *Proc. American Control Conference*, pages 1530–1535, Denver, CO, June 2003a.

P. A. Vela and J. W. Burdick. Control of underactuated mechanical systems with drift using higher-order averaging theory. In *Proc. IEEE Conference on Decision and Control*, pages 3111–3117, Maui, HI, Decebmer 2003b.

P. A. Vela and J. W. Burdick. Control of biomimetic locomotion via averaging theory. In *Proc. IEEE International Conference on Robotics and Automation*, pages 1482–1489, Taipei, Taiwan, September 2003c.

P. A. Vela, K. A. Morgansen, and J. W. Burdick. Underwater locomotion from oscillatory shape deformations. In *Proc. IEEE Conference on Decision and Control*, pages 2074–2080, Las Vegas, NV, December 2002.

S. Weibel and J. Baillieul. Averaging and energy methods for robust open-loop control of

mechanical systems. In J. Baillieul, S. S. Sastry, and H. J. Sussmann, editors, *Essays on Mathematical Robotics*, pages 203–269. Springer, 1998.

S. Weibel, J. Baillieul, and T. J. Kaper. Small-amplitude periodic motions of rapidly forced mechanical systems. In *Proc. Conference on Decision and Control*, pages 533–539, New Orleans, LA, December 1995.

S. Weibel, J. Baillieul, and B. Lehman. Equilibria and stability of an n-pendulum forced by rapid oscillations. In *Proc. Conference on Decision and Control*, pages 1147–1152, San Diego, CA, December 1997.

R. J. Wood. The first takeoff of a biologically inspired at-scale robotic insect. *IEEE Transactions on Robotics*, 24(2):341–347, 2008.